

# Compositional and functional diversity of primitive minimal coacervates in a nucleic acid-peptide world

Karina K. Nakashima,<sup>1,2,†</sup> Fatma Zohra Mihoubi,<sup>1,2,†</sup> Jagandeep S. Saraya,<sup>3</sup> Kieran O. Russell,<sup>4</sup> Fidan Rahmatova,<sup>1,2</sup> James D. Robinson,<sup>3</sup> Maria Julia Maristany,<sup>4,5</sup> Jan Huertas,<sup>4,6</sup> Roger Rubio-Sánchez,<sup>7</sup> Rosana Collepardo-Guevara,<sup>4,5,6\*</sup> Derek K. O'Flaherty,<sup>3\*</sup> and Claudia Bonfio<sup>1,2,\*</sup>

<sup>1</sup>Department of Biochemistry, University of Cambridge, CB2 1GA Cambridge, UK

<sup>2</sup>Institut de Science et d'Ingénierie Supramoléculaires, CNRS UMR 7006, University of Strasbourg, 67000 Strasbourg, France

<sup>3</sup>Department of Chemistry, University of Guelph, ON N1G 2W1, Guelph, Canada

<sup>4</sup>Yusuf Hamied Department of Chemistry, University of Cambridge, CB2 1EW Cambridge, UK

<sup>5</sup>Cavendish Laboratory, Department of Physics, University of Cambridge, CB3 0HE, Cambridge, UK

<sup>6</sup>Department of Genetics, University of Cambridge, CB2 3EH, Cambridge, UK

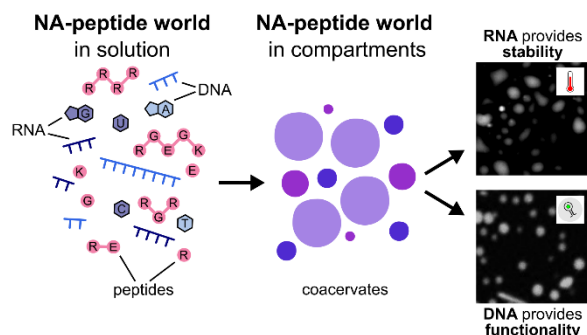
<sup>7</sup>Department of Chemical Engineering and Biotechnology, University of Cambridge, CB3 0AS Cambridge, UK

<sup>†</sup>These authors contributed equally

\*corresponding authors: [rc597@cam.ac.uk](mailto:rc597@cam.ac.uk), [doflaher@uoguelph.ca](mailto:doflaher@uoguelph.ca), [cb2036@cam.ac.uk](mailto:cb2036@cam.ac.uk)

## Abstract

The RNA-peptide world hypothesis postulates the early co-evolution of RNA and peptides, leading to the emergence of non-enzymatic RNA replication and peptide synthesis. Although nucleotides and amino acids were shown to form and polymerise under prebiotic conditions, the origin of their synergy, ubiquitously preserved in the central dogma of modern biology, remains unclear. We propose that the cooperation between DNA, RNA and peptides might have stemmed from their co-localisation in early compartments. Here we show that heterogeneous mixtures of prebiotic oligonucleotides and peptides spontaneously assemble into primitive coacervates. Experimental and computational studies reveal that peptide/nucleic acid coacervates are more robust and form over a broader range of conditions than peptide/peptide analogues. Notably, RNA-based coacervates exhibit exceptional stability and, in the presence of DNA, minimal viscosity, facilitating the diffusion of reactive oligonucleotides and supporting prebiotic RNA chemistry. Our findings suggest that coacervation may have occurred in the early on the evolutionary timeline, fostering the emergence of a nucleic acid-peptide world. This study provides new insights into the prebiotic role of coacervates, reconsidering their significance in the origins of life and the emergence of primitive replication and translation systems.



## Introduction

The RNA-peptide world hypothesis proposes the early co-evolution of RNAs and peptides, from which RNA replication and peptide synthesis may have emerged.<sup>1,2</sup> It was recently shown that RNA nucleotides and amino acids form non-enzymatically, alongside DNA nucleotides, in prebiotic conditions<sup>3-5</sup> and polymerise into short RNA and DNA oligomers, and peptides.<sup>6-8</sup> Although no defined prebiotic role has been proposed for DNA until its “genetic takeover” of RNA,<sup>9</sup> canonical and non-canonical RNAs were reported to template RNA and DNA polymerisation<sup>10</sup> and direct peptide synthesis,<sup>1,2,11</sup> and short peptides derived from the ribosomal core enhanced ribozyme activity.<sup>12</sup> Yet, how the primordial synergy between nucleic acids and peptides originated remains unknown. An intriguing hypothesis relies on the ability of the building blocks of life to cooperate upon co-localisation by means of compartmentalisation early on the evolutionary timeline.<sup>13</sup>

Biomolecular condensates, generated through the liquid-liquid phase separation of RNA and proteins, have been proposed as vestiges of primitive cells<sup>14</sup> because of their ability to spatially regulate cellular biochemistry.<sup>15</sup> Employed as *in vitro* models of biomolecular condensates, complex coacervates comprising homopeptides and functional oligonucleotides, e.g., ribozymes, were shown to take up dilute solutes, enable diffusion within and between the compartment and its environment, and host prebiotic reactions, e.g., ribozymatic activity.<sup>14,16-21</sup> Complex coacervation results from electrostatic interactions between oppositely charged polymers, such as positively charged polyarginines or polylysines, and negatively charged inorganic polyphosphates, polyglutamates, polyaspartates or sequence-specific nucleic acids.<sup>14,19,22,23</sup> However, in any prebiotic scenario, non-coded oligomerisation pathways would have likely afforded complex mixtures of peptides, DNA and RNA oligomers of limited length and high compositional heterogeneity.<sup>6,24,25</sup> As such, the prebiotic feasibility of coacervates, *i.e.*, whether they would have spontaneously emerged from simple, prebiotic molecules or relied upon the synthesis of long, coded, functional polymers (*i.e.*, homopeptides and ribozymes), has been overlooked.

Here we show that even short, mixed tri- and dipeptides form coacervates with prebiotically plausible heterogeneous oligonucleotides. Through experimental and computational studies, our findings indicate that coacervation could have occurred early in the evolutionary timeline, possibly simultaneously with the emergence of a nucleic acid-peptide world.

For the first time in a prebiotic context, we systematically compare peptide/peptide and peptide/nucleic acid coacervates and demonstrate that the latter form under a much broader range of conditions; and that RNA-based coacervates are remarkably more stable than both peptide/DNA and

peptide/peptide analogues. Importantly, we find that the extraordinary stability of RNA-based coacervates is minimally affected by the presence of DNA, which in turn makes RNA-based coacervates less viscous and thus more suitable to host prebiotic RNA chemistry by enhancing the diffusion of reactive oligonucleotides. Our results suggest that DNA played an early role in compartmentalisation to enable the emergence of primitive coacervates capable of hosting RNA biochemistry. Our work reconsiders the significance of primitive coacervates to support replication and translation in a general “compartmentalised nucleic acid-peptide world” to further our understanding of the possible the origins of life.

## Results and discussion

### Short peptides enable coacervation

Proteins and peptides are typically soluble only in a narrow pH, temperature and salt concentration range. Outside that range, they tend to amorphaously precipitate or aggregate in solid amyloid fibrils, or nano- or micro-structures.<sup>14</sup> However, some proteins and peptides have also been shown to form coacervates. This propensity to undergo phase separation strongly depends on the protein or peptide composition and charged and/or aromatic residues in intra- or intermolecular interactions, which lead to coacervation.<sup>14</sup> Arginine (Arg, R) residues interact with negatively charged monomers, such as nucleotides, through ionic and cation- $\pi$  interactions.<sup>26–28</sup> Such contacts are among the most frequent in RNA/protein complexes.<sup>29</sup> Recently, model Arg decamers were shown to undergo liquid-liquid phase separation in the presence of negatively charged molecules of low multivalency, e.g., nucleotide phosphates and decamers of glutamic acid (Glu, E) or aspartic acid (Asp, D).<sup>19</sup> Despite the ability of long homopolymeric peptides to generate biomimetic coacervates, their abundance on early Earth is questionable because it implies highly selective incorporation of certain amino acids during polymerisation or an environment enriched in a single amino acid. Either scenario is prebiotically implausible. Libraries of early amino acids likely included arginine among ten canonical amino acids, but no aromatics (e.g., phenylalanine or tyrosine),<sup>3</sup> and non-coded prebiotic peptide syntheses are mostly non-selective.<sup>6</sup> As such, it is unclear whether coacervates would have formed in prebiotic mixtures of heterogeneous peptides and oligonucleotides.

To further our understanding of the prebiotic plausibility of coacervates, we identified the minimal prebiotic requirements to direct phase separation. We systematically screened the phase space for mixtures of short coacervating (*i.e.*, enabling coacervation)<sup>23</sup> peptides and oligonucleotides (Fig. 1a). We employed mixed-sequence single-stranded (ss) DNA oligomers as model polyanions, to prevent any potential bias derived from a given nucleobase, and *N*- and *C-termini* unprotected peptides as polycationic counterparts (Figs. S1–S9, and Tables S1 and S2). Most peptide/nucleic acid combinations led to coacervation (Figs. 1a and S10). Precipitation of solid-like aggregates was detected when both types of polymers reached a certain length (8 Arg residues and 40 nucleotides). However, Arg monomers ( $R_1$ ) or dimers ( $R_2$ ) result in soluble mixtures regardless of the length of the DNA strand. Notably, peptide length has a greater influence than DNA length on the phase behaviour of peptide/nucleic acid mixtures. Although a mixture of  $R_3$  and  $DNA_8$  is soluble, four extra nucleobases ( $DNA_{12}$ ) enable coacervation with  $R_3$ ; yet phase separation with  $DNA_8$  only requires a single-unit increase in peptide length ( $R_4$ ).

To understand how the molecular features of coacervating peptides influence the stability of the resulting coacervates, we varied peptide length, sequence and charge in the presence of a mixed-sequence oligonucleotide ( $DNA_{20}$ ). Turbidity measurements upon titration of NaCl allowed us to determine the critical salt concentration (CSC) of peptide/DNA mixtures (Figs. 1b and S11, and Tables S3 and S4). CSC is

conventionally taken as an indication of coacervate robustness<sup>19</sup> and defined as the highest NaCl concentration tolerated before complete dissolution of the droplets.

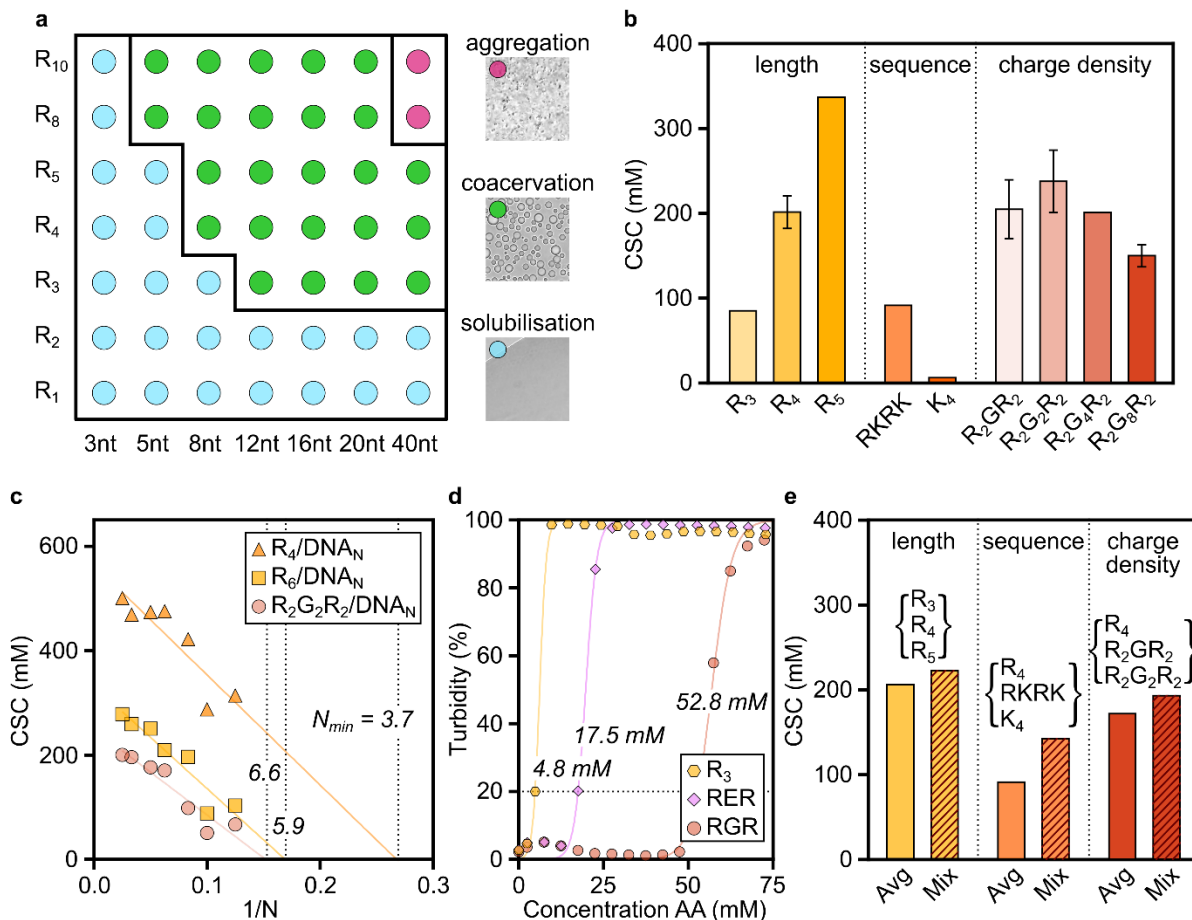
Increasing the length of an Arg homopeptide led to higher CSC values of the corresponding coacervates, thus indicating a strong correlation between peptide length and the strength of peptide interactions with DNA (Fig. 1b). Peptides of alternating D-Arg and L-Arg led to slightly destabilised coacervates compared to their homochiral counterparts, suggesting that peptide conformation and secondary structure affects, to a minor extent, coacervate stability (Table S3). Replacing Arg residues with lysines (Lys, K) resulted in gradual dissolution of the coacervates, likely due to the lower frequency of cation- $\pi$  interactions of nucleobases with Lys over Arg (Fig. 1b).<sup>30,31</sup> Our findings indicate that a minimum number of Arg residues per peptide and the same stereochemistry are required for coacervation.

Inspired by a first attempt to compare homo- and heteropeptides in coacervates,<sup>17</sup> we probed the influence of peptide sequence in governing coacervation by testing a library of peptides that contained a fixed number of Arg residues and an increasing number of glycines (Gly, G). All peptides screened had positive charge (+4) but varied in their charge density. When R<sub>2</sub>G<sub>2</sub>R<sub>2</sub> was mixed with DNA<sub>20</sub> in place of R<sub>4</sub>, we observed an 18% increase in salt stability of the resulting coacervates, likely due to the increased peptide length compensating for the 33.3% decrease in charge density of the peptide (Fig. 1b and Table S4). However, a further reduction in charge density, by incorporating more Gly residues (e.g., R<sub>2</sub>G<sub>4</sub>R<sub>2</sub> or R<sub>2</sub>G<sub>8</sub>R<sub>2</sub>), led to a decrease in salt stability. These findings suggest that, in a prebiotic setting in which heteropeptides were likely more abundant than Arg homopeptides, the stability of primitive coacervates greatly depended on both sequence and length of their peptide components,<sup>30</sup> but less so on their stereochemistry.

To assess the effect of peptide charge on phase separation, we determined the CSC for coacervates made of a series of peptides (R<sub>4</sub>, R<sub>6</sub> and R<sub>2</sub>G<sub>2</sub>R<sub>2</sub>) with oligonucleotides of various lengths (DNA<sub>N</sub>). In agreement with predictions for long polymers,<sup>32</sup> we observed a linear relationship between the CSC and the inverse of polymer length (1/N) for primitive coacervates. We estimated the minimal oligonucleotide length required for coacervation with any given peptide to delineate the precise co-existence boundaries in the related phase space (Fig. 1c and Table S5). For example, we calculated that R<sub>6</sub> undergoes coacervation only if a DNA tetramer is present ( $N_{\min} \geq 3.7$ ). Conversely, a shorter or less-charged peptide (e.g., R<sub>4</sub> or R<sub>2</sub>G<sub>2</sub>R<sub>2</sub>) would require longer DNA oligomers ( $N_{\min} \geq 6$ ) to undergo phase separation, which suggests that peptides with different sequences and lengths, but the same charge (e.g., R<sub>4</sub> and R<sub>2</sub>G<sub>2</sub>R<sub>2</sub>), have similar molecular requirements for coacervation. We thus assessed phase separation of R<sub>2</sub>G<sub>n</sub>R<sub>2</sub> peptides (n = 0, 2, 8). In all cases, stable coacervates were observed with DNA<sub>7</sub>, but not with DNA<sub>6</sub> (Fig. S12), which confirms that net charge has a more prominent role than length in modulating coacervation.<sup>19</sup>

In parallel, we studied the propensity of peptides with the same length, but different charge (e.g., R<sub>3</sub>, RGR and RER), to phase separate in the presence of DNA<sub>16</sub> (Figs. 1d and S13). The minimal concentration of R<sub>3</sub> required to enable coacervation was 4.8 mM; replacing an Arg residue with Gly or Glu induces a 9-fold and 3.5-fold concentration increase, respectively (Fig. 1d). Elongating the peptide, but maintaining its charge, also increases the amount of peptide required for coacervation (Fig. S13). As such, substituting arginine with glycine is more detrimental to coacervation than substitution with glutamic acid, which is in agreement with studies on inorganic polyphosphates.<sup>22</sup> Although replacing one arginine with glutamic acid lowers the peptide charge, it also potentially allows for more hydrogen bonding interactions with itself and DNA<sub>16</sub>, which would explain the lower coacervation onset for RER than RGR trimers.

Without a genetic code input to determine peptide sequences, a varied mixture of peptides could have formed on early Earth. We thus investigated whether peptide mixtures would undergo coacervation in the presence of oligonucleotides (Fig. 1e). We studied three model systems in which peptides differ in their length ( $R_3$ ,  $R_4$ ,  $R_5$ ), sequence ( $R_4$ , RKRK,  $K_4$ ) or charge density ( $R_4$ ,  $R_2G_2R_2$ ,  $R_2G_2R_2$ ). Remarkably, we found that all mixtures systematically had higher CSCs than the average value for their individual components, even for peptides incapable of coacervation on their own (e.g.,  $K_4$ ) (Table S4). These results demonstrate that coacervates may have readily formed with a range of mixed-sequence positively charged peptides resulting from non-enzymatic polymerisation processes<sup>6,24,33</sup> and benefitted from recruiting shorter, non-coacervating peptides.



**Figure 1.** The length, sequence and charge of arginine-based peptides influence the phase behaviour of primitive peptide/DNA coacervates. (a) Phase diagram of peptide/DNA coacervates, outlining the minimal peptide and DNA oligomer lengths required for coacervation. DNA sequences comprise the motif (ACTG)<sub>n</sub>, except for 3nt, which is dA<sub>3</sub>. (b) Critical salt concentrations (CSCs) of coacervates as a function of peptide length, sequence and charge density. Experiments were performed in the presence of DNA<sub>20</sub> ([positively charged amino acid] = 20 mM). (c) Estimated minimal length for DNA oligomers to undergo coacervation with peptides of the same charge ( $R_4$  and  $R_2G_2R_2$ ) and length ( $R_6$  and  $R_2G_2R_2$ ).  $N_{min}$  is obtained for CSC = 0 from the linear regression discussed in the Supplementary Information. (d) Titration curves of a DNA<sub>16</sub> solution ([nt] = 10 mM) with  $R_3$ , RER or RGR peptides. The dotted lines indicate the onset of coacervation (*i.e.*, the concentration above which coacervation is observed). (e) Critical salt concentrations (CSCs) of equimolar mixtures of peptides compared to the average of the individual CSCs of the mixture components. The three mixtures tested in the presence of DNA<sub>20</sub> ([nt] = 5 mM) are:  $R_3$ ,  $R_4$  and  $R_5$  (length mixture);  $R_2G_2R_2$ ,  $R_2G_2R_2$  and  $R_4$  (charge density mixture); and  $K_4$ , RKRK and  $R_4$  (sequence mixture). Each peptide in the

mixture was present in equimolar amino acid concentration ([amino acid] = 6.67 mM). Abbreviations: R = Arginine, G = Glycine, E = Glutamic acid, K = Lysine, nt = nucleotide, DNA<sub>N</sub> = mixed-sequence oligonucleotide of varied length.

### RNA coacervates are highly stable

Ribozymes or long sequence-specific nucleic acids (NAs) reportedly undergo phase separation with positively charged ions, polyamines and peptides.<sup>16–18,34–36</sup> However, prebiotic polymerisation processes would have mainly produced short, non-functional oligonucleotides, for which the *coacervating* propensity is unknown. In view of the prebiotic plausibility of both ribonucleotides and deoxyribonucleotides,<sup>5,37,38</sup> we investigated the propensity of single-stranded (ss) DNA and RNA oligomers for coacervation. Evidence suggests DNA would have been present in an RNA world,<sup>39–42</sup> but its role remains unclear<sup>39</sup> until the “genetic takeover” of RNA by DNA as information carrier.<sup>9</sup>

We first assessed the salt stability of coacervates made of Arg tetramers (R<sub>4</sub>) with DNA<sub>8</sub> ((ACTG)<sub>2</sub>) or RNA<sub>8</sub> ((ACUG)<sub>2</sub>) and compared it with that of previously studied<sup>19</sup> coacervates comprising negatively charged peptides (Glu decamers, E<sub>10</sub>) (Tables S1 and S2). CSC values at different [Arg]:[nucleotide] ratios were plotted to delineate the phase diagram of peptide/peptide and peptide/nucleic acid mixtures (Figs. 2a and S14–S16 and Table S6).

In line with previous observations,<sup>19</sup> we found that R<sub>4</sub>/E<sub>10</sub> mixtures do not form coacervates. When a longer positively charged peptide (R<sub>10</sub>) was used with E<sub>10</sub>, the maximum salt stability of the resulting coacervates was obtained when the two peptides were present in equimolar charge concentrations. A re-entrant tendency was observed with excess R<sub>10</sub>, which suggests that peptide/peptide mixtures form coacervates only when the charge concentration mismatch is minimal (Fig. 2a). When E<sub>10</sub> was replaced by DNA<sub>8</sub> and RNA<sub>8</sub>, we observed coacervation across a broader range of conditions (Figs. S17–S19). Upon increasing the concentration of arginine while keeping fixed that of oligonucleotide, salt stability curves plateaued at 8:1 [Arg]:[nucleotide]. No re-entrant behaviour was observed even with a high polymer charge mismatch, thus generating wider phase co-existence regions than those of peptide/peptide coacervates (Fig. 2a). The propensity of DNA oligonucleotides to undergo phase separation with peptides in mismatched charge concentrations suggests that the peptide/DNA coacervates may have been more likely to occur in a prebiotic setting than their peptide/peptide analogues.

Surprisingly, the salt tolerance of R<sub>4</sub>/RNA<sub>8</sub> is 2.3 times higher relative to that of the R<sub>4</sub>/DNA<sub>8</sub> mixture, rising from 110.0 mM to 249.0 mM NaCl at 8:1 [Arg]:[nucleotide]. A greater tendency of RNA oligomers to form coacervates over their DNA counterparts was also confirmed by measuring the minimal concentration of oligonucleotide and peptide required for coacervation, which is 2-fold lower for R<sub>4</sub>/RNA<sub>8</sub> mixtures relative to R<sub>4</sub>/DNA<sub>8</sub> mixtures (Fig. 2b). Intrigued by the enhanced salt stability of peptide/RNA coacervates, we used hot-stage epifluorescence microscopy<sup>43</sup> to evaluate their temperature susceptibility relative to analogous peptide/DNA coacervates (Figs. 2c and S20).

Along the heating ramp, full dissolution of the R<sub>4</sub>/DNA<sub>8</sub> coacervates was observed at ≈45°C. Conversely, R<sub>4</sub>/RNA<sub>8</sub> coacervates showcase greater thermal stability, dissolving only at ≈60°C. In both cases, cooling led to coacervation, which confirmed the reversibility of the assembly process. Although an additional hydroxyl group was shown to mildly increase the CSC of coacervates comprising small metabolites,<sup>44</sup> the unprecedented difference in the salt and thermal stability of DNA and RNA coacervates suggests stronger interactions between RNA and peptides than between DNA and peptides.

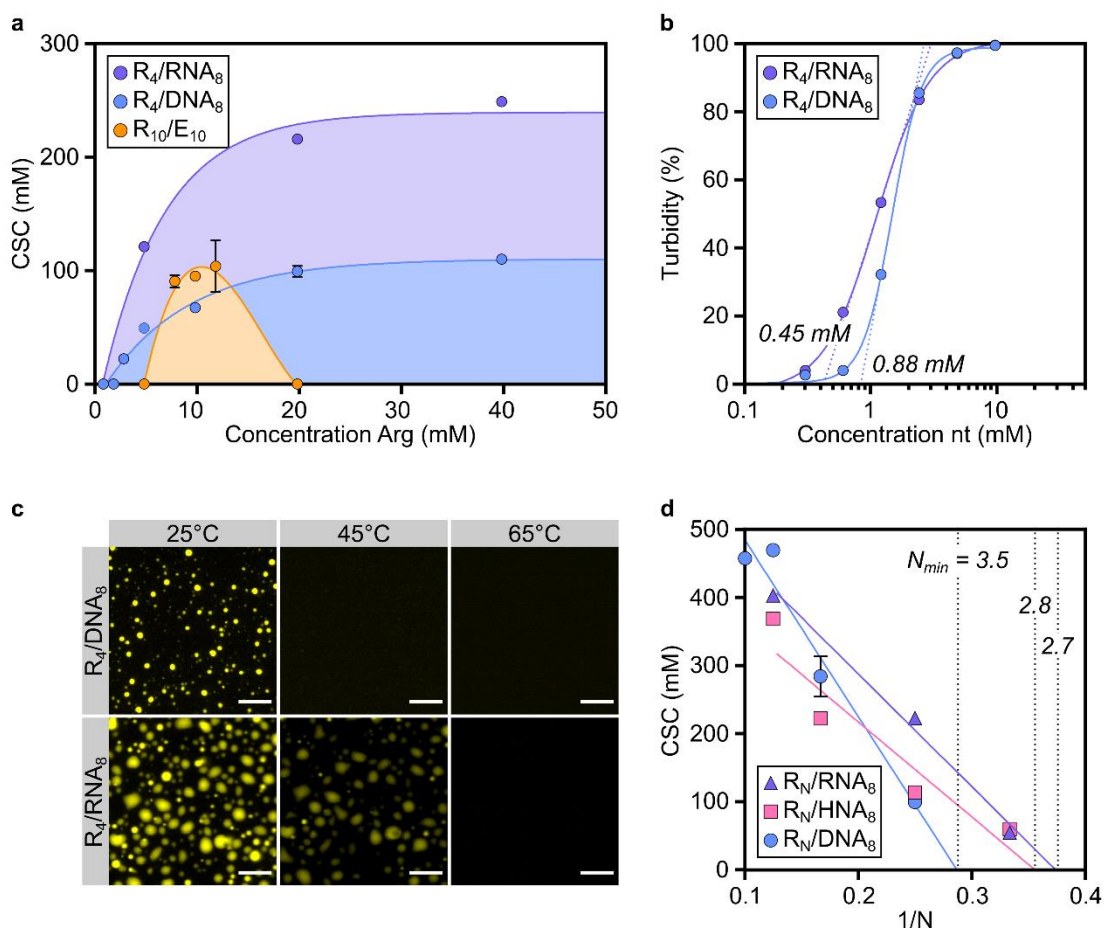
The differences in thermal and salt stability observed for  $R_4/DNA_8$  and  $R_4/RNA_8$  coacervates suggest distinct minimal coacervation requirements with respect to the length of peptides when RNA oligomers are used instead of DNA analogues. We found that  $RNA_8$ , but not  $DNA_8$ , forms coacervates with Arg trimers ( $R_3$ ) (CSC = 54.2 mM) (Table S3). Similarly, droplets were observed when  $RNA_{20}$  was mixed with  $R_2$  (Table S7 and Fig. S21). We next computed the minimal peptide length ( $N_{min}$ ) required for coacervation for a series of oligonucleotides ( $DNA_8$ ,  $RNA_8$ ,  $DNA_{12}$  and  $RNA_{12}$ ) (Figs. 2d and S22). We confirmed that at least an Arg tetramer is required to form coacervates with  $DNA_8$  ( $N_{min} \geq 3.5$ ), whereas coacervation occurs with  $RNA_8$  and the shorter  $R_3$  ( $N_{min} \geq 2.7$ ) (Table S5), which is in close agreement with qualitative screening (Fig. 1a). Because chimeric RNA-DNA oligonucleotides would have likely emerged from a prebiotic pool of ribonucleotides and deoxyribonucleotides,<sup>37,38,45</sup> we also tested an oligonucleotide comprising 50% RNA and 50% DNA nucleotides ( $HNA_8$ ) and observed an  $N_{min}$  value similar to that obtained for  $RNA_8$  ( $N_{min} \geq 2.8$ ) (Fig. 2d). An analogous trend was observed for longer oligonucleotides, with  $RNA_{12}$ , hybrid strands ( $HNA_{12}$ ) and mixed DNA-RNA oligomers predicted to form coacervates with Arg trimers (Fig. S23). These results suggest that the effect of ribonucleotides or RNA oligomers in a heterogeneous mixture with Arg peptides could have overcome that of deoxyribonucleotides and DNA oligomers and led to the emergence of coacervates with minimal length requirements and salt stability similar to those of a pure peptide/RNA system.

Homopolymeric DNA and RNA sequences have been widely studied for their ability to form coacervate models.<sup>32,46</sup> However, purines are only slightly more reactive than pyrimidines in template-free non-enzymatic RNA polymerisation,<sup>47</sup> so heteropolymeric sequences would have likely been more abundant than homopolymeric analogues on early Earth. We thus investigated how oligonucleotide sequence and charge influences coacervation.

Polycytosine and polyguanine decamers formed solid-like aggregates; but polyadenine and polythymine decamers formed coacervates with substantially lower CSCs than those made of heteropolymeric DNA sequences comprising all four nucleotides (Fig. S24). Similarly, the minimal oligonucleotide length required for coacervation with  $R_6$  is almost 2-fold higher for polyadenine ( $polyA_N$ ) than for mixed-sequence oligonucleotides ( $N_{min} = 6.6$  vs 3.7, respectively) (Fig. S25). Therefore, short, mixed-sequence oligonucleotides exhibit a higher propensity towards coacervation than less prebiotic, homopolymeric strands. Conversely, increasing the oligonucleotide charge, by means of phosphate groups on the 5' and 3' ends, causes the formation of clusters of coacervates and, in time, solid-like aggregates (Fig. S26), potentially due to the additional electrostatic interactions with the more exposed, terminal phosphate groups.

Following the observations that coacervation with low charge density heteropeptides is possible and that an  $R_2/RNA_{20}$  mixture forms coacervates, we investigated whether *N*- and *C-termini* unprotected peptide heterodimers ( $R_2$ , RG and RE) could undergo phase separation with short RNAs (Fig. S21 and Table S7). As expected, none of the peptide dimers phase separated with  $DNA_8$  and  $DNA_{12}$ . Surprisingly, we observed coacervation for RG and RE, but not  $R_2$ , when mixed with  $RNA_8$ . RG (charge = +1) requires an amino acid concentration of 40 mM to form coacervates, whereas RE (charge = 0) undergoes phase separation in the same conditions employed for  $R_3$  and  $R_4$  (20 mM amino acid concentration), likely due to RE participating in a wider range of interactions relative to RG. Our results indicate that, even in a prebiotic scenario where short, heterogeneous peptides, RNA and DNA oligomers were present, phase separation

likely occurred and potentially impacted the chemistry taking place at the dawn of a nucleic acid-peptide world.



**Figure 2.** Peptide/RNA coacervates exhibit higher robustness than peptide/DNA coacervates. (a) Salt stability of peptide/peptide and oligonucleotide/peptide coacervates. Critical salt concentrations (CSCs) were measured through turbidity measurements of peptide/peptide and oligonucleotide/peptide solutions by titration with NaCl in 25 mM HEPES, pH 7.5 and at room temperature. In all experiments, the anion concentration was kept constant ( $[nt] = 5$  mM and  $[glutamic\ acid] = 10$  mM). (b) Turbidity curves for  $R_4/DNA_8$  and  $R_4/RNA_8$  as a function of nucleotide concentration. The dotted lines are tangents to the inflection point, used to determine the minimal concentration required for coacervation (indicated in the graph). (c) Thermal stability of  $R_4$  coacervates with  $DNA_8$  and  $RNA_8$ . 1%  $Cy_3$ -(TGAC) $_2$  was used for visualization. Scale bars are 10  $\mu\text{m}$ . (d) Estimation of the minimal peptide length ( $N_{min}$ ) required for coacervation for a given nucleic acid composition. Abbreviations: R = Arginine, E = Glutamic acid, nt = nucleotide,  $DNA_8$  = 8-deoxyribonucleotide-long mixed-sequence oligonucleotide ((ACTG) $_2$ ),  $RNA_8$  = 8-ribonucleotide-long mixed-sequence oligonucleotide ((ACUG) $_2$ ),  $HNA_8$  = 8-nucleotide-long mixed-sequence oligonucleotide comprising deoxyribonucleotides and ribonucleotides (ArCrUGArCrUG).

### Peptides interact more with RNA than DNA

To elucidate the distinct features of the interactions between peptides and DNA or RNA strands and rationalise the different salt and thermal stabilities of the resulting coacervates, we carried out atomistic force-field simulations of four mixtures:  $R_3/DNA_8$ ,  $R_4/DNA_8$ ,  $R_3/RNA_8$  and  $R_4/RNA_8$ . Our models contain eight single-stranded (ss) oligonucleotides with thirty-six Arg peptides in explicit solvent and ions. For each



mixture, we analysed the trajectories to quantify the frequency of intermolecular contacts between Arg peptides and oligonucleotides.

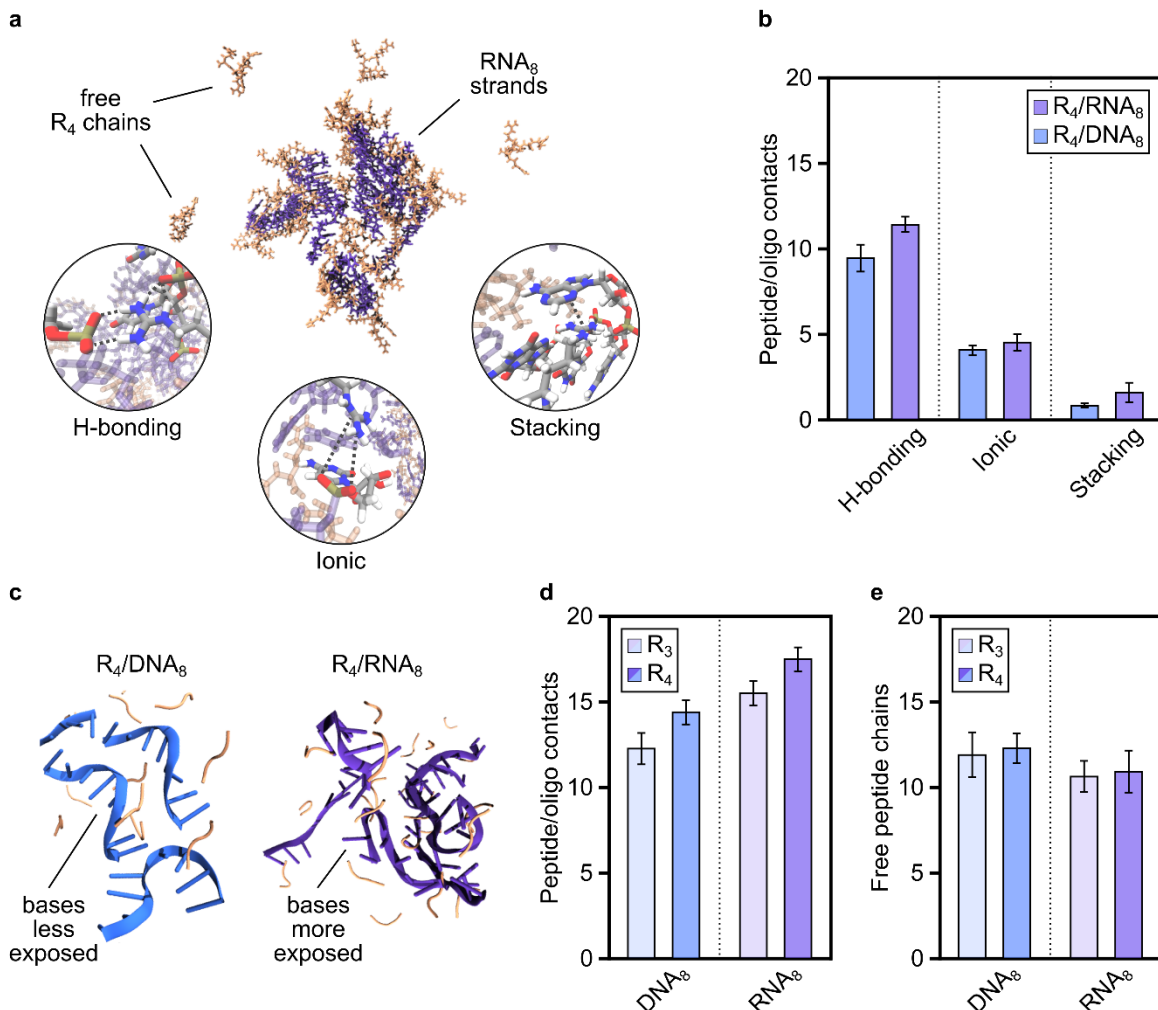
Arginine is known to interact with RNA through multiple modes,<sup>48</sup> yet any distinction between RNA and DNA oligomers to undergo coacervation has never been explored, due to the focus on probing the differences between double-stranded and single-stranded DNA (for their significance in genomic function),<sup>49,50</sup> and the outdated assumption that RNA preceded DNA on early Earth.<sup>51</sup>

We identified three main intermolecular interaction modes: ionic (here defined as non-hydrogen bonding contacts between the positively charged sidechain of Arg and the backbone phosphate group in both oligonucleotides), hydrogen bonding, and stacking, including  $\pi$ - $\pi$  stacking and cation- $\pi$  interactions between the positively charged Arg sidechain and the nucleobases in both oligonucleotides (Fig. 3a). Across all interaction classes, RNA<sub>8</sub> consistently forms more contacts with Arg peptides than DNA<sub>8</sub>, with differences being most pronounced in stacking interactions (96% increase in contact points for RNA<sub>8</sub> over DNA<sub>8</sub>) and hydrogen bonding *via* the nucleobase (Figs. 3b, S27 and S28, and Tables S8 and S9). Despite their relatively low frequency, the enhanced strength of cation- $\pi$  interactions, demonstrated through quantum mechanical calculations of model systems relative to ionic or hydrogen bonding in aqueous media,<sup>52</sup> suggests that even minor variations in their occurrence can have a significant energetic impact. As such, the higher number of stacking interactions present in the RNA<sub>8</sub> systems are expected to be a key contributor to the higher thermodynamic stability of RNA<sub>8</sub>-based coacervates, as also shown by the studies on the thermal stability of coacervates (Fig. 2c).

The higher frequency of intermolecular interactions observed for RNA<sub>8</sub> over DNA<sub>8</sub> are attributed to conformational differences between the two nucleic acids, likely due to the additional hydroxyl group in the sugar moiety of ribonucleotides. In contrast to DNA<sub>8</sub>, RNA<sub>8</sub> adopts a more expanded, unfolded structure with Arg peptides (Fig. 3c), which enables its nucleobases to engage more readily in intermolecular hydrogen bonding and stacking interactions with Arg residues. Our all-atom simulations reveal that the higher propensity of RNA<sub>8</sub> versus DNA<sub>8</sub> to acquire an expanded, unfolded structure within the coacervate phase results in an increased density of intermolecular interactions and an enthalpic gain for coacervation.<sup>53</sup> This observation aligns with previous structural analyses that reveal stronger and more frequent  $\pi$ - $\pi$  contacts of Arg with RNA nucleobases than with DNA nucleobases.<sup>54</sup> Several other factors likely contribute, such as uracil's weaker stacking interactions with other nucleobases compared to thymine<sup>55</sup> and the higher tendency of DNA to adopt compact helical conformations.<sup>56</sup>

The total number of intermolecular contacts that RNA<sub>8</sub> or DNA<sub>8</sub> form with Arg peptides (Figs. 3d and S29, and Table S10) correlates well with experimentally observed phase separation propensity (Fig. 2). Indeed, simulations on the R<sub>3</sub>/DNA<sub>8</sub> system (the only mixture that does not form coacervates) show the lowest number of intermolecular contacts. Notably, elongating the peptide chain by one Arg residue (from R<sub>3</sub> to R<sub>4</sub>) results in an 18 and 16% increase in hydrogen bonding and ionic interactions, respectively (Fig. S27). This increase in the total number of interactions for the R<sub>4</sub>/DNA<sub>8</sub> system aligns well with our experimental finding that R<sub>4</sub> is the minimum peptide length required for coacervation with DNA<sub>8</sub> (Fig. 2d). In contrast, the R<sub>3</sub>/RNA<sub>8</sub> mixture has a similar number of intermolecular contacts to R<sub>4</sub>/DNA<sub>8</sub> due to the more abundant hydrogen bonding and stacking interactions characteristic of RNA<sub>8</sub>, and thus undergo coacervation. This observation and the fact that excess peptide remains in the simulation box at equilibrium (Figs. 3e and S30, and Table S11) suggests that the intrinsic physicochemical differences between DNA and RNA can explain their observed different sensitivity to peptide length.

Our simulations reveal striking differences in how Arg peptides interact with DNA and RNA, which allow us to explain the macroscopic differences in the phase separation behaviour that we observed experimentally. RNA<sub>8</sub> exhibits a notably higher frequency of stacking and hydrogen bonding with Arg peptides than DNA<sub>8</sub> (Fig. 3b), which likely underpins the increased resilience to both salt concentration (Fig. 2a) and temperature (Fig. 2c), and thus the thermodynamic stability of RNA-based coacervates.



**Figure 3.** Computational investigations reveal contact modes and frequency of interactions in peptide/nucleic acid coacervates. (a) Representative atomistic force-field simulation snapshot of the R<sub>4</sub>/RNA<sub>8</sub> mixture, showing a cluster of RNA and peptide, and unbound peptide in excess. Inset shows the interaction modes, e.g., hydrogen bonding, ionic interactions, and cation- $\pi/\pi$ - $\pi$  stacking. The simulations were performed with OpenMM 8.1.2, leveraging the CUDA platform in mixed precision mode, using the Amber14SB force field for peptides, OL3 parameters for RNA, and bsc1 for DNA. See Supplementary Information for more details. (b) Comparison between the number of DNA and RNA interactions with arginine peptides (per frame, per nucleotide), separated into three categories: hydrogen bonding, ionic interactions and stacking. (c) Simplified rendering of R<sub>4</sub>/DNA<sub>8</sub> (blue) and R<sub>4</sub>/RNA<sub>8</sub> (purple) clusters, showing the helical, structured conformation acquired by DNA strands and the more disordered folding acquired by RNA strands, which leaves ribonucleotides exposed to interact with peptides. (d) Number of peptide/oligonucleotide contacts (all modes of interaction), which represents the total number of intermolecular contacts that one molecule of RNA<sub>8</sub> or DNA<sub>8</sub> forms with R<sub>3</sub> or R<sub>4</sub>. (e) Excess peptide remaining in the simulation box at equilibrium for RNA<sub>8</sub> or DNA<sub>8</sub> coacervates with R<sub>3</sub> or R<sub>4</sub>. Abbreviations: R = Arginine, DNA<sub>8</sub> = 8-deoxyribonucleotide-long mixed sequence ((ACTG)<sub>2</sub>), RNA<sub>8</sub> = 8-ribonucleotide-long mixed-sequence oligonucleotide ((ACUG)<sub>2</sub>).

## Nucleic acids quickly diffuse in primitive DNA coacervates

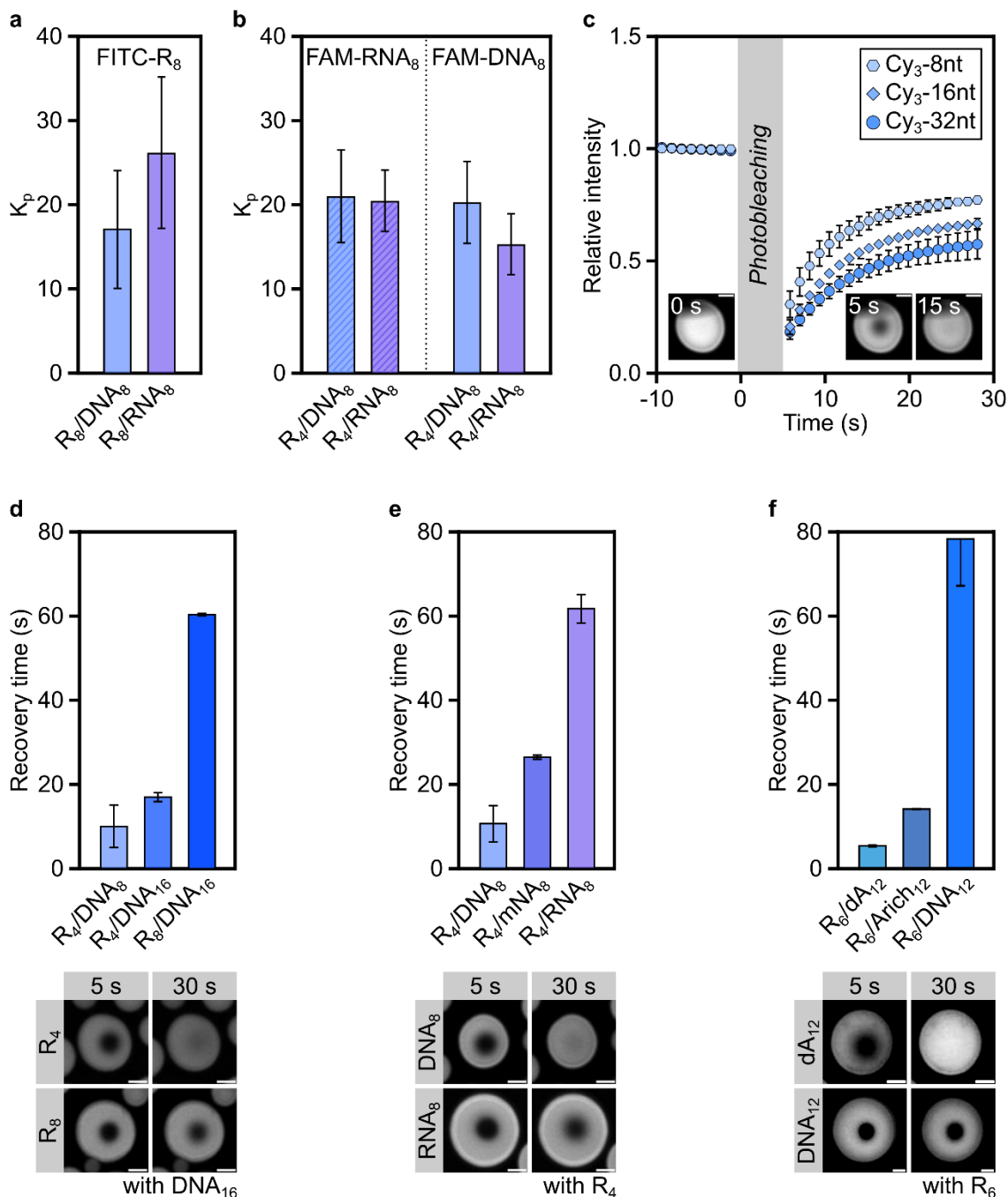
*Model* coacervates can increase the local concentration of dilute solutes, including oligonucleotides, and potentially facilitate replication reactions.<sup>18,57</sup> Whether the composition of *primitive* coacervates would influence their ability to recruit peptides and oligonucleotides is unknown. The partition coefficients for several fluorescently labelled probes (FITC-R<sub>8</sub>, FAM-DNA<sub>8</sub> and FAM-RNA<sub>8</sub>) was measured by confocal microscopy (Table S12). FITC-R<sub>8</sub> exhibited a 1.5 times higher partition coefficient in R<sub>8</sub>/RNA<sub>8</sub> than in R<sub>8</sub>/DNA<sub>8</sub> coacervates (Fig. 4a), likely due to the greater number of contacts between Arg peptides and RNA (Fig. 3b). FAM-DNA<sub>8</sub> and FAM-RNA<sub>8</sub> partitioned similarly in R<sub>4</sub>/DNA<sub>8</sub> coacervates, yet R<sub>4</sub>/RNA<sub>8</sub> coacervates recruited 1.3-fold more FAM-RNA<sub>8</sub> instead of FAM-DNA<sub>8</sub> (Fig. 4b). The difference in partition coefficients for RNA-based coacervates likely results from the higher energetic cost of recruiting a conformationally rigid and less interacting DNA probe into RNA coacervates.<sup>58</sup> Importantly, oligonucleotides that are too short to undergo phase separation are efficiently recruited in primitive coacervates (Fig. S31).

Diffusion rates within coacervates are also important for nucleic acid reactivity, e.g., ribozymatic functionality and non-enzymatic RNA polymerisation. Specifically, coacervates with long RNA strands (>50 nucleotides)<sup>17</sup> or Arg homopeptides<sup>18</sup> are known to be extremely viscous and inhibit ribozymatic activity. We thus characterised the fluidity of primitive coacervates by focusing on the diffusion of recruited oligonucleotides by means of Fluorescence Recovery After Photobleaching (FRAP).

Firstly, we explored the influence of probe size on its diffusion within minimal coacervates, by employing three model Cy3-labelled probes of different lengths (Fig. 4c). Empirical recovery times ( $\tau$ ) for all probes are 5–95 seconds, which indicates extraordinarily fluid primitive coacervates (Table S13) compared to previously studied coacervate models which display recovery times on the scale of several minutes.<sup>17</sup> As expected, the empirical recovery time is proportional to the length of the probe and that of the coacervate components, which is correlated to the viscosity of the coacervate (Figs. 4d, S32 and S33). Interestingly, peptide length has a stronger effect on coacervate fluidity than oligonucleotide length: the recovery time of a 8-nucleotide long probe in R<sub>4</sub>/DNA<sub>8</sub> coacervates is nearly half of that observed in R<sub>4</sub>/DNA<sub>16</sub> coacervates (10 s and 18 s, respectively), whereas the use of R<sub>8</sub> instead of R<sub>4</sub> for coacervation induces a 3-fold increase in the recovery time of the probe. These results align with those reported for coacervate stability and its stronger dependence on peptide, rather than oligonucleotide length (Fig. 1a and Table S3).

Secondly, we investigated the potential effect of coacervate composition on probe diffusion. The empirical recovery times in R<sub>4</sub>/DNA<sub>8</sub> and R<sub>4</sub>/RNA<sub>8</sub> coacervates confirm a relatively low viscosity for all systems. Yet, we found that the probe is strikingly more mobile in DNA-based than in RNA-based coacervates (empirical recovery times of 10 s and 62 s, respectively) (Figs. 4e and S34). These findings suggest that the stronger and more frequent interactions occurring between RNA and Arg-peptides (Fig. 3) lead to coacervates with higher viscosity and, thus, slower probe diffusion compared to their DNA-based analogues. Similarly, coacervates made up of adenosine-rich oligonucleotides that interact less (Table S9) result in faster recovery than those made of mixed-sequence oligonucleotides (Fig. 4f). Notably, the addition of salt or short non-coacervating DNA oligonucleotides to primitive coacervates results in lower empirical recovery times, and thus lower viscosity, by weakening the interactions between the coacervate components (Fig. S35 and Table S13).

Overall, our findings showcase the remarkable low viscosity of primitive coacervates compared to artificial systems proposed so far as models for primitive cells. The lower tendency of DNA to interact with peptides compared to RNA could have led to the emergence of coacervates with extraordinary fluidity and fast diffusion of partitioned peptides and nucleic acids, a seeming requirement<sup>17</sup> for prebiotic RNA activity. Notably, nucleic acid-based coacervates comprising both RNA and DNA would have exhibited remarkable fluidity, thanks to the ability of DNA to mitigate RNA-peptide interactions without impacting coacervate stability (Fig. 2d), hinting at an early synergy between RNA and DNA.



**Figure 4.** Composition of primitive peptide/NA coacervates modulates their biophysical properties. (a) Partitioning of a labelled peptide (1% FITC- $R_8$ ) in peptide/nucleic acid coacervates. (b) Partitioning of labelled oligonucleotides (1%

FAM-DNA<sub>8</sub> or 1% FAM-RNA<sub>8</sub>) in peptide/nucleic acid coacervates. (c) Example of FRAP profiles for the investigated peptide/nucleic acid coacervates. The fit of three probes in R<sub>4</sub>/DNA<sub>8</sub> coacervates is included for clarity. (d) Recovery time for probe Cy3-8nt in coacervates of varying peptide and DNA length: R<sub>4</sub>/DNA<sub>8</sub>, R<sub>4</sub>/DNA<sub>16</sub> and R<sub>6</sub>/DNA<sub>16</sub>. A 20 mM:5 mM [Arg]:[nucleotide] ratio was used for these experiments. (e) Recovery time of probe Cy3-8nt in coacervates comprising R<sub>4</sub> and DNA<sub>8</sub>, RNA<sub>8</sub> or a DNA<sub>8</sub>:RNA<sub>8</sub> (1:1 ratio) mixture (mNA<sub>8</sub>). A 20 mM:5 mM [Arg]:[nucleotide] ratio was used for these experiments. (f) Recovery time of probe Cy3-8nt in coacervates comprising R<sub>6</sub> and DNA<sub>12</sub>, dA<sub>12</sub> or an A-rich sequence, Arich<sub>12</sub>. A 20 mM:10 mM [Arg]:[nucleotide] ratio was used for these experiments. Scale bar: 2 μm. Abbreviations: R = Arginine, nt = nucleotide, DNA<sub>8</sub> = 8-deoxyribonucleotide-long mixed-sequence oligonucleotide ((ACTG)<sub>2</sub>), DNA<sub>16</sub> = 16-deoxyribonucleotide-long mixed-sequence oligonucleotide ((ACTG)<sub>4</sub>), RNA<sub>8</sub> = 8-ribonucleotide-long mixed-sequence oligonucleotide ((ACUG)<sub>2</sub>), τ = empirical recovery time.

### Primitive coacervates enable RNA polymerisation

The RNA-peptide world hypothesis posits an evolutionary period in which primitive lifeforms relied heavily on the catalytic properties and information carrying capabilities of RNA alongside peptides.<sup>59,60</sup> Non-enzymatic RNA replication is thought, however, to have played a pivotal role prior to the rise of an RNA replicase (or ribozymes with an analogous function) to effectively replicate the RNA genome.<sup>61</sup> We thus investigated whether primitive coacervates could have supported RNA folding and function, e.g., non-enzymatic RNA polymerisation.

As a preliminary assessment, we used a well-studied split version of the Broccoli aptamer<sup>43,62</sup> in solutions that contained R<sub>4</sub>/RNA<sub>8</sub>, R<sub>4</sub>/DNA<sub>8</sub> or R<sub>4</sub>/DNA<sub>16</sub> coacervates, and measured the fluorescence intensity of the bound fluorogenic probe, 3,5-difluoro-4-hydroxybenzylidene imidazolinone (DFHBI) (Figs. S36 and S37). The fluorescence of the light-up aptamer, and thereby its secondary structure, was fully preserved within R<sub>4</sub>/DNA<sub>8</sub> coacervates, but only partially maintained in R<sub>4</sub>/RNA<sub>8</sub> coacervates or in coacervates comprising sufficiently long DNAs such that non-homogeneous partitioning was observed (Figs. 5a and 5b). These findings indicate that coacervates made of short DNA oligonucleotides and Arg peptides — characterised by weaker and less abundant interactions, and hence remarkable fluidity, than their RNA-based counterparts (Fig. 3b) — enable more efficient nucleic acid folding.

Non-enzymatic genome copying is thought to be a crucial process in the emergence and evolution of early lifeforms, particularly in the rise of functional RNA sequences.<sup>61</sup> Although it was shown that coacervates comprising synthetic polycations, including polyallyldiammonium chloride, supported template-directed RNA elongation, highly viscous coacervates comprising polyarginines and RNA oligonucleotides (R<sub>10</sub>/rA<sub>11</sub>) inhibited RNA reactivity.<sup>18</sup> Yet, encouraged by the extraordinary fluidity of DNA-based coacervates, we investigated whether the efficiency of non-enzymatic RNA polymerisation would be preserved in the presence of primitive coacervates (Fig. 5c).

Primer extension reactions are useful model experiments that reflect the first step of non-enzymatic genome replication. Here, a fluorescently labelled primer hybridised to a complementary template (containing a GG overhang within the template strand) (Table S2) was added to a solution of DNA-based or RNA-based coacervates. Primer extension reactions were initiated upon addition of the activated dinucleotide<sup>63</sup> and MgCl<sub>2</sub> and assessed by gel electrophoresis (Figs. 5d and S38, and Tables S14 and S15). Control experiments performed in the presence of the *host* oligonucleotide (*i.e.*, involved in coacervation, but not engaged in primer extension), but without peptide, showed that the reaction is as efficient in the presence of bystander oligonucleotides as in their absence (Fig. S39), as long as no complementarity exists between host and primer/template oligonucleotides.

Due to the reactivity of nucleophilic amines towards the activated dimer (Fig. S40), we expected Arg peptides to compromise primer extension. In the presence of R<sub>6</sub>, 12-deoxyribonucleotide-long polyadenine strands (dA<sub>12</sub>) and NaCl (to prevent phase separation), the efficiency of primer extension was 1.5 times lower than without peptide after 24 hours (Figs. S41 and S42). These findings suggest that non-enzymatic RNA polymerisation may have been inefficient in crowded prebiotic settings in which reactive peptides were abundant. Consequently, we wondered whether, upon coacervation, peptides would have a less detrimental effect on non-enzymatic RNA polymerisation.

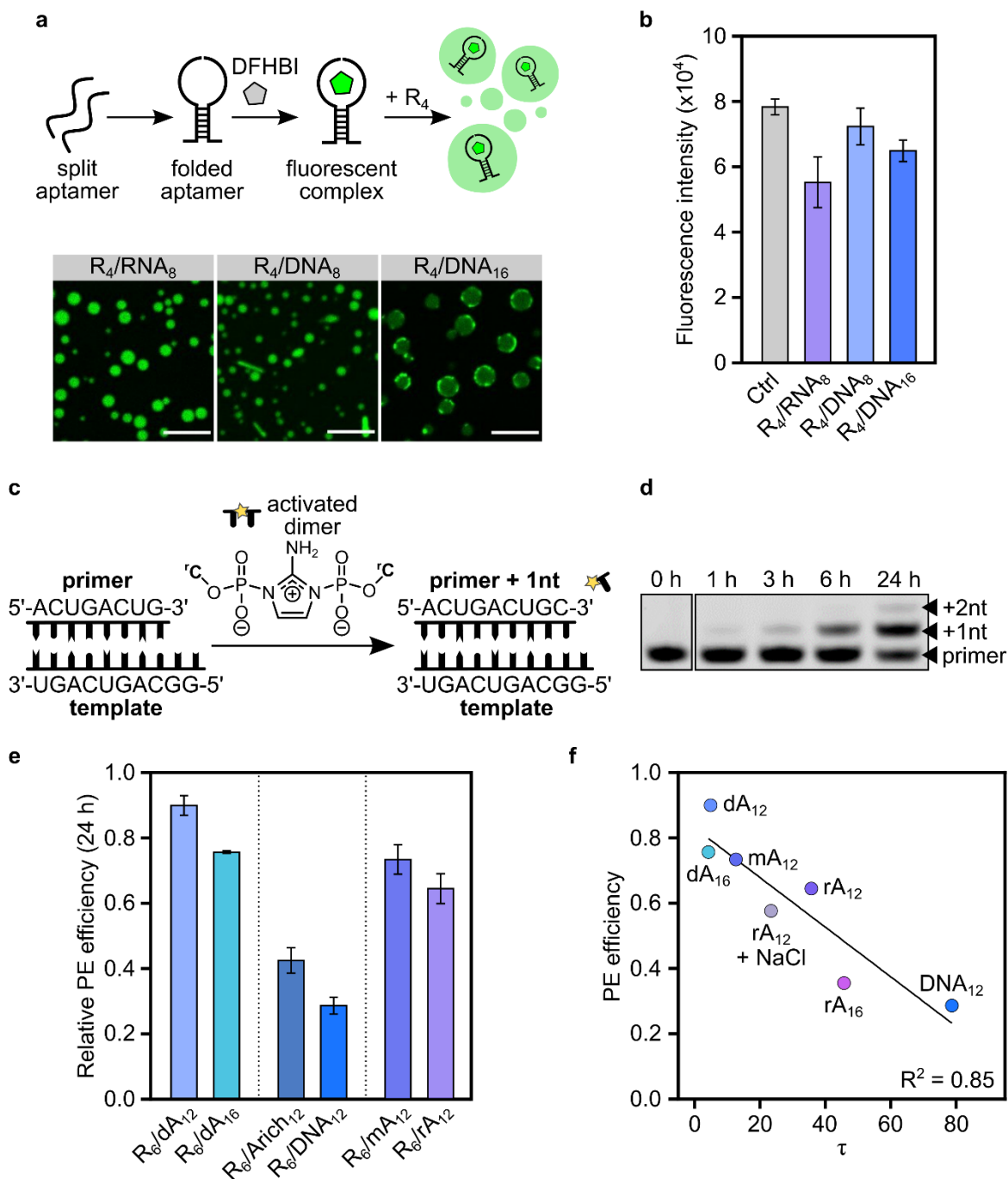
When primer extension was performed in the presence of R<sub>6</sub>/dA<sub>12</sub> coacervates, the reaction efficiency was mostly restored ( $\approx$ 90% extended primer after 24 hours) (Figs. 5d, 5e, S41 and S42). Similar yields of primer extension were obtained for a different primer-template system (Fig. S43) to support the generalisability of our findings. As expected, by changing the charge ratio between *coacervating* peptide and oligonucleotide, thus increasing the excess of free peptide in solution (without affecting the composition of the dense phase, Fig. S44), the reaction efficiency partially decreased (63% after 24 hours) (Fig. S45).

We next sought to understand the relationship between the viscosity of primitive coacervates and the functionality of their guest RNA strands (Fig. 5f). We thus explored the suitability of coacervates comprising host oligonucleotides of different composition, length and sequence, for non-enzymatic primer extension. When the reaction was performed in relatively viscous coacervates composed of longer polyadenine strands (dA<sub>16</sub> in lieu of dA<sub>12</sub>), primer extension was still observed (76% after 24 hours), albeit with lower efficiency (Figs. 5e and S46). Similarly, when RNA (rA<sub>12</sub>) was used for coacervation, 64% extended primer was detected (Figs. 5e and S46). Coacervates comprising mixed DNA and RNA oligonucleotides (mA<sub>12</sub>, *i.e.*, dA<sub>12</sub>:rA<sub>12</sub> 1:1 ratio) showed an intermediate efficiency of primer extension (73% after 24 hours) (Figs. 5e and S47). These results confirm that the viscosity of coacervates, which is a result of their composition (Figs. 4d-f), directly effects RNA chemistry (Fig. 5f).

Based on the propensity of each nucleotide to interact with Arg peptides (Table S9), we hypothesised that mixed-sequence oligonucleotide coacervates would exhibit diminished capability of supporting RNA polymerisation. As expected, we observed a high level of inhibition in R<sub>4</sub>/DNA<sub>12</sub> coacervates (36% after 24 hours) (Figs. S48). Increasing the adenine content in the host oligonucleotide sequence (Arich<sub>12</sub>), which lowered the viscosity of the resulting coacervates, resulted in higher primer extension yields (41% after 24 hours) (Figs. 5e and S49). Elongating the peptide (R<sub>6</sub> in place of R<sub>4</sub>) also increased the yield of primer extension (47% after 24 hours) (Figs. S48) despite the enhanced viscosity of the resulting coacervates (Table S13), which suggests that the stability of primitive coacervates also plays a role in enabling efficient RNA polymerisation. Interestingly, although RNA polymerisation is fully suppressed in coacervates with a host RNA sequence that is fully complementary to the guest RNA template, host DNA coacervates tolerate complementary guest RNA and a degree of primer extension (29% with complementary RNA template versus 47% for non-complementary RNA template) (Fig. S50). This finding may be due to the higher stability of RNA:RNA duplexes relative to DNA:RNA hybrids.<sup>64,65</sup>

Overall, although ribozyme activity and template-directed RNA polymerisation are inhibited in model polyarginine/RNA coacervates,<sup>17,18</sup> we show for the first time that primitive DNA-based coacervates can fully preserve RNA folding and efficiently support non-enzymatic RNA primer extension, namely due to their highly fluid nature. Notably, the remarkable differences in stability, fluidity and functionality between DNA and RNA coacervates are suggestive of a nucleic-acid-peptide world scenario in which all precursors of the

central dogma of biology could have played distinct, key biochemical roles with potential to support the emergence of life.



**Figure 5.** Primitive coacervates are compatible with prebiotic RNA chemistry and functionality. (a) Schematic representation and confocal micrographs of the split Broccoli aptamer reconstitution in primitive coacervates. Scale bar: 10  $\mu$ m (b) Total DFHBI emission in Broccoli aptamer samples after addition of R<sub>4</sub> (to trigger coacervation). In the 1-phase control, no oligonucleotide strand other than the split aptamer was present, and no peptide was added. (c) Schematic representation of the PE reaction. For all reactions involved in this study, 5 mM Mg<sup>2+</sup> was used as catalyst. (d) Representative denaturing polyacrylamide gel image of PE in R<sub>6</sub>/dA<sub>12</sub> coacervates at different time points. (e) Relative PE efficiency as a function of oligonucleotide composition or length. Error bars represent S.E.M from at least

two independent experiments. (f) Relationship between PE efficiency and empirical recovery time in R<sub>6</sub>-based coacervates (20 mM:10 mM [Arg]:[nt]). Abbreviations: R = Arginine, nt = nucleotide, PE = primer extension, dA<sub>12</sub> = 12-deoxyribonucleotide-long polyadenine oligonucleotide, dA<sub>16</sub> = 16-deoxyribonucleotide-long polyadenine oligonucleotide, rA<sub>12</sub> = 12-ribonucleotide-long polyadenine oligonucleotide, mA<sub>12</sub> = dA<sub>12</sub>:rA<sub>12</sub> 1:1 ratio, Arich<sub>12</sub> = 12-deoxyribonucleotide-long A-rich-sequence oligonucleotide (AAGTAAAGTAAA), DNA<sub>12</sub> = 12-deoxyribonucleotide-long mixed-sequence oligonucleotide ((ACTG)<sub>3</sub>).

## Conclusions

Complex coacervates, formed upon liquid-liquid phase separation of oppositely charged polymers, have long been suggested as models of primitive cells. Yet, the low prebiotic plausibility of the coacervating components studied, commonly designed to maximise coacervate stability or functionality, led to the notion that the emergence of coacervates succeeded the synthesis of long, sequence-specific, functional polymers (*i.e.*, homopeptides and ribozymes). Our work challenges this assumption by demonstrating that short, mixed-sequence peptides and oligonucleotides spontaneously undergo phase separation to generate primitive coacervates, which likely impacted prebiotic RNA chemistry.

The prebiotic plausibility of short peptides, RNA and DNA oligomers, and their intertwined role in the central dogma of biology, suggest their cooperation, likely due to co-localisation, early on the evolutionary timeline. Our work shows that primitive coacervates can be generated by liquid-liquid phase separation of short, heterogeneous peptides and oligonucleotides (*i.e.*, peptide dimers and trimers, RNA and DNA octamers). These findings suggest that compartmentalisation *via* coacervation could have occurred simultaneously to the early stages of non-coded amino acid and nucleotide polymerisation. In contrast with peptide-peptide coacervates, these minimal nucleic acid-peptide coacervates showcase enhanced stability to high concentration mismatch of their components and elevated salinity, thus loosening the chemical constraints on the prebiotic environments that could have accommodated coacervation.

The seemingly inevitable tendency of short heterogeneous peptides and oligonucleotides to undergo phase separation suggests that coacervates were unlikely selected as a fitness advantage at a late evolutionary stage, but rather were a consequence of prebiotic molecular composition in an early nucleic acid-peptide world.

Primitive coacervates can be effectively described by all-atom simulations of peptide/nucleic acid condensation. Mixtures comprising RNA oligonucleotides are characterised by a higher number of contacts between arginine residues and nucleotides compared to DNA-based counterparts, likely due to the more extended and less structured conformation acquired by RNA over DNA upon phase separation. Although both nucleic acid/peptide coacervates exhibit enhanced stability and fluidity over previously reported models, we show for the first time that the chemical diversity of RNA and DNA is mirrored in the diverse properties (stability, fluidity and functionality) of the resulting coacervates.

Our work offers a set of guiding molecular principles to generate models of biomolecular condensates. Fine-tuning the fluidity of coacervates by modulating the DNA-to-RNA ratio enabled us to explore RNA chemistries (e.g., ribozymatic activity) that were, until now, considered incompatible with primitive coacervates. More broadly, this study highlights how small molecular differences in oligonucleotide or peptide composition or length can have remarkable macromolecular effects on the material properties of the resulting coacervates. The possibilities to explore the effect of other molecular alterations, including



employing non-canonical nucleotides or amino acids, or building blocks with opposite chirality, on coacervate functionality are arguably unlimited.

Non-enzymatic RNA copying would have been important prior to the rise of a ribozyme capable of replication. Testing its compatibility with primitive coacervates was thus critical. We found that coacervate stability, charge and, most importantly, fluidity are key factors that control the chemical copying of RNA, with a high degree of predictability. The novel observation that DNA-based coacervates more efficiently preserve RNA secondary structures and support non-enzymatic RNA polymerisation suggests that, before the “genetic takeover” of RNA, DNA oligonucleotides might have played a key role in compartmentalisation by enabling the emergence of coacervates compatible with primitive RNA activity. All in all, the seemingly inevitability of coacervation invites us to revisit prebiotic chemistry for its compatibility and efficacy in phase-separated environments; and the unique ability of primitive DNA-containing coacervates to efficiently preserve RNA folding and support RNA functionality offers a new trajectory for the early evolution of primitive cells with sequence-dependent phenotypes.

## Acknowledgements

We thank Jean-Daniel Fauny and Romain Vauchelles (IBMC, Unistra) for access to the confocal microscopy facility, Valentin Bauer (ISIS, Unistra) for support with SPPS and peptide purification, and Tiemei Lu for input on the initial experimental setup. We thank Prof. Pietro Cicuta and Dr Jurij Kotar (Cavendish Laboratory) for support to obtain a dataset on the temperature stability of minimal coacervates. We also thank Dr David A. Russell (University of Cambridge) for insightful comments on the manuscript and relevant literature provided. We further thank Dr Vikki Cantrill for her support in editing this manuscript.

The authors acknowledge funding from the NWO (Dutch Research Council) via a Rubicon Fellowship (019.222EN.011 to K.K.N.), the Human Frontier Science Program Organization (HFSP) via an Early Career Research Grant (RGY00062/2022, <https://doi.org/10.52044/HFSP.RGY00622022.pc.gr.153594>, to C.B. and D.K.O.), the ERC (Starting Grant) under the European Union’s Horizon Europe research and innovation programme (GA 101162933 to C.B.), the Federation of European Biochemical Society via a FEBS Excellence Award (to C.B.), the Agence Nationale de la Recherche via an ANR AAPG JCJC 2022 (to C.B.), the CSC Graduate School funded by the Agence Nationale de la Recherche (CSC-IGS ANR-17-EURE-0016 for doctoral funding to F.R.), the University of Strasbourg Institute for Advanced Study (USIAS) via a USIAS Fellowship (to C.B.), the Foundation Jean-Marie Lehn, the Biotechnology and Biological Sciences Research Council via a BBSRC Discovery Fellowship (BB/X010228/1 to R.R.S.), the UKRI EPSRC under the UK Government’s guarantee scheme (EP/Z002028/1 to R.C.G.), following funding by the ERC (Consolidator Grant) under the European Union’s Horizon Europe research and innovation programme, the Winton Programme for Physics of Sustainability (for doctoral funding to M.J.M.), the NSERC via a NSERC Discovery Grant (RGPIN 2020-05043 to D.K.O.) and a NSERC Alliance Catalyst Grant (ALLRP 57555822 to D.K.O.). This project made use of time on HPC granted via the UK High-End Computing Consortium for Biomolecular Simulation, HECBioSim (<http://hecbiosim.ac.uk>), supported by EPSRC (EP/R029407/1 to R.C.G.).

## References

1. Müller, F. *et al.* A prebiotically plausible scenario of an RNA–peptide world. *Nature* **605**, 279–284 (2022).

2. Su, M., Roberts, S. J. & Sutherland, J. D. RNA-directed peptide synthesis across a nicked loop. *Nucleic Acids Research* 11415–11422 (2024).
3. Patel, B. H., Percivalle, C., Ritson, D. J., Duffy, C. D. & Sutherland, J. D. Common origins of RNA, protein and lipid precursors in a cyanosulfidic protometabolism. *Nature Chem* **7**, 301–307 (2015).
4. Becker, S. *et al.* Unified prebiotically plausible synthesis of pyrimidine and purine RNA ribonucleotides. *Science* **366**, 76 LP – 82 (2019).
5. Teichert, J. S., Kruse, F. M. & Trapp, O. Direct Prebiotic Pathway to DNA Nucleosides. *Angewandte Chemie International Edition* **58**, 9944–9947 (2019).
6. Canavelli, P., Islam, S. & Powner, M. W. Peptide ligation by chemoselective aminonitrile coupling in water. *Nature* **571**, 546–549 (2019).
7. Gibard, C., Bhowmik, S., Karki, M., Kim, E.-K. & Krishnamurthy, R. Phosphorylation, oligomerization and self-assembly in water under potential prebiotic conditions. *Nature Chemistry* **10**, 212–217 (2018).
8. Forsythe, J. G. *et al.* Ester-Mediated Amide Bond Formation Driven by Wet-Dry Cycles: A Possible Path to Polypeptides on the Prebiotic Earth. *Angewandte Chemie - International Edition* **54**, 9871–9875 (2015).
9. Leu, K., Obermayer, B., Rajamani, S., Gerland, U. & Chen, I. A. The prebiotic evolutionary advantage of transferring genetic information from RNA to DNA. *Nucleic Acids Res* **39**, 8135–8147 (2011).
10. O’Flaherty, D. K., Zhou, L. & Szostak, J. W. Nonenzymatic Template-Directed Synthesis of Mixed-Sequence 3’-NP-DNA up to 25 Nucleotides Long Inside Model Protocells. *J. Am. Chem. Soc.* **141**, 10481–10488 (2019).
11. Jash, B., Tremmel, P., Jovanovic, D. & Richert, C. Single nucleotide translation without ribosomes. *Nat. Chem.* **13**, 751–757 (2021).
12. Tagami, S., Attwater, J. & Holliger, P. Simple peptides derived from the ribosomal core potentiate RNA polymerase ribozyme function. *Nature Chem* **9**, 325–332 (2017).
13. Ghosh, B., Bose, R. & Tang, T.-Y. D. Can coacervation unify disparate hypotheses in the origin of cellular life? *Current Opinion in Colloid & Interface Science* **52**, 101415 (2021).
14. Abbas, M., Lipiński, W. P., Wang, J. & Spruijt, E. Peptide-based coacervates as biomimetic protocells. *Chem. Soc. Rev.* **50**, 3690–3705 (2021).
15. Banani, S. F., Lee, H. O., Hyman, A. A. & Rosen, M. K. Biomolecular condensates: organizers of cellular biochemistry. *Nat Rev Mol Cell Biol* **18**, 285–298 (2017).
16. Drobot, B. *et al.* Compartmentalised RNA catalysis in membrane-free coacervate protocells. *Nat Commun* **9**, 3643 (2018).
17. Iglesias-Artola, J. M. *et al.* Charge-density reduction promotes ribozyme activity in RNA–peptide coacervates via RNA fluidization and magnesium partitioning. *Nat. Chem.* **14**, 407–416 (2022).
18. Poudyal, R. R. *et al.* Template-directed RNA polymerization and enhanced ribozyme catalysis inside membraneless compartments formed by coacervates. *Nat Commun* **10**, 490 (2019).

19. Cakmak, F. P., Choi, S., Meyer, M. O., Bevilacqua, P. C. & Keating, C. D. Prebiotically-relevant low polyion multivalency can improve functionality of membraneless compartments. *Nat Commun* **11**, 5949 (2020).
20. Nakashima, K. K., Van Haren, M. H. I., André, A. A. M., Robu, I. & Spruijt, E. Active coacervate droplets are protocells that grow and resist Ostwald ripening. *Nat Commun* **12**, 3819 (2021).
21. Fraccia, T. P. & Martin, N. Non-enzymatic oligonucleotide ligation in coacervate protocells sustains compartment-content coupling. *Nat Commun* **14**, 2606 (2023).
22. Dai, S. *et al.* An inorganic mineral-based protocell with prebiotic radiation fitness. *Nat Commun* **14**, 7699 (2023).
23. Blocher McTigue, W. C. & Perry, S. L. Protein Encapsulation Using Complex Coacervates: What Nature Has to Teach Us. *Small* **16**, 1907671 (2020).
24. Fox, S. W. & Nakashima, T. The assembly and properties of protobiological structures: The beginnings of cellular peptide synthesis. *Biosystems* **12**, 155–166 (1980).
25. Verlander, M. S. & Orgel, L. E. Analysis of high molecular weight material from the polymerization of adenosine cyclic 2', 3'-phosphate. *J Mol Evol* **3**, 115–120 (1974).
26. Krainer, G. *et al.* Reentrant Liquid Condensate Phase of Proteins is Stabilized by Hydrophobic and Non-Ionic interactions. *Biophysical Journal* **120**, 28a (2021).
27. Bremer, A. *et al.* Deciphering how naturally occurring sequence features impact the phase behaviours of disordered prion-like domains. *Nat. Chem.* **14**, 196–207 (2022).
28. Joseph, J. A. *et al.* Physics-driven coarse-grained model for biomolecular phase separation with near-quantitative accuracy. *Nat Comput Sci* **1**, 732–743 (2021).
29. Jones, S. Protein-RNA interactions: a structural analysis. *Nucleic Acids Research* **29**, 943–954 (2001).
30. Fisher, R. S. & Elbaum-Garfinkle, S. Tunable multiphase dynamics of arginine and lysine liquid condensates. *Nat Commun* **11**, 4628 (2020).
31. Kumar, K. *et al.* Cation- $\pi$  interactions in protein-ligand binding: theory and data-mining reveal different roles for lysine and arginine. *Chem. Sci.* **9**, 2655–2665 (2018).
32. Lu, T., Nakashima, K. K. & Spruijt, E. Temperature-Responsive Peptide-Nucleotide Coacervates. *J. Phys. Chem. B* **125**, 3080–3091 (2021).
33. Verlander, M. S., Lohrmann, R. & Orgel, L. E. Catalysts for the self-polymerization of adenosine cyclic 2',3'-phosphate. *J Mol Evol* **2**, 303–316 (1973).
34. Le Vay, K. K., Salibi, E., Ghosh, B., Tang, T. D. & Mutschler, H. Ribozyme activity modulates the physical properties of RNA-peptide coacervates. *eLife* **12**, e83543 (2023).
35. Samanta, A., Sabatino, V., Ward, T. R. & Walther, A. Functional and morphological adaptation in DNA protocells via signal processing prompted by artificial metalloenzymes. *Nat. Nanotechnol.* **15**, 914–921 (2020).

36. Codispoti, S. *et al.* The interplay between peptides and RNA is critical for protoribosome compartmentalization and stability. *Nucleic Acids Research* gkae823 (2024) doi:10.1093/nar/gkae823.
37. Xu, J. *et al.* Selective prebiotic formation of RNA pyrimidine and DNA purine nucleosides. *Nature* **582**, 60–66 (2020).
38. Xu, J., Green, N. J., Russell, D. A., Liu, Z. & Sutherland, J. D. Prebiotic Photochemical Coproduction of Purine Ribo- and Deoxyribonucleosides. *J. Am. Chem. Soc.* **143**, 14482–14486 (2021).
39. Kim, S. C., O’Flaherty, D. K., Giurgiu, C., Zhou, L. & Szostak, J. W. The Emergence of RNA from the Heterogeneous Products of Prebiotic Nucleotide Synthesis. *J. Am. Chem. Soc.* **143**, 3267–3279 (2021).
40. Nakata, M. *et al.* End-to-End Stacking and Liquid Crystal Condensation of 6– to 20–Base Pair DNA Duplexes. *Science* **318**, 1276–1279 (2007).
41. Dirscherl, C. F. *et al.* A heated rock crack captures and polymerizes primordial DNA and RNA. *Phys. Chem. Chem. Phys.* **25**, 3375–3386 (2023).
42. Fraccia, T. P. *et al.* Abiotic ligation of DNA oligomers templated by their liquid crystal ordering. *Nat Commun* **6**, 6424 (2015).
43. Rubio-Sánchez, R. *et al.* Thermally Driven Membrane Phase Transitions Enable Content Reshuffling in Primitive Cells. *J. Am. Chem. Soc.* **143**, 16589–16598 (2021).
44. Smokers, I. B. A., Van Haren, M. H. I., Lu, T. & Spruijt, E. Complex Coacervation and Compartmentalized Conversion of Prebiotically Relevant Metabolites. *ChemSystemsChem* **4**, e202200004 (2022).
45. Bhowmik, S. & Krishnamurthy, R. The role of sugar-backbone heterogeneity and chimeras in the simultaneous emergence of RNA and DNA. *Nat. Chem.* **11**, 1009–1018 (2019).
46. Aumiller, W. M., Pir Cakmak, F., Davis, B. W. & Keating, C. D. RNA-Based Coacervates as a Model for Membraneless Organelles: Formation, Properties, and Interfacial Liposome Assembly. *Langmuir* **32**, 10042–10053 (2016).
47. Costanzo, G. *et al.* Non-Enzymatic Oligomerization of 3’, 5’ Cyclic AMP. *PLoS ONE* **11**, e0165723 (2016).
48. Paloni, M., Bussi, G. & Barducci, A. Arginine multivalency stabilizes protein/RNA condensates. *Protein Science* **30**, 1418–1426 (2021).
49. Renger, R. *et al.* Co-condensation of proteins with single- and double-stranded DNA. *Proceedings of the National Academy of Sciences* **119**, e2107871119 (2022).
50. Alberts, B. *et al.* *Molecular Biology of the Cell*. (Garland Science, 2002).
51. Joyce, G. F. & Szostak, J. W. Protocells and RNA Self-Replication. *Cold Spring Harb Perspect Biol* **10**, a034801 (2018).
52. Gallivan, J. P. & Dougherty, D. A. A Computational Study of Cation– $\pi$  Interactions vs Salt Bridges in Aqueous Media: Implications for Protein Engineering. *J. Am. Chem. Soc.* **122**, 870–874 (2000).

53. Garaizar, A., Sanchez-Burgos, I., Collepardo-Guevara, R. & Espinosa, J. R. Expansion of Intrinsically Disordered Proteins Increases the Range of Stability of Liquid–Liquid Phase Separation. *Molecules* **25**, 4705 (2020).
54. Wilson, K. A., Kung, R. W., D'souza, S. & Wetmore, S. D. Anatomy of noncovalent interactions between the nucleobases or ribose and  $\pi$ -containing amino acids in RNA–protein complexes. *Nucleic Acids Research* **49**, 2213–2225 (2021).
55. Brown, R. F., Andrews, C. T. & Elcock, A. H. Stacking Free Energies of All DNA and RNA Nucleoside Pairs and Dinucleoside-Monophosphates Computed Using Recently Revised AMBER Parameters and Compared with Experiment. *J. Chem. Theory Comput.* **11**, 2315–2328 (2015).
56. Oweida, T. J., Kim, H. S., Donald, J. M., Singh, A. & Yingling, Y. G. Assessment of AMBER Force Fields for Simulations of ssDNA. *J. Chem. Theory Comput.* **17**, 1208–1217 (2021).
57. Choi, S., Meyer, M. O., Bevilacqua, P. C. & Keating, C. D. Phase-specific RNA accumulation and duplex thermodynamics in multiphase coacervate models for membraneless organelles. *Nat. Chem.* **14**, 1110–1117 (2022).
58. Nakashima, K. K., Vibhute, M. A. & Spruijt, E. Biomolecular Chemistry in Liquid Phase Separated Compartments. *Front. Mol. Biosci.* **6**, (2019).
59. Crick, F. H. C. The origin of the genetic code. *Journal of Molecular Biology* **38**, 367–379 (1968).
60. Orgel, L. E. Evolution of the genetic apparatus. *Journal of Molecular Biology* **38**, 381–393 (1968).
61. Szostak, J. W. The eightfold path to non-enzymatic RNA replication. *Journal of Systems Chemistry* **3**, 1–14 (2012).
62. Alam, K. K., Tawiah, K. D., Lichte, M. F., Porciani, D. & Burke, D. H. A Fluorescent Split Aptamer for Visualizing RNA–RNA Assembly In Vivo. *ACS Synth. Biol.* **6**, 1710–1721 (2017).
63. Walton, T. & Szostak, J. W. A Highly Reactive Imidazolium-Bridged Dinucleotide Intermediate in Nonenzymatic RNA Primer Extension. *J. Am. Chem. Soc.* **138**, 11996–12002 (2016).
64. Sugimoto, N. *et al.* Thermodynamic Parameters To Predict Stability of RNA/DNA Hybrid Duplexes. *Biochemistry* **34**, 11211–11216 (1995).
65. Freier, S. M. *et al.* Improved free-energy parameters for predictions of RNA duplex stability. *Proceedings of the National Academy of Sciences* **83**, 9373–9377 (1986).

# Compositional and functional diversity of primitive minimal coacervates in a nucleic acid-peptide world

Karina K. Nakashima,<sup>1,2,†</sup> Fatma Zohra Mihoubi,<sup>1,2,†</sup> Jagandeep S. Saraya,<sup>3</sup> Kieran O. Russell,<sup>4</sup> Fidan Rahmatova,<sup>1,2</sup> James D. Robinson,<sup>3</sup> Maria Julia Maristany,<sup>4,5</sup> Jan Huertas,<sup>4,6</sup> Roger Rubio-Sánchez,<sup>7</sup> Rosana Collepardo-Guevara,<sup>4,5,6\*</sup> Derek K. O’Flaherty,<sup>3\*</sup> and Claudia Bonfio<sup>1,2,\*</sup>

<sup>1</sup>Department of Biochemistry, University of Cambridge, CB2 1GA Cambridge, UK

<sup>2</sup>Institut de Science et d’Ingénierie Supramoléculaires, CNRS UMR 7006, University of Strasbourg, 67000 Strasbourg, France

<sup>3</sup>Department of Chemistry, University of Guelph, ON N1G 2W1, Guelph, Canada

<sup>4</sup>Yusuf Hamied Department of Chemistry, University of Cambridge, CB2 1EW Cambridge, UK

<sup>5</sup>Cavendish Laboratory, Department of Physics, University of Cambridge, CB3 0HE, Cambridge, UK

<sup>6</sup>Department of Genetics, University of Cambridge, CB2 3EH, Cambridge, UK

<sup>7</sup>Department of Chemical Engineering and Biotechnology, University of Cambridge, CB3 0AS Cambridge, UK

<sup>†</sup>These authors contributed equally

\* corresponding authors: [rc597@cam.ac.uk](mailto:rc597@cam.ac.uk), [doflaher@uoguelph.ca](mailto:doflaher@uoguelph.ca), [cb2036@cam.ac.uk](mailto:cb2036@cam.ac.uk)

## Supplementary Information

### Contents

Materials and Methods .....	2
Sample Preparation .....	3
Experimental Methods .....	3
Computational Methods .....	7
Supplementary Tables .....	10
Supplementary Figures .....	36
References .....	86

## Materials and Methods

Reagents were purchased from Merck and Thermo Fisher and used without further purification unless otherwise stated. Polyuridylic acid (polyU) potassium salt (MW 600–1000 kDa, ~2000–3200 bases) was purchased from Merck. *N*-benzoyl-dA, *N*-isobutyryl-dG, *N*-acetyl-dC and dT phosphoramidites, and 2'-*O*-TBDMS protected, *N*-benzoyl-rA, *N*-isobutyryl-rG, *N*-acetyl-rC and rU phosphoramidites, and 6-FAM amidite (CLP-9777) were purchased from ChemGenes (Wilmington, MA). Oligonucleotides were purchased from Integrated DNA Technologies (IDT) and Eurofins or synthesised in-house when indicated. Peptides were purchased as TFA salts from GenScript or synthesised in-house when indicated. Sep-Pak C18 classic cartridge was purchased from Waters (Milford, MA). Water coming into contact with DNA/RNA oligomers was 18 M $\Omega$  grade.

Fmoc solid phase peptide synthesis (Fmoc-SPPS) was carried out on an induction heating-assisted PurePrep<sup>®</sup> Chorus synthesiser (Gyros Protein Technologies) pressurised with 4.5 N<sub>2</sub> and equipped with two independent reaction vessel slots with both induction heating and a UV-monitoring detector. Reverse-phase high-performance liquid chromatography (RP-HPLC) purifications on peptides were performed using an Agilent semi-preparative HPLC system equipped with a 1260 Infinity II binary pump, 1260 Infinity II variable wavelength detector with 3 mm preparative cell, and a 1290 Infinity II preparative open-bed sampler/collector with a 20 mL injection loop on a ReproSil Pur 120 C18-AQ 250 x 25 mm 5  $\mu$ m particle size column from DrMaisch GmbH. Purification of oligonucleotides was performed using a DNAPac<sup>™</sup> PA200 column with a Vanquish<sup>™</sup> analytical purification high-performance liquid chromatography (HPLC) system. DNA and RNA melting temperatures and base pairing probabilities were assessed using NUPACK 4.0 (<https://www.nupack.org/>). pH monitoring was performed using a Mettler Toledo FiveEasy pH meter and adjustments were made with aqueous solutions of NaOH or HCl as appropriate. The turbidity of mixtures was determined using a BMG Labtech CLARIOstar<sup>plus</sup>. Concentrations were calculated using the Beer-Lambert equation (molar extinction coefficients were estimated using the OligoAnalyzer<sup>™</sup> Tool (IDT)).

Coacervates were imaged using a Nikon Eclipse TS2 inverted epifluorescence microscope equipped with a Moment A21K635003 camera (0.63 $\times$  adaptor) and a 60 $\times$  oil immersion objective. Alternatively, coacervates were imaged using a Zeiss Axio Observer Z1 spinning disk confocal microscope equipped with a Yokogawa CSU confocal head and a 63 $\times$  oil immersion objective. Images were processed using Fiji (<http://rsb.info.nih.gov/ij/>). Thermal studies were performed using a home-built Nikon Eclipse Ti-E inverted microscope equipped with a 20 $\times$  objective lens (Nikon, Plan Fluor, N.A. 0.75) and a Grasshopper3 GS3-U3-23S6M camera (Point Gray Research). The illumination was provided by single-colour light-emitting diodes (LEDs) using a filter set for Texas Red. Temperature ramps were performed using a custom-built script, enabling precise manipulation of the instrument in terms of time, temperature, and illumination as required. FRAP experiments were performed using a Leica TCS SP5 laser scanning confocal microscope (Cavendish Laboratory, Cambridge) equipped with an HCX PL Apo 40 $\times$  DRY (NA 0.85) objective lens and a HeNe laser (633 nm, 10 mW). DNA and RNA oligonucleotides (ONs) were synthesised using an ABI-394 DNA synthesiser. UV measurements on oligonucleotides were taken at 260 nm using an Agilent BioTek Epoch Microplate Spectrophotometer, reading each sample at least 3 times and correcting each value by a blank measurement. Polyacrylamide gels were imaged on an Amersham TYPHOON using the Cy2 laser at 25-50  $\mu$ m pixel size.

Average and standard deviation values refer to  $n \geq 3$  replicates. Statistical significance was determined using unpaired t-tests (ns  $P > 0.05$ ; \*  $P \leq 0.1$ ; \*\*  $P \leq 0.01$ ; \*\*\*  $P \leq 0.001$ ; \*\*\*\*  $P \leq 0.0001$ ).

## Sample Preparation

**Stock solutions.** Peptide stocks were prepared in MilliQ water at a concentration of 100 mM based on the molecular weight of the TFA salt. The pH of E<sub>10</sub> (glutamic acid decamer) was adjusted with ammonia for complete dissolution. Solutions were sonicated, stored at -20°C, and vortexed for 1 minute before use. Single-strand DNA and RNA oligonucleotide stocks were prepared in DNase/RNase-free water at a strand concentration of approximately 1 mM. To facilitate the solubilisation of the oligonucleotides, solutions were heated to 50°C for 5 minutes and cooled down to room temperature before the measurement. The concentration was checked on a diluted solution (250-500×), measuring the absorbance at 260 nm.

**Coacervate preparation.** Coacervates were prepared in a 10-100 µL scale by adding, respectively, MilliQ water, HEPES buffer (from a 500 mM stock buffer solution, pH 7.4), DNA or RNA (~1 mM oligonucleotide stock) and peptide (100 mM stock). Aptamer and fluorescent probes were added at last unless otherwise stated. Mixing was done by gently tapping the microtube to avoid reducing droplet size for imaging. Mixtures were assessed by light microscopy to confirm the presence of liquid droplets. Note: in FRAP and aptamer experiments, the peptide was added at last to enable the fast incorporation of fluorescent dyes.

**Preparation of observation chambers.** A passivated glass coverslip #1.5 was used as the observation surface in all experiments. Glass passivation was performed to prevent wetting. A 5 wt% solution of partially hydrolysed polyvinyl alcohol (PVA, 13-23k) was spread on top of clean coverslips and let adsorb for 1 hour inside a covered petri dish. The coverslips were rinsed thoroughly with distilled water and once with MilliQ before being dried with compressed air. For long imaging experiments (FRAP, K<sub>p</sub> measurements, thermal ramps), 2-6 µL chambers were prepared using double-sided 3M tape (GPT-020F, 0.2 mm) and a hole-punch (2-4 mm Ø) and sealed using 10 mm Ø coverslips to prevent evaporation.

## Experimental Methods

**Fmoc solid-phase peptide synthesis (Fmoc-SPPS).** R<sub>4</sub>, R<sub>2</sub>, RER, RG, GR, RE, R<sub>2</sub>E<sub>2</sub>R<sub>2</sub>, (D-R-L-R)<sub>2</sub> and (D-R-L-R)<sub>4</sub> were synthesised according to previously published SPPS procedures by using Fmoc-protected amino acids.<sup>1</sup> 0.50 mmol of commercially available, pre-loaded Wang resin was added to a plastic reactor equipped with a fritted plastic insert. The resin was allowed to swell in DMF for 30 minutes. For the deprotection step, 20% piperidine in DMF (5 mL/0.5 mmol) was added to the resin. The resin was left to react for 2 minutes before the removal of the solvent. The treatment was repeated with 20% piperidine in DMF and left shaking for 15 minutes. The solvent was removed, and the resin was washed with DCM/DMF (5 x 5 mL). For the coupling step, Fmoc-protected amino acids (Fmoc-AA-OH) (3.0 equiv. relative to the resin loading) were dissolved in dry DMF. A solution of 2-(1H-benzotriazol-1-yl)-1,1,3,3-tetramethyluronium hexafluorophosphate (HBTU, 3.8 equiv.) was added to the Fmoc-AA-OH solution, followed by *N,N*-Diisopropylethylamine (DIPEA, 6.0 equiv.), and added to the resin. The resulting mixture was agitated on a laboratory shaker for 45 minutes. DMF washes of the resin (5 x 5.0 mL) were performed before deprotection. Cycles of coupling and deprotection steps were performed to obtain the desired peptide sequence. After the final Fmoc removal, the resin was washed with DMF (3x), DCM (3x), and MeOH (3x) and left to dry under a high vacuum overnight.



For cleavage, the resin was treated with the cleavage solution (trifluoroacetic acid (TFA):H<sub>2</sub>O:triisopropyl silane 95:2.5:2.5 volume ratio) for 2 hours. TFA-peptide solutions were collected, and the resin was washed with TFA (2x3 mL). The collected fractions were concentrated under nitrogen flow and added to cold diethyl ether, leading to the precipitation of the peptide. The precipitate was centrifuged for 5 minutes at 3000 rpm and washed with cold diethyl ether (10 mL). The resulting peptide was dissolved in acetonitrile:water 1:5 (10 mL) and lyophilised. Peptides were purified by RP-HPLC. Elution was performed at a flow rate of 10 mL/min using a linear gradient of acetonitrile and ultrapure water (both containing 0.1% LCMS grade formic acid). The gradient ranged from 20% to 80% acetonitrile over 1 hour. UV absorption at 220 nm and 254 nm was used to monitor the collection of unprotected peptides. Fractions containing the target product were identified by mass spectrometry and lyophilised.

**R<sub>2</sub>E<sub>2</sub>R<sub>2</sub>**: <sup>1</sup>H-NMR (500 MHz, D<sub>2</sub>O) δ (ppm) 4.29–4.15 (m, 4H), 3.97 (t, J = 6.4 Hz, 1H), 3.25–2.89 (m, 8H), 2.47–2.18 (m, 4H), 2.02–1.30 (m, 20H).

**(D-R-L-R)<sub>2</sub>**: <sup>1</sup>H-NMR (500 MHz, D<sub>2</sub>O) δ (ppm) 4.30–3.20 (m, 2H), 4.05–3.95 (m, 1H), 3.50–3.02 (m, 9H), 1.97–1.28 (m, 16H).

**(D-R-L-R)<sub>4</sub>**: <sup>1</sup>H-NMR (500 MHz, D<sub>2</sub>O) δ (ppm) 4.44–3.94 (m, 7H), 3.33–2.86 (m, 16H), 2.05–1.28 (m, 32H).

**R<sub>4</sub>**: <sup>1</sup>H-NMR (500 MHz, D<sub>2</sub>O) δ (ppm) 3.95–3.86 (m, 3H), 3.19–3.10 (m, 8H), 1.95–1.79 (m, 8H), 1.73–1.51 (m, 8H).

**RRR**: <sup>1</sup>H-NMR (500 MHz, D<sub>2</sub>O) δ (ppm) 4.34–4.28 (m, 1H), 4.28–4.22 (m, 1H), 3.97 (t, J = 6.4 Hz, 1H), 2.42 (t, J = 7.4 Hz, 2H), 2.08–1.64 (m, 6H), 1.63–1.44 (m, 4H).

**R<sub>2</sub>**: <sup>1</sup>H-NMR (500 MHz, D<sub>2</sub>O) δ (ppm) 4.44–4.35 (m, 1H), 4.09 (t, J = 6.4 Hz, 1H), 3.25 (t, J = 6.8 Hz, 2H), 2.58–2.44 (m, 2H), 2.28–1.61 (m, 6H).

**RG**: <sup>1</sup>H-NMR (500 MHz, D<sub>2</sub>O) δ (ppm) 4.14–3.98 (m, 3H), 3.25 (t, J = 6.8 Hz, 2H), 2.03–1.91 (m, 2H), 1.80–1.64 (m, 2H).

**GR**: <sup>1</sup>H-NMR (500 MHz, D<sub>2</sub>O) δ (ppm) 4.47–4.40 (m, 1H), 3.90 (s, 2H), 3.23 (t, J = 6.8 Hz, 2H), 2.02–1.59 (m, 4H).

**RE**: <sup>1</sup>H-NMR (500 MHz, D<sub>2</sub>O) δ (ppm) 4.48–4.32 (m, 1H), 4.12 (t, J = 5.9 Hz, 1H), 3.24 (q, J = 7.2 Hz, 3H), 2.19–1.43 (m, 8H).

**Synthesis of imidazolium-bridged dicytidyl dimer intermediate.** The dimer used for primer extension was synthesised and purified as previously reported.<sup>2</sup> Cytidine 5'-monophosphate (0.5 mmol) was dissolved in dimethyl sulfoxide and reacted with 2-aminoimidazole hydrochloride (0.23 mmol) under vigorous stirring. Triphenylphosphine (5 mmol), 2,2'-dipyridyl disulfide (5 mmol), and triethylamine (10 mmol) were then added sequentially to the solution, which was stirred for 30 minutes. A sample was taken for <sup>31</sup>P NMR analysis to monitor reaction progress. The reaction mixture was subsequently precipitated by adding it to pre-cooled acetone (250 mL), diethyl ether (250 mL), and sodium perchlorate (saturated in acetone), followed by centrifugation and washing of the resulting solid with acetone and diethyl ether. The pellet was dried under a high vacuum to remove residual solvent.

**Oligonucleotide solid-phase synthesis.** DNA and RNA oligonucleotides were assembled using standard reagents and standard manufacturer protocols on a 1 μmol scale. DMTr-removal reagent consisted of 3% trichloroacetic acid in dichloromethane, the activator consisted of 0.25 M 5-ethylthio tetrazole in

acetonitrile, the oxidiser consisted of a 0.02 M solution of iodine in pyridine:water:tetrahydrofuran (8:16:76 volume ratio), and the capping reagents consisted of (Cap A) a solution of acetic anhydride:pyridine:tetrahydrofuran (10:10:80 volume ratio) and (Cap B) a 10% (v/v) solution of *N*-methylimidazole in tetrahydrofuran. All oligonucleotides were deprotected from the solid support using 25% ammonium hydroxide:ethanol 4:1 volume ratio (1mL total volume) for 17 h at 55°C and concentrated in a Savant SC 110A SpeedVac® Plus to a pellet. Oligonucleotides were then purified by ion exchange chromatography.

RNA oligomers were desilylated in DMSO:triethylamine trihydrofluoride 2:3 volume ratio (100 µL:150 µL) for 2 hours at 65°C and then precipitated in cooled 1-butanol for 1 hour. Upon centrifugation, the pellet was recovered, and the supernatant was discarded. The pellet was further washed with 200 µL of 1-butanol. Deprotected oligonucleotides were purified by Strong Anion-Exchange (SAX) HPLC with solvent A (50 mM Tris buffer pH 7.6, 10% v/v MeCN) and solvent B (50 mM Tris pH 7.6, 1 M NaCl, 10% v/v MeCN), with a standard gradient of 0-75% over 15 minutes. Purified samples were desalted using Sep-Pak C18 Classic Cartridge (Water™). The Sep-Pak C18 cartridge was conditioned with 10 mL of MeCN, 10 mL of MeCN:water 1:1 volume ratio and 10 mL of 100 mM pH 7 NaOAc. The purified oligo was diluted to at least 2% v/v MeCN (1:4 dilution with water) and flowed through the cartridge at least twice for column loading. The bound oligonucleotide was washed with water (~25 mL), eluted from the column with 4 mL of MeCN:water 1:1 volume ratio, and concentrated into a pellet using a DNA concentrator.

**Determination of the critical salt concentration (CSC).** The robustness of complex coacervates is commonly assessed by their stability to salt, typically NaCl. The critical salt concentration corresponds to the highest NaCl concentration tolerated before the complete dissolution of coacervates. Turbidity was indirectly measured on a plate reader, reading the absorbance at 600 nm and using the relation:

$$\text{Turbidity} = 100 - \text{Transmittance}_{\%} = 100(1 - 10^{\text{Abs}_{\text{blank}} - \text{Abs}})$$

Samples of 100 µL (or 20 µL in the case of peptide/RNA mixtures) were prepared in 96-well plates (or 384-well plates) and titrated with concentrated stocks of NaCl (1, 3 or 5 M). The concentration of the salt stock was chosen to minimise the dilution of the sample during titrations (20% maximum dilution) and maximise the number of points measured during the steep decay of absorbance. At the end of the titration, all mixtures reached the turbidity of the blank (100 µL of MilliQ). The titration curves have a sigmoidal shape, and the CSC was calculated as follows: (i) the exact concentration of NaCl was calculated at each point, taking into account the total volume in the well; (ii) the curve (turbidity vs NaCl concentration) was fitted every three points with a linear equation; (iii) the linear fit with the highest linear coefficient (absolute value) was used to identify the tangent at the inflection point ( $y = ax + b$ ). The CSC was thus calculated as  $CSC = -\frac{a}{b}$ .

**Coacervation onset.** We define the coacervation onset as the amino acid concentration required for each peptide to form coacervates in the presence of oligonucleotides, assessed by turbidity measurements. Turbidity measurements were performed by monitoring absorbance at 600 nm in a plate reader upon titration of the oligonucleotide solution with a concentrated peptide stock until absorbance reached its maximum. As previously discussed, absorption was converted to turbidity, and the onset concentration corresponds to the amino acid concentration for turbidity > 20%.

**Minimal complex concentration for coacervation.** We define the minimal complex concentration as the minimal concentration of peptide:oligonucleotide 4:1 concentration ratio required for coacervation. Coacervates were prepared as in previous experiments (20 mM amino acid concentration and 5 mM nucleotide concentration, 20  $\mu$ L samples), then serially diluted in a 384-well plate. Absorbance at 600 nm was converted to turbidity, and the minimal complex concentration for peptide/oligonucleotide mixtures was determined as the intercept between the x-axis and the tangent to the inflection point of the sigmoidal curve.

**Temperature stability with hot stage epifluorescence microscopy.** Borosilicate glass capillaries (internal section of 2 x 0.2 mm) were passivated using the same protocol as the coverslips. One capillary end was sealed with optical glue and cured under UV light ( $\lambda = 365$  nm) for 5 minutes. Peptide/oligonucleotide mixtures containing 1% of Cy3-(TGAC)<sub>2</sub> were introduced in the capillary (approx. 30  $\mu$ L), which was then completely sealed with a two-component epoxy resin and hardener glue. Glass capillaries were placed on a coverslip and subsequently on a copper plate connected to a Peltier element, enabling fine control over temperature.

**Fluorescence Recovery After Photobleaching (FRAP).** Cy3-labelled DNA oligonucleotides (Cy3-(TGAC)<sub>2</sub>, Cy3-(TGAC)<sub>4</sub> and Cy3-(TGAC)<sub>8</sub>, labelled on the 5') were chosen as FRAP probes for peptide/oligonucleotide coacervates. Coacervates were prepared as described previously, with the peptide added last to the microtube. Imaging was done ca. 30 minutes after sample preparation and placement in the observation chamber.

For each measurement, a droplet was chosen in the centre of the field of view (512x512 px) and imaged for 10 frames (every 1.117 s). A circular region of interest (ROI), selected inside the droplet (smaller than the droplet) before the acquisition, was bleached using the 633 nm laser line at 100% intensity. Post-bleaching images were collected at the same framerate until ROI intensity reached a plateau, which for our samples varied between 30-250 s (all profiles available in SI). Pre- and post-bleaching imaging was performed using the 633 nm laser line at 4-6% intensity and pinhole size set to 1 AU. A standard photomultiplier tube was used as a detector (480-720 nm). Three droplets in different FOVs were bleached for each sample, and the recovery curves were averaged.

**Partition coefficients.** Partitioning of fluorescent client molecules was quantified using the equation<sup>3</sup>

$$K_p = \frac{I_{\text{droplet}} - I_{\text{dark}}}{I_{\text{dilute phase}} - I_{\text{dark}}}$$

The fluorescence intensity inside the droplet,  $I_{\text{droplet}}$ , was averaged among all droplets in the field of view (FOV) using a particle analysis plugin from ImageJ and a low threshold to prevent underestimation. The intensity of the dilute phase was averaged for the entire FOV after droplets were removed.  $I_{\text{dark}}$  corresponds to the intensity measured in a sample lacking any fluorophore at the same laser power used for the respective sample. Client molecules used include: Cy3-(TGAC)<sub>2</sub>, Cy3-(ACTG)<sub>2</sub>, FITC-r(ACUG)<sub>2</sub>, Cy3-dA<sub>11</sub> and Magnesium Green.

**Broccoli aptamer reconstitution.** A minimal version of the Broccoli aptamer was split in strand A (5'-r(GCGGAGACGGUCGGUCCAGAU), 23nt) and strand B (5'-r(UAUCUGUCGAGUAGAGUGUGGGCUCG), 27nt) and its reconstitution was followed by DFHBI fluorescence in the presence of KCl. A 2000× DFHBI stock was prepared in DMSO and diluted 100× in 25 mM HEPES buffer before being added to the sample. The samples were prepared to ensure that coacervation takes place after aptamer reconstitution by mixing in the following order (unless otherwise stated): MilliQ, 25 mM HEPES buffer, 10 mM KCl, DNA<sub>8</sub>/RNA<sub>8</sub>/DNA<sub>16</sub> (5 mM nt), strand A (10 μM), strand B (10 μM), 5 mM DFHBI and peptide (20 mM amino acid). Measurements were performed before and after adding the peptide; fluorescence was recorded every 15 minutes for 1 hour. For microscopy, coacervates containing the Broccoli aptamer and DFHBI were prepared and left to incubate for 30 minutes in sealed microscopy chambers.

**Primer Extension Reaction.** Primer extension reactions in the presence of coacervates were performed with 25 mM HEPES (pH 8.0), R<sub>4</sub> or R<sub>6</sub> 20–40 mM (amino acid concentration), nucleic acid host strand 5–10 mM (nucleotide concentration), 3 μM 6-FAM-labelled primer and 4 μM template. Activated dimer stocks were resuspended in water, resulting in a stock concentration of 100 mM. The required amount for the host strand was dried in a centrifuge tube using a DNA concentrator, followed by resuspension in water (5 μL). Buffer was then added, followed by peptide and premixed primer-template duplex. The reaction was initiated by the addition of activated CC dimer (2.5 mM final concentration), followed by MgCl<sub>2</sub> (5 mM final concentration) and water (to reach a final reaction volume of 20 μL). The reaction was mixed vigorously and immediately aliquoted (4 μL) for the various time points (0 h, 1 h, 3 h, 6 h, 24 h). Timepoints were quenched using 8 M urea (36 μL) containing 72 mM NaCl.

Control primer extension experiments were repeated as described above but with NaCl (1 M) added to dissolve the coacervates. Aliquots for control experiments containing NaCl were quenched using 8M urea (36 μL). Additional control experiments were repeated without the presence of peptide, with and without 1 M NaCl. Note that all volumes were adjusted to a final volume of 20 μL by varying the amount of water added.

All primer extension species were heated to 100°C for 2 min, and 3 μL aliquots were resolved by 20% (19:1) denaturing PAGE with 8 M urea. Polyacrylamide gels were cast using 20% (acrylamide:bis-acrylamide 19:1) denaturing gels (8 M urea) and run in 1× TBE buffer (89 mM Tris, 89 mM boric acid, and 2 mM EDTA) in a 16 cm wide x 14 cm long x 0.8 cm thick gel. Gels were pre-run at 10 W for at least 30 minutes before loading. Gels were initially run at 3 W until the markers (95% formamide, 0.025% bromophenol blue, 0.025% xylene cyanol) had loaded onto the gel matrix and separated. The cell voltage was then increased to 8 W and run for at least two hours. Gels were imaged on an Amersham TYPHOON. All band intensities were quantified using the ImageQuant™ software (using the background reduction function and manual band detection).

## Computational Methods

**Atomistic Force-Field simulations.** The simulations were performed using the Amber14SB force field for peptides,<sup>4</sup> OL3 parameters for RNA,<sup>5</sup> and bsc1 for DNA.<sup>6</sup> All systems were solvated using the TIP4P-FB water model,<sup>7</sup> and compatible ion parameters were applied for sodium (Na<sup>+</sup>) and chloride (Cl<sup>-</sup>) ions.

Temperature control was managed by a Langevin thermostat, set to 298 K with a friction coefficient of 1 ps<sup>-1</sup>. For simulations conducted in the isothermal-isobaric (NPT) ensemble, the pressure was maintained at 1 atmosphere using a Monte Carlo barostat<sup>8</sup> with updates applied every 25 steps.

Using the LFMiddle discretisation scheme,<sup>9</sup> the Langevin integrator was employed to propagate the system dynamics. Hydrogen mass repartitioning was used, enabling a time step of 4 fs during the production simulations, which was further supported by constraining all bonds involving hydrogen atoms using the CCMA algorithm.<sup>10</sup> Non-bonded interactions were computed with a cutoff distance of 0.9 nm. Long-range electrostatics were handled using the Particle Mesh Ewald (PME) method.<sup>11</sup> All simulations were performed using OpenMM 8.1.2,<sup>12</sup> leveraging the CUDA platform in mixed precision mode. Energy minimisation was performed using OpenMM's built-in local energy minimiser, which utilises the L-BFGS optimisation algorithm<sup>13</sup> until it converged to a tolerance of 10 kJ mol<sup>-1</sup> nanometer<sup>-1</sup>.

**Monomer Preparation.** Initial monomer structures were built using PyMOL 2.5.7.<sup>14</sup> Single-stranded RNA and DNA 8-mers were constructed in an extended conformation approximating B-form dihedral angles. Peptides composed of polyarginine were prepared in an extended conformation. Peptides were modelled with protonated N-termini (NH<sub>3</sub><sup>+</sup>) and deprotonated C-termini (COO<sup>-</sup>) to reflect physiological conditions. Nucleotides were prepared without the 3' phosphate group to match experimental conditions. Each monomer's initial configuration was solvated in a cubic box with a minimum of 5 Å between any solute atom and the box edge. The systems were neutralised, and ionic strength adjusted to 30 mM NaCl. Energy minimisation was performed, followed by a 100 ns NVT equilibration at 298 K. Evenly spaced configurations from the last 80 ns of the monomer simulations were extracted to build multi-chain systems.

**Multi-Chain System Preparation.** Multi-chain systems were constructed by placing monomers using Packmol 20.14.4,<sup>15</sup> enforcing a minimum distance of 10.0 Å between any two atoms to prevent overlaps. Each system consisted of 8 nucleotides (either RNA or DNA) and 36 polyarginine peptides, with one nucleotide and four peptides placed randomly within each octant of a cubic box with a side length of 140.0 Å. The assembled systems were solvated in a cubic box 145.0 Å per side, ensuring a minimum of 5 Å between any solute atom and the box edge under periodic boundary conditions, before being neutralised and brought to an ionic strength of 100 mM NaCl.

**Equilibration Protocol.** After minimisation, the systems were relaxed through the following steps:

- 250 ps of NPT simulation at 298 K and 1 atm with heavy atom positional restraints of 15 kcal mol<sup>-1</sup> Å<sup>-2</sup> applied to all peptide and nucleotide heavy atoms, using a 2 fs time step.
- 250 ps of unrestrained NPT simulation at 298 K and 1 atm, with a 2 fs time step.
- 500 ps of unrestrained NVT simulation using a 2 fs time step.

**Production Simulations.** Production simulations were carried out in the NVT ensemble for 800 ns per replicate, with 5 independent replicates for each system, totalling 3.0 μs of simulation time per system. Each replicate began from an independently prepared configuration and used different random number seeds to ensure statistical independence.

Trajectory frames were saved every 0.8 ns. The last 200 ns of each simulation (corresponding to 500 frames) were used for contact analysis. Contacts between molecules were defined based on a cutoff distance of 0.45 nm between heavy atoms and were analysed using a custom Python script utilising CuPy.

**Interaction Analysis.** Trajectories were analysed using the Python package MDTraj.<sup>16</sup> Hydrogen bonds were assessed using the Wernet-Nillson criteria.<sup>17</sup> Ionic interactions were defined as occurring when the CZ atom from an arginine sidechain approaches OP1 or OP2 atoms from a phosphate group closer than 0.6 nm without a hydrogen bond being established between the two residues. Following previous work,<sup>18</sup> Arg-nucleobase stacking interactions were defined as occurring when the CZ atom from an arginine sidechain approaches the centre-of-geometry of a nucleobase ring with the angle between the planes of the guanidium group and the nucleobase ring less than 30°.

**Coarse Grained Model.** Coarse grained simulations were carried out using an OpenMM implementation of the newly released residue level coarse-grained model Mpipi-Recharged, which is designed to accurately model the liquid-liquid phase separation of highly charged biomolecular condensates.<sup>19</sup> The model employs a one-bead-per-residue representation for amino acids and unstructured single-stranded RNA. Parameters are available for all 20 natural amino acids and uridine in RNA. Full details of the model and its parameters are available in the recent publication.

**Coarse Grained Simulation Procedure.** Using the Mpipi-Recharged model, direct coexistence simulations<sup>20</sup> of various mixtures of polyR peptide and polyU RNA were performed. For each system we simulated, initial extended configurations of monomers were prepared and relaxed for 10 ns at 300 K. Following this, copies of the relaxed monomer were placed into a rectangular box on a regular grid pattern. The periodic boxes used were approximately 144 nm x 24 nm x 24 nm and periodic boundary conditions were applied in all 3 directions. An OpenMM CustomExternalForce was then used to pull all monomers to the center of the box. After 10 ns of pulling, a dense slab formed at the center of the box, at which point the pulling force was switched off. Subsequently, the systems were simulated for 1 ms without the external force to allow the formation of coexisting high- and low-density phases. All multichain coarse-grained simulations were carried out at a temperature of 300 K and an implicit salt concentration of 100 mM NaCl. Integration was carried out using a LangevinMiddleIntegrator with timestep of 10 fs and collision frequency of 0.01 / ps.

**Coarse Grained Simulation Analysis.** Custom Python scripts utilising MDTraj and CuPy were used to analyse coarse grained simulations.<sup>21</sup> Contacts were defined as occurring when two coarse grained beads  $i$  and  $j$  are closer than  $0.5(\sigma_i + \sigma_j) + 0.1$  nm, where  $\sigma_i$  is the characteristic length scale associated with bead  $i$ .

## Supplementary Tables

**Table S1.** Peptide sequences used in the present work. All sequences are written *N*- to *C*-termini, are not protected (*i.e.*, H-peptide-OH) and used as TFA salts (SIH = Synthesised in-house).

Peptide sequence	Net charge	Charge density	Source
<b>Dimers</b>			
RG	1	0.5	SIH
GR	1	0.5	SIH
RE	0	0	SIH
R <sub>2</sub>	2	1	SIH
<b>Trimers</b>			
R <sub>3</sub>	3	1	GenScript
RGR	2	0.67	GenScript
RER	1	0.33	SIH
<b>Tetramers</b>			
R <sub>4</sub>	4	1	SIH, GenScript
K <sub>4</sub>	4	1	GenScript
RKRK	4	1	GenScript
(D-R-L-R) <sub>2</sub>	4	1	SIH
RG <sub>2</sub> R	2	0.5	GenScript
R <sub>4</sub> -HCl	4	1	GenScript
<b>Pentamers</b>			
R <sub>5</sub>	5	1	GenScript
R <sub>2</sub> GR <sub>2</sub>	4	0.8	GenScript
<b>Hexamers</b>			
R <sub>2</sub> G <sub>2</sub> R <sub>2</sub>	4	0.67	GenScript
R <sub>6</sub>	6	1	GenScript
R <sub>2</sub> E <sub>2</sub> R <sub>2</sub>	2	0.33	SIH
<b>Other lengths</b>			
R <sub>7</sub>	7	1	GenScript
R <sub>8</sub>	8	1	GenScript
(D-R-L-R) <sub>4</sub>	8	1	SIH
R <sub>2</sub> G <sub>4</sub> R <sub>2</sub>	4	0.5	GenScript
R <sub>9</sub>	9	1	GenScript
R <sub>10</sub>	10	1	GenScript
E <sub>10</sub>	-10	1	GenScript
R <sub>2</sub> G <sub>8</sub> R <sub>2</sub>	4	0.33	GenScript

**Table S2.** Oligonucleotide acronyms and sequences used in the present work (SIH = synthesised in-house).

Name	Sequence	Source
dA <sub>3</sub>	5'-AAA-3'	SIH
DNA <sub>5</sub>	5'-ACTGA-3'	IDT
DNA <sub>6</sub>	5'-ACTGAC-3'	IDT
DNA <sub>7</sub>	5'-ACTGACT-3'	IDT
DNA <sub>8</sub>	5'-ACTGACTG-3'	IDT
DNA <sub>10</sub>	5'-ACTGACTGAC-3'	IDT
DNA <sub>12</sub>	5'-ACTGACTGACTG -3'	IDT
DNA <sub>16</sub>	5'-ACTGACTGACTGACTG-3'	IDT
DNA <sub>20</sub>	5'-ACTGACTGACTGACTGACTG-3'	IDT
DNA <sub>40</sub>	5'-ACTGACTGACTGACTGACTGACTGACTGACTGACTGACTG-3'	IDT
dA <sub>10</sub>	5'-AAAAAAAAAAAA-3'	IDT
dT <sub>10</sub>	5'-TTTTTTTTTTT-3'	IDT
dC <sub>10</sub>	5'-CCCCCCCCCCC-3'	IDT
dG <sub>10</sub>	5'-GGGGAGGGGA-3'	IDT
Cy3-5nt	5'-TCAGT-Cy <sub>3</sub> -3'	IDT
Cy3-8nt	5'-Cy3-TGACTGAC-3'	IDT
Cy3-16nt	5'-Cy3-TGACTGACTGACTGAC-3'	IDT
Cy3-32nt	5'-Cy3-TGACTGACTGACTGACTGAC-3'	IDT
Cy3-dA <sub>11</sub>	5'-Cy3-AAAAAAAAAAA-3'	IDT
DNA <sub>8</sub> * <sup>a</sup>	5'-CAGTCAGT-3'	IDT
HNA <sub>8</sub>	5'-ArCrUGArCrUG-3'	IDT
RNA <sub>8</sub>	5'-r(ACUGACUG)-3'	IDT, SIH
HNA <sub>12</sub>	5'-ArCrUGArCrUGArCrUG-3'	IDT
RNA <sub>12</sub>	5'-r(ACUGACUGACUG)-3'	IDT, SIH
RNA <sub>20</sub>	5'-r(ACUGACUGACUGACUGACUG)-3'	IDT, SIH
dA <sub>11</sub>	5'-AAAAAAAAAAAA-3'	Eurofins
dA <sub>21</sub>	5'-AAAAAAAAAAAAAAAAAAAAAAAA-3'	Eurofins
dA <sub>31</sub>	5'-AAAAAAAAAAAAAAAAAAAAAAAAAAAAAAAA-3'	Eurofins
dA <sub>41</sub>	5'-AA-3'	Eurofins
dA <sub>51</sub>	5'- AA-3'	Eurofins
dA <sub>12</sub>	5'-AAAAAAAAAAAA-3'	SIH
dA <sub>16</sub>	5'-AAAAAAAAAAAA-3'	SIH
dT <sub>16</sub>	5'-TTTTTTTTTTTTTTTT-3'	SIH
rA <sub>12</sub>	5'-r(AAAAAAAAAAAAA)-3'	SIH
rA <sub>16</sub>	5'-r(AAAAAAAAAAAAA)-3'	SIH
Arich <sub>12</sub>	5'-AAGTAAAGTAAA-3'	SIH
Template <sup>b</sup>	5'-r(GGGUCGAGCG)-3'	SIH
FAM-RNA <sub>8</sub> (primer) <sup>b</sup>	5'-FAM-r(CGCUCGAC)-3'	SIH
Template <sup>c</sup>	5'-r(GGCAGUCAGU)-3'	SIH
FAM-RNA <sub>8</sub> (primer) <sup>c</sup>	5'-FAM-r(ACUGACUG)-3'	SIH



FAM-DNA <sub>8</sub>	5'-FAM-ACTGACTG-3'	SIH
DNA <sub>11</sub> -Phos	5'-ACTGACTGACT-Phos-3'	IDT
Phos-DNA <sub>10</sub> -Phos	5'-Phos-CTGACTGACT-Phos-3'	IDT
Broccoli aptamer A	5'-r(GCGGAGACGGUCGGGUCCAGAU)-3'	Eurofins
Broccoli aptamer B	5'-r(UAUCUGUCGAGUAGAGUGUGGGCUCCGC)-3'	Eurofins

<sup>a</sup> DNA<sub>8</sub>\* is the complementary sequence to DNA<sub>8</sub>

<sup>b</sup> primer/template system referred to as non-complementary to the host oligonucleotide

<sup>c</sup> primer/template system referred to as complementary to the host oligonucleotide

**Table S3.** Critical salt concentrations (CSCs) measured for mixtures comprising 20 mM amino acid of Arg homopeptides and 5 mM nucleotide (unless otherwise stated) in 25 mM HEPES pH 7.4 and room temperature.

Peptide	Oligonucleotide	CSC (mM, NaCl)
R <sub>3</sub>	DNA <sub>8</sub>	0
R <sub>3</sub>	HNA <sub>8</sub>	59.7
R <sub>3</sub>	RNA <sub>8</sub>	54.2
R <sub>3</sub>	DNA <sub>12</sub>	38.8 ± 4.7
R <sub>3</sub>	HNA <sub>12</sub>	52.7
R <sub>3</sub>	RNA <sub>12</sub>	205.2
R <sub>3</sub>	DNA <sub>12</sub> :RNA <sub>12</sub> 1:1	44.7
R <sub>4</sub>	DNA <sub>8</sub>	99.3 ± 4.7
R <sub>4</sub>	HNA <sub>8</sub>	113.7
R <sub>4</sub>	RNA <sub>8</sub>	215.9
(D-R-L-R) <sub>2</sub>	DNA <sub>8</sub>	78.3
R <sub>4</sub>	DNA <sub>12</sub>	196.4
R <sub>4</sub>	HNA <sub>12</sub>	237.8
R <sub>4</sub>	RNA <sub>12</sub>	379.2
R <sub>4</sub>	DNA <sub>12</sub> :RNA <sub>12</sub> 1:1	258.5
(D-R-L-R) <sub>2</sub>	DNA <sub>12</sub>	152.8
R <sub>4</sub>	DNA <sub>16</sub>	212.6
R <sub>4</sub>	DNA <sub>20</sub>	201.6 ± 19.3
R <sub>4</sub>	RNA <sub>20</sub>	430.7
R <sub>4</sub>	DNA <sub>40</sub>	278.1
R <sub>4</sub>	polyU	492.9
R <sub>6</sub>	DNA <sub>6</sub>	143.6
R <sub>6</sub>	DNA <sub>8</sub>	313.7
R <sub>6</sub>	HNA <sub>8</sub>	222.1
R <sub>6</sub>	RNA <sub>8</sub>	210.7
R <sub>6</sub>	dA <sub>10</sub>	99.9
R <sub>6</sub>	dA <sub>11</sub>	123.4
R <sub>6</sub>	dA <sub>12</sub> <sup>a</sup>	280.1

Peptide	Oligonucleotide	CSC (mM, NaCl)
R <sub>6</sub>	rA <sub>12</sub> <sup>a</sup>	508.4
R <sub>6</sub>	DNA <sub>12</sub> <sup>a</sup>	409.2
R <sub>6</sub>	DNA <sub>12</sub>	415.9 ± 6.1
R <sub>6</sub>	HNA <sub>12</sub>	431.9
R <sub>6</sub>	RNA <sub>12</sub>	693.8
R <sub>6</sub>	DNA <sub>12</sub> :RNA <sub>12</sub> 1:1	422.4
R <sub>6</sub>	Arich <sub>12</sub> <sup>a</sup>	261.7
R <sub>6</sub>	dA <sub>15</sub>	153.5
R <sub>6</sub>	dA <sub>16</sub> <sup>a</sup>	296.4
R <sub>6</sub>	DNA <sub>16</sub>	475.1
R <sub>6</sub>	DNA <sub>20</sub>	473.8
R <sub>6</sub>	dA <sub>31</sub>	243.5
R <sub>6</sub>	DNA <sub>40</sub>	500.0
R <sub>6</sub>	dA <sub>41</sub>	256.6
R <sub>6</sub>	dA <sub>51</sub>	269.8
R <sub>7</sub>	DNA <sub>7</sub>	369.3
R <sub>8</sub>	DNA <sub>8</sub>	503 ± 33.7
R <sub>8</sub>	HNA <sub>8</sub>	368.6
R <sub>8</sub>	RNA <sub>8</sub>	402.6
(D-R-L-R) <sub>4</sub>	DNA <sub>8</sub>	424.9
R <sub>8</sub>	DNA <sub>12</sub>	601.8 ± 45.3
(D-R-L-R) <sub>4</sub>	DNA <sub>12</sub>	509.8
R <sub>8</sub>	DNA <sub>16</sub>	743.5
R <sub>8</sub>	DNA <sub>20</sub>	684.2 ± 55.4
R <sub>10</sub>	dA <sub>10</sub>	258.2
R <sub>10</sub>	dT <sub>10</sub>	279.0
R <sub>10</sub>	DNA <sub>10</sub>	583.8 ± 37.1
R <sub>10</sub>	DNA <sub>12</sub>	634.2

<sup>a</sup> [nt] = 10 mM

**Table S4.** Critical salt concentrations (CSCs) measured for peptide mixtures (and respective controls) and Arg-containing heteropeptides with oligonucleotides (5 mM nucleotide) at 25 mM HEPES pH 7.4 and room temperature.

Composition	[aa] (mM)	CSC (mM)
R <sub>3</sub> /DNA <sub>20</sub>	6.67	19.8
R <sub>3</sub> /DNA <sub>20</sub>	20	85.0
R <sub>4</sub> /DNA <sub>20</sub>	6.67	174.8
R <sub>4</sub> /DNA <sub>20</sub>	20	207.4 ± 27.2
R <sub>5</sub> /DNA <sub>20</sub>	20	348.1
R <sub>3</sub> /R <sub>4</sub> /R <sub>5</sub> /DNA <sub>20</sub>	20	230.5
R <sub>2</sub> GR <sub>2</sub> /DNA <sub>20</sub>	25	204.6
RG <sub>2</sub> R/DNA <sub>20</sub>	13.3	0
R <sub>4</sub> /RG <sub>2</sub> R/DNA <sub>20</sub>	13.3	147.1
R <sub>2</sub> G <sub>2</sub> R <sub>2</sub> /DNA <sub>20</sub>	30	237.8
R <sub>2</sub> G <sub>4</sub> R <sub>2</sub> /DNA <sub>20</sub>	20	143.4
R <sub>2</sub> G <sub>4</sub> R <sub>2</sub> /DNA <sub>20</sub>	40	163.3
R <sub>2</sub> G <sub>8</sub> R <sub>2</sub> /DNA <sub>20</sub>	20	85.2
R <sub>2</sub> G <sub>8</sub> R <sub>2</sub> /DNA <sub>20</sub>	60	140.8
R <sub>2</sub> GR <sub>2</sub> /DNA <sub>20</sub>	20	163.3
R <sub>2</sub> G <sub>2</sub> R <sub>2</sub> /DNA <sub>20</sub>	20	170.0
R <sub>4</sub> /R <sub>2</sub> GR <sub>2</sub> /R <sub>2</sub> G <sub>2</sub> R <sub>2</sub> /DNA <sub>20</sub>	20	200.1
RKRK/DNA <sub>20</sub>	6.67	50.3
RKRK/DNA <sub>20</sub>	20	91.5
R <sub>4</sub> /RKRK/DNA <sub>20</sub>	13.3	182.0
K <sub>4</sub> /DNA <sub>20</sub>	6.67	0
K <sub>4</sub> /RKRK/DNA <sub>20</sub>	13.3	82.8
R <sub>4</sub> /K <sub>4</sub> /DNA <sub>20</sub>	13.3	141.5
RGR/DNA <sub>20</sub>	13.3	0
R <sub>3</sub> /RER/DNA <sub>20</sub>	13.3	32.1
R <sub>3</sub> /RER/RGR/DNA <sub>20</sub>	20	40.0
R <sub>1</sub> /DNA <sub>8</sub>	20	0
R <sub>4</sub> /R <sub>1</sub> (3:1)/DNA <sub>8</sub>	20	84.3
R <sub>4</sub> /R <sub>1</sub> (1:1)/DNA <sub>8</sub>	20	40.4
R <sub>1</sub> /DNA <sub>20</sub>	20	0
R <sub>4</sub> /R <sub>1</sub> (3:1)/DNA <sub>20</sub>	20	201.9
R <sub>4</sub> /R <sub>1</sub> (1:1)/DNA <sub>20</sub>	20	139.8

**Table S5.** Parameters calculated from the linear fit ( $CSC = a(1/N) + b$ ) for the CSCs of peptides and oligonucleotides when one (or both) lengths are varied.

Peptide	Oligonucleotide	a	b	R <sup>2</sup>	Calculated N <sub>min</sub> (-a/b)	Empirical N <sub>min</sub>
R <sub>2</sub> G <sub>2</sub> R <sub>2</sub>	DNA <sub>N</sub>	-1640.8	256.5	0.89	6.4	7
R <sub>4</sub>	DNA <sub>N</sub>	-1963.3	332.1	0.89	5.9	7
R <sub>6</sub>	DNA <sub>N</sub>	-2107.8	564.4	0.81	3.7	5
R <sub>6</sub>	polyA <sub>N</sub>	-2105.7	308.3	0.99	6.8	11
R <sub>4</sub>	RNA <sub>N</sub>	-2906.4	59.22	0.95	4.9	8 <sup>a</sup>
R <sub>N</sub>	DNA <sub>12</sub>	-2561.6	866.9	0.99	2.9	3
R <sub>N</sub>	DNA <sub>20</sub>	-2951.5	1007.6	0.90	2.9	3
R <sub>N</sub>	DNA <sub>N</sub>	-7477.5	1420.2	0.94	5.3	6
R <sub>N</sub>	DNA <sub>8</sub>	-2588.7	742.7	0.96	3.5	4
R <sub>N</sub>	HNA <sub>8</sub>	-1610.3	564.4	0.89	3.0	3
R <sub>N</sub>	RNA <sub>8</sub>	-1653.8	616.9	0.99	2.7	3
R <sub>N</sub>	RNA <sub>12</sub>	-2835.8	1104.2	0.96	2.6	3
R <sub>N</sub>	HNA <sub>12</sub>	-2275.5	809.7	0.99	2.8	3
R <sub>N</sub>	RNA <sub>12</sub> :DNA <sub>12</sub> 1:1	-2266.0	808.4	0.99	2.8	3

Shortest RNA oligonucleotide tested

**Table S6.** Critical salt concentrations (CSCs) measured for peptide/peptide and peptide/oligonucleotide coacervates at different component concentrations (phase diagram studies). Concentrations refer to amino acid (aa) or nucleotide (nt) concentrations.

Mixture	[aa] (mM)	[nt] (mM)	CSC (mM)
R <sub>4</sub> /DNA <sub>8</sub>	2	5	0
	3	5	22.3
	5	5	49.4
	10	5	67.3
	20	5	99.3 ± 4.7
	40	5	110.0
	20	1	0
	20	2	51.8
	20	5	99.3 ± 4.7
	20	10	122.7
	20	15	118.6
	20	20	140.1
R <sub>3</sub> /DNA <sub>12</sub>	5	5	0
	10	5	0
	15	5	25.0
	20	5	38.8 ± 4.7
	30	5	36.7
	40	5	20.7
	60	5	47.0
	20	2.5	30.7
	20	5	38.8 ± 4.7
	20	10	46.4
	20	15	37.8
	20	20	23.2
R <sub>4</sub> /DNA <sub>20</sub>	3	5	93.0
	5	5	123.5
	10	5	175.9
	15	5	213.8
	20	5	201.6 ± 19.3
	30	5	270.3
R <sub>8</sub> /DNA <sub>20</sub>	3	5	391.5
	5	5	503.8
	10	5	503.0
	15	5	609.0
	20	5	684.2 ± 55.4
	30	5	674.8
R <sub>10</sub> /E <sub>10</sub> <sup>a</sup>	5	10	0
	8	10	90.6 ± 5.6
	10	10	95.2 ± 0.4
	12	10	103.8 ± 22.9
	20	10	0
	10	5	0
	10	8	81.9 ± 12.9
	10	12	107.5 ± 6.1
	10	15	93.7 ± 5.7
	10	20	84.8
	10	40	0

Concentrations reported are [Arg] and [Glu]

**Table S7.** Amino acid concentrations required for the coacervation of dipeptides with oligonucleotides of different lengths. *N/A* stands for ‘non-applicable’.

Peptide dimer	Oligonucleotide	Phase	Amino acid concentration required
<b>R<sub>2</sub></b>	DNA <sub>8</sub>	Soluble	<i>N/A</i>
	DNA <sub>12</sub>	Soluble	<i>N/A</i>
	DNA <sub>20</sub>	Soluble	<i>N/A</i>
	RNA <sub>8</sub>	Soluble	<i>N/A</i>
	RNA <sub>12</sub>	<b>Droplets</b>	60 mM
	RNA <sub>20</sub>	<b>Droplets</b>	40 mM
<b>RG, GR</b>	DNA <sub>8</sub>	Soluble	<i>N/A</i>
	DNA <sub>12</sub>	Soluble	<i>N/A</i>
	DNA <sub>20</sub>	Soluble	<i>N/A</i>
	RNA <sub>8</sub>	<b>Droplets</b>	40 mM
	RNA <sub>12</sub>	<b>Droplets</b>	40 mM
	RNA <sub>20</sub>	<b>Droplets</b>	20 mM
<b>RE</b>	DNA <sub>8</sub>	Soluble	<i>N/A</i>
	DNA <sub>12</sub>	<b>Droplets</b>	40 mM
	DNA <sub>20</sub>	<b>Droplets</b>	40 mM
	RNA <sub>8</sub>	<b>Droplets</b>	20 mM
	RNA <sub>12</sub>	<b>Droplets</b>	20 mM
	RNA <sub>20</sub>	<b>Droplets</b>	20 mM

**Table S8.** Number of contacts per oligonucleotide strand with arginine residues, as computed with atomistic simulations. Results are categorised by mode of interaction for a given peptide/nucleic acid combination. Each value in a repeat is an average value for all oligonucleotide chains of that peptide/oligonucleotide mixture over time.

Number of contacts	Mixture			
	R <sub>3</sub> /DNA <sub>8</sub>	R <sub>3</sub> /RNA <sub>8</sub>	R <sub>4</sub> /DNA <sub>8</sub>	R <sub>4</sub> /RNA <sub>8</sub>
	H-bonding			
Repeat 1	8.32	10.30	9.35	11.06
Repeat 2	7.28	9.06	10.48	10.94
Repeat 3	8.82	11.17	8.71	11.81
Repeat 4	8.15	9.38	9.16	11.68
Repeat 5	7.56	10.58	9.69	11.42
Average	<b>8.02</b>	<b>10.1</b>	<b>9.48</b>	<b>11.4</b>
Standard deviation	0.55	0.8	0.59	0.3
	Ionic			
Repeat 1	3.19	3.51	4.28	3.95
Repeat 2	3.38	4.37	4.30	4.24
Repeat 3	4.04	4.18	3.70	4.98
Repeat 4	3.99	4.28	4.09	4.71
Repeat 5	3.05	3.52	4.06	4.57
Average	<b>3.53</b>	<b>3.97</b>	<b>4.09</b>	<b>4.49</b>
Standard deviation	0.41	0.38	0.22	0.36
	Stacking			
Repeat 1	0.68	1.59	0.71	1.70
Repeat 2	0.72	1.30	0.77	1.48
Repeat 3	0.95	1.40	0.92	0.88
Repeat 4	0.53	1.34	0.97	2.01
Repeat 5	0.74	1.59	0.83	2.03
Average	<b>0.726</b>	<b>1.44</b>	<b>0.840</b>	<b>1.62</b>
Standard deviation	0.135	0.13	0.097	0.42

**Table S9.** Number of contacts per oligonucleotide strand with arginine residues, as computed with atomistic simulations. Results are categorised by mode of interaction per nucleobase for a given peptide/nucleic acid combination. Each value in a repeat is an average value for all oligonucleotide chains of that peptide/oligonucleotide mixture over time.

Number of contacts	R <sub>3</sub> /DNA <sub>8</sub>			
	A	C	G	T
	<b>H-bonding</b>			
Repeat 1	1.29	2.68	2.27	2.08
Repeat 2	1.12	2.75	1.64	1.78
Repeat 3	0.99	2.54	3.05	2.24
Repeat 4	1.16	2.90	2.21	1.88
Repeat 5	1.08	2.62	1.90	1.96
Average	<b>1.13</b>	<b>2.70</b>	<b>2.22</b>	<b>1.99</b>
SEM	0.10	0.12	0.48	0.16
	<b>Ionic</b>			
Repeat 1	0.33	0.94	0.86	1.06
Repeat 2	0.62	1.00	0.77	0.98
Repeat 3	0.73	0.93	1.17	1.20
Repeat 4	0.63	0.83	1.25	1.28
Repeat 5	0.37	0.79	0.89	1.00
Average	<b>0.54</b>	<b>0.90</b>	<b>0.99</b>	<b>1.10</b>
SEM	0.16	0.08	0.19	0.12
	<b>Stacking</b>			
Repeat 1	0.33	0.12	0.08	0.15
Repeat 2	0.32	0.18	0.15	0.07
Repeat 3	0.24	0.14	0.38	0.19
Repeat 4	0.16	0.14	0.11	0.13
Repeat 5	0.27	0.14	0.19	0.14
Average	<b>0.27</b>	<b>0.14</b>	<b>0.18</b>	<b>0.14</b>
SEM	0.06	0.02	0.11	0.04

Number of contacts	R <sub>3</sub> /RNA <sub>8</sub>			
	A	C	G	U
	<b>H-bonding</b>			
Repeat 1	1.00	3.27	3.26	2.76
Repeat 2	1.30	2.61	2.79	2.36
Repeat 3	1.22	3.00	3.58	3.37
Repeat 4	1.43	2.59	2.52	2.84
Repeat 5	1.26	2.81	3.70	2.81
Average	<b>1.24</b>	<b>2.86</b>	<b>3.17</b>	<b>2.83</b>
SEM	0.14	0.25	0.45	0.32
	<b>Ionic</b>			
Repeat 1	0.86	0.82	0.75	1.09
Repeat 2	0.74	1.24	1.12	1.27
Repeat 3	0.77	0.96	1.36	1.09
Repeat 4	0.50	1.25	1.12	1.41
Repeat 5	0.58	0.87	0.92	1.15
Average	<b>0.69</b>	<b>1.03</b>	<b>1.05</b>	<b>1.20</b>
SEM	0.13	0.18	0.21	0.12
	<b>Stacking</b>			
Repeat 1	0.34	0.42	0.49	0.34
Repeat 2	0.34	0.38	0.37	0.20
Repeat 3	0.40	0.24	0.51	0.25
Repeat 4	0.24	0.34	0.45	0.32
Repeat 5	0.44	0.29	0.55	0.31
Average	<b>0.35</b>	<b>0.33</b>	<b>0.47</b>	<b>0.29</b>
SEM	0.07	0.06	0.06	0.05



Number of contacts	R <sub>4</sub> /DNA <sub>8</sub>			
	A	C	G	T
	H-bonding			
Repeat 1	1.18	3.59	2.24	2.34
Repeat 2	1.77	3.41	2.92	2.39
Repeat 3	1.19	2.73	2.46	2.33
Repeat 4	1.35	2.66	2.61	2.54
Repeat 5	1.08	3.26	2.75	2.60
Average	<b>1.31</b>	<b>3.13</b>	<b>2.59</b>	<b>2.44</b>
SEM	0.24	0.37	0.23	0.11
	Ionic			
Repeat 1	0.58	1.16	1.11	1.43
Repeat 2	0.58	1.24	1.21	1.28
Repeat 3	0.46	0.78	1.33	1.13
Repeat 4	0.68	0.68	1.54	1.20
Repeat 5	0.52	1.02	1.25	1.26
Average	<b>0.56</b>	<b>0.98</b>	<b>1.29</b>	<b>1.26</b>
SEM	0.07	0.22	0.14	0.10
	Stacking			
Repeat 1	0.26	0.15	0.14	0.16
Repeat 2	0.26	0.16	0.25	0.11
Repeat 3	0.29	0.22	0.26	0.15
Repeat 4	0.36	0.20	0.24	0.17
Repeat 5	0.30	0.20	0.24	0.09
Average	<b>0.29</b>	<b>0.18</b>	<b>0.23</b>	<b>0.14</b>
SEM	0.04	0.03	0.04	0.03

Number of contacts	R <sub>4</sub> /RNA <sub>8</sub>			
	A	C	G	U
	H-bonding			
Repeat 1	1.20	3.05	3.50	3.31
Repeat 2	1.61	2.41	3.78	3.14
Repeat 3	1.58	3.01	4.01	3.20
Repeat 4	1.62	4.05	2.89	3.12
Repeat 5	1.53	3.50	3.58	2.81
Average	<b>1.51</b>	<b>3.20</b>	<b>3.55</b>	<b>3.12</b>
SEM	0.16	0.55	0.38	0.17
	Ionic			
Repeat 1	0.47	1.11	1.13	1.24
Repeat 2	0.62	1.18	0.97	1.47
Repeat 3	0.73	1.33	1.32	1.60
Repeat 4	0.66	1.40	1.31	1.34
Repeat 5	0.63	1.12	1.37	1.45
Average	<b>0.62</b>	<b>1.23</b>	<b>1.22</b>	<b>1.42</b>
SEM	0.09	0.12	0.15	0.12
	Stacking			
Repeat 1	0.40	0.24	0.61	0.45
Repeat 2	0.26	0.32	0.57	0.33
Repeat 3	0.16	0.21	0.30	0.22
Repeat 4	0.45	0.44	0.52	0.61
Repeat 5	0.33	0.41	0.67	0.62
Average	<b>0.32</b>	<b>0.33</b>	<b>0.53</b>	<b>0.45</b>
SEM	0.10	0.09	0.13	0.16

**Table S10.** Number of total contacts per oligonucleotide strand with arginine residues, as computed with atomistic simulations. The number of contacts established with unique arginine residues or unique peptide chains is also specified. Each value in a repeat is an average value for all oligonucleotide chains of that peptide/oligonucleotide mixture over time.

Number of contacts	Mixture			
	R <sub>3</sub> /DNA <sub>8</sub>	R <sub>3</sub> /RNA <sub>8</sub>	R <sub>4</sub> /DNA <sub>8</sub>	R <sub>4</sub> /RNA <sub>8</sub>
	Total contacts			
Repeat 1	12.19	15.40	14.33	16.71
Repeat 2	11.37	14.72	15.55	16.66
Repeat 3	13.81	16.75	13.34	17.68
Repeat 4	12.66	15.00	14.23	18.40
Repeat 5	11.35	15.70	14.58	18.01
<b>Average</b>	<b>12.3</b>	<b>15.5</b>	<b>14.4</b>	<b>17.5</b>
Standard deviation	0.9	0.7	0.7	0.7
	With unique arginine residues			
Repeat 1	6.30	7.43	7.46	8.25
Repeat 2	6.09	6.93	8.35	7.51
Repeat 3	7.36	7.61	7.38	8.61
Repeat 4	6.90	7.03	7.46	8.55
Repeat 5	5.83	6.90	7.81	8.45
<b>Average</b>	<b>6.50</b>	<b>7.18</b>	<b>7.69</b>	<b>8.28</b>
Standard deviation	0.56	0.29	0.36	0.40
	With unique peptide chains			
Repeat 1	3.88	4.42	3.99	4.01
Repeat 2	3.97	4.14	3.96	3.90
Repeat 3	4.45	4.55	3.73	4.61
Repeat 4	4.35	4.28	3.54	4.40
Repeat 5	3.52	4.10	3.72	4.22
<b>Average</b>	<b>4.03</b>	<b>4.30</b>	<b>3.79</b>	<b>4.23</b>
Standard deviation	0.34	0.17	0.17	0.25

**Table S11.** Number of free peptide chains for a given mixture, as computed with atomistic simulations. Each value in a repeat is an average value for all oligonucleotide chains of that peptide/oligonucleotide mixture over time.

Number of free peptides	Mixture			
	R <sub>3</sub> /DNA <sub>8</sub>	R <sub>3</sub> /RNA <sub>8</sub>	R <sub>4</sub> /DNA <sub>8</sub>	R <sub>4</sub> /RNA <sub>8</sub>
Repeat 1	12.5	11.4	13.7	10.6
Repeat 2	14.2	8.9	11.2	11.1
Repeat 3	11.1	11.2	12.8	12.3
Repeat 4	10.6	11.0	12.1	11.8
Repeat 5	11.2	10.7	11.7	8.8
Average	<b>11.9</b>	<b>10.6</b>	<b>12.3</b>	<b>10.9</b>
Standard deviation	1.3	0.9	0.9	1.2

**Table S12.** Partition coefficients calculated from confocal fluorescence microscopy images.  $K_p$  values were calculated from fluorescence intensities measured using Fiji.

Peptide	Oligonucleotide	Probe	$I_{in}$	$I_{out}$	$K_p$	N
R <sub>4</sub>	DNA <sub>8</sub>	FAM-DNA <sub>8</sub>	12672.9	898.9	20.3 ± 4.85	201
R <sub>4</sub>	RNA <sub>8</sub>	FAM-DNA <sub>8</sub>	10117.3	1805.5	15.3 ± 3.6	308
R <sub>4</sub>	DNA <sub>8</sub>	FAM-RNA <sub>8</sub>	15148.5	1767.7	21.0 ± 5.5	214
R <sub>4</sub>	RNA <sub>8</sub>	FAM-RNA <sub>8</sub>	11540.0	1449.1	20.5 ± 3.6	363
R <sub>8</sub>	DNA <sub>8</sub>	FITC-R <sub>8</sub>	40.4	2.06	19.9 ± 9.4	519
R <sub>8</sub>	RNA <sub>8</sub>	FITC-R <sub>8</sub>	37.0	1.5	24.9 ± 10.4	365
R <sub>4</sub>	DNA <sub>8</sub>	Broccoli aptamer	1917.9	125.6	15.3 ± 8.3	59
R <sub>4</sub>	RNA <sub>8</sub>	Broccoli aptamer	2704.9	249.1	11.6 ± 3.0	366
R <sub>4</sub>	DNA <sub>16</sub>	Broccoli aptamer	2797.3	224.4	11.1 ± 5.8	307
R <sub>10</sub>	E <sub>10</sub>	Broccoli aptamer	4825.2	175.6	30.8 ± 11.3	321
R <sub>3</sub>	DNA <sub>12</sub>	Cy <sub>3</sub> -A <sub>11</sub>	5062.7	262.1	19.1 ± 5.9	120
		Cy <sub>3</sub> -A <sub>31</sub>	12193.2	517.5	23.5 ± 7.8	180
		Cy <sub>3</sub> -A <sub>51</sub>	12837.7	642.3	20.1 ± 7.2	197
R <sub>4</sub>	DNA <sub>8</sub>	Cy <sub>3</sub> -A <sub>11</sub>	14126.5	547.5	25.8 ± 10.3	331
		Cy <sub>3</sub> -A <sub>31</sub>	18301.1	672.2	26.8 ± 9.0	330
		Cy <sub>3</sub> -A <sub>51</sub>	14905.3	480.5	32.5 ± 11.5	324
R <sub>4</sub>	DNA <sub>8</sub>	Mg Green, 0 mM Mg <sup>2+</sup>	3848.0	6651.0	0.58	-
R <sub>4</sub>	RNA <sub>8</sub>	Mg Green, 0 mM Mg <sup>2+</sup>	2756.4	4383.3	0.63	-
R <sub>10</sub>	E <sub>10</sub>	Mg Green, 0 mM Mg <sup>2+</sup>	786.1	3409.5	0.23	-
R <sub>4</sub>	DNA <sub>8</sub>	Mg Green, 5 mM Mg <sup>2+</sup>	4122.8	8821.8	0.47	-
R <sub>4</sub>	RNA <sub>8</sub>	Mg Green, 5 mM Mg <sup>2+</sup>	2617.9	6242.7	0.42	-
R <sub>10</sub>	E <sub>10</sub>	Mg Green, 5 mM Mg <sup>2+</sup>	443.3	3919.1	0.11	-
R <sub>3</sub>	DNA <sub>12</sub>	Cy3-8nt	29.6	0.1	133.3 ± 54.9	133
		Cy3-16nt	49.3	0.4	108.3 ± 67.2	171
		Cy3-32nt	47.6	1.1	52.9 ± 16.9	209
R <sub>4</sub>	DNA <sub>8</sub>	Cy3-8nt	72.3	1.8	38.9 ± 13.3	106
		Cy3-16nt	64.8	1.6	46.2 ± 17.8	131
		Cy3-32nt	38.8	1.7	33.9 ± 15.1	175
R <sub>4</sub>	DNA <sub>16</sub>	Cy3-8nt	32.2	1.8	19.1 ± 4.6	124
		Cy3-16nt	26.9	0.7	45.1 ± 19.5	89
		Cy3-32nt	25.4	1.8	13.4 ± 4.6	124
R <sub>8</sub>	DNA <sub>16</sub>	Cy3-8nt	26.4	0.4	61.4 ± 21.3	122
		Cy3-16nt	23.2	2.2	11.9 ± 4.7	209
		Cy3-32nt	18.3	0.4	42.6 ± 27.1	135
R <sub>4</sub>	RNA <sub>8</sub>	Cy3-8nt	40.5	1.3	30.4 ± 10.5	98
R <sub>4</sub>	dsDNA <sub>8</sub> <sup>a</sup>	Cy3-8nt	33.4	0.7	48.5 ± 16.6	40
R <sub>10</sub>	dA <sub>10</sub>	Cy3-dA <sub>11</sub>	58.4	0.7	83.1 ± 31.1	115
R <sub>10</sub>	dT <sub>10</sub>	Cy3-dA <sub>11</sub>	53.2	2.1	25.4 ± 8.2	172

R <sub>10</sub>	dC <sub>10</sub>	Cy3-dA <sub>11</sub>	60.1	1.6	36.9 ± 12.5	181
R <sub>10</sub>	DNA <sub>10</sub>	Cy3-dA <sub>11</sub>	138.1	2.4	15.9 ± 4.5	139

<sup>a</sup> ds denotes double-stranded DNA, prepared with DNA<sub>8</sub> and DNA<sub>8</sub>\* oligonucleotides.

**Table S13.** Parameters obtained from fitting FRAP profiles to the exponential decay:  $y = y_0 + A_1e^{-t/\tau}$ , where  $y$  is the normalised fluorescence and  $t$  is the time since photobleaching.


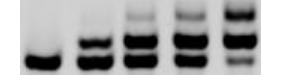

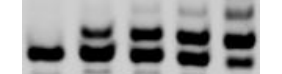
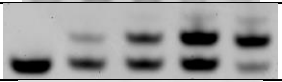
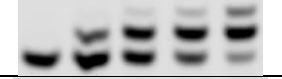
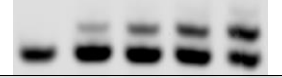
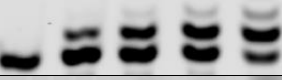
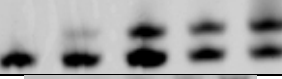
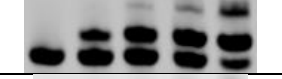


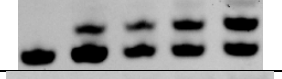
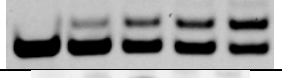

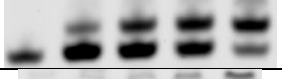
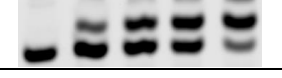
Peptide	Oligonucleotide	Probe	$y_0$	$A_1$	$\tau$ (s)	$R^2$
R <sub>3</sub>	DNA <sub>12</sub> <sup>a</sup>	Cy3-8nt	0.96	-1.13	5.86	0.996
		Cy3-16nt	0.78	-0.79	6.73	0.994
		Cy3-32nt	0.55	-0.84	5.17	0.999
R <sub>4</sub>	DNA <sub>8</sub> <sup>a</sup>	Cy3-8nt	0.78	-1.16	10.06 ± 5.02 <sup>a</sup>	0.999
		Cy3-16nt	0.68	-1.08	6.64	0.999
		Cy3-32nt	0.60	-0.85	7.83	0.999
R <sub>4</sub>	DNA <sub>8</sub> :RNA <sub>8</sub> 1:1 <sup>a</sup>	Cy3-8nt	0.72	-0.66	26.24	0.995
R <sub>4</sub>	RNA <sub>8</sub> <sup>a</sup>	Cy3-8nt	0.56	-0.46	61.5 ± 4.7	0.998
R <sub>4</sub>	dsDNA <sub>8</sub> <sup>a</sup>	Cy3-8nt	0.96	-0.92	8.9	0.999
		Cy3-16nt	0.55	-0.35	10.6	0.980
R <sub>4</sub>	DNA <sub>12</sub> <sup>b</sup>	Cy3-8nt	0.83	-0.79	13.14	0.996
R <sub>4</sub>	DNA <sub>16</sub> <sup>a</sup>	Cy3-8nt	0.79	-0.76	18.25	0.999
		Cy3-16nt	0.69	-0.60	26.06	0.999
		Cy3-32nt	0.66	-0.54	25.97	0.996
R <sub>6</sub>	dA <sub>12</sub> <sup>b</sup>	Cy3-8nt	0.76	-0.90	4.93 ± 0.89	0.864
R <sub>6</sub>	mA <sub>12</sub> (dA <sub>12</sub> :rA <sub>12</sub> 1:1) <sup>b</sup>	Cy3-8nt	0.75	-0.71	12.69	0.973
R <sub>6</sub>	dA <sub>3</sub> :rA <sub>12</sub> 1:1 <sup>b</sup>	Cy3-8nt	0.70	-0.77	12.46	0.861
R <sub>6</sub>	rA <sub>12</sub> <sup>a</sup>	Cy3-8nt	0.63	-0.53	27.77	0.945
R <sub>6</sub>	rA <sub>12</sub> <sup>b</sup>	Cy3-8nt	0.44	-0.30	35.79 ± 2.82	0.951
R <sub>6</sub>	rA <sub>12</sub> <sup>b,c</sup>	Cy3-8nt	0.61	-0.49	23.49	0.937
R <sub>6</sub>	DNA <sub>12</sub> <sup>b</sup>	Cy3-8nt	0.42	-0.24	78.77	0.840
R <sub>6</sub>	Arich <sub>12</sub> <sup>b</sup>	Cy3-8nt	0.76	-0.74	14.56	0.993
R <sub>6</sub>	dA <sub>16</sub> <sup>b</sup>	Cy3-8nt	0.84	-1.30	4.27	0.850
R <sub>6</sub>	rA <sub>16</sub> <sup>b</sup>	Cy3-8nt	0.46	-0.37	45.81	0.988
R <sub>8</sub>	DNA <sub>16</sub> <sup>a</sup>	Cy3-8nt	0.60	-0.41	61.95	0.999
		Cy3-16nt	0.53	-0.37	80.62	0.999
		Cy3-32nt	0.47	-0.30	94.68	0.999
R <sub>10</sub>	dA <sub>10</sub> <sup>a</sup>	Cy3-dA11	0.69	-1.18	3.36	0.994
R <sub>10</sub>	dT <sub>10</sub> <sup>a</sup>	Cy3-dA11	0.64	-0.53	9.70	0.995
R <sub>10</sub>	dC <sub>10</sub> <sup>a</sup>	Cy3-dA11	0.63	-0.63	6.15	0.999
R <sub>10</sub>	DNA <sub>10</sub> <sup>a</sup>	Cy3-dA11	0.72	-0.60	28.5	0.998

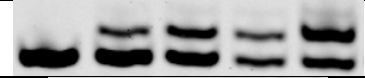
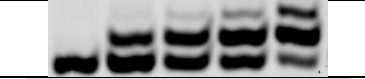

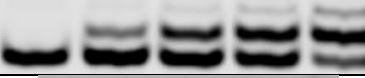
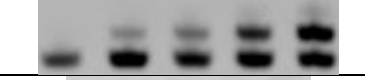
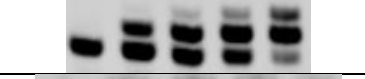
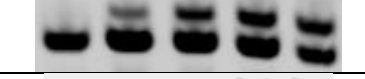

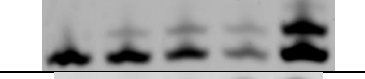
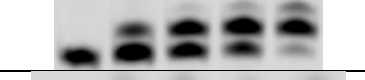

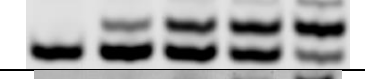
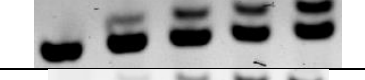
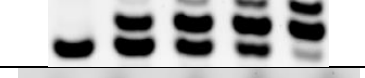

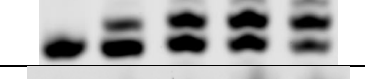
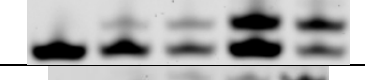
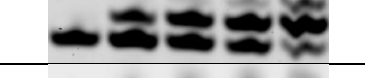

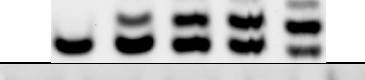
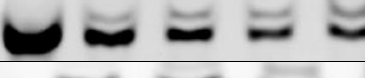
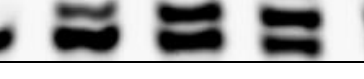
<sup>a</sup> [Arg] = 20 mM, [nt] = 5 mM

<sup>b</sup> [Arg] = 20 mM, [nt] = 10 mM

<sup>c</sup> 50mM [NaCl]

**Table S14.** Representative denaturing polyacrylamide gel image of PE in primitive coacervates. A = w/ peptide, no NaCl (coacervates); B = no peptide, no NaCl; C = w/ peptide, w/ NaCl; D = no peptide, w/ NaCl.

Mixture	Conditions	0h, 1h, 3h, 6h, 24h
R <sub>4</sub> /dA <sub>12</sub> 40:5 [Arg]:[nt]	A	
	B	
	C	
	D	
R <sub>6</sub> /dA <sub>12</sub> 20:10 [Arg]:[nt] <sup>a</sup>	A	
	B	
	C	
	D	
R <sub>6</sub> /dA <sub>12</sub> 20:10 [Arg]:[nt]	A	
	B	
	C	
	D	
R <sub>6</sub> /rA <sub>12</sub> 20:10 [Arg]:[nt] <sup>a</sup>	A	
	A (+ 50 mM NaCl)	
	B	
	C	
	D	

R <sub>6</sub> /mA <sub>12</sub> 20:10 [Arg]:[nt] <sup>a</sup>	A	
	B	
	C	
	D	
R <sub>6</sub> /dA <sub>12</sub> 40:5 [Arg]:[nt] <sup>a</sup>	A	
	B	
	C	
	D	
R <sub>6</sub> /rA <sub>12</sub> 40:5 [Arg]:[nt] <sup>a</sup>	A	
	B	
	C	
	D	
R <sub>6</sub> /mA <sub>12</sub> 40:5 [Arg]:[nt] <sup>a</sup>	A	
	B	
	C	
	D	
R <sub>6</sub> /dA <sub>16</sub> 20:10 [Arg]:[nt] <sup>a</sup>	A	
	B	
	C	
	D	
R <sub>6</sub> /rA <sub>16</sub> 20:10 [Arg]:[nt] <sup>a</sup>	A	
	B	



	C	
	D	
R <sub>4</sub> /dT <sub>16</sub> 20:10 [Arg]:[nt]	A	
	B	
	C	
	D	
R <sub>6</sub> /dT <sub>16</sub> 20:10 [Arg]:[nt]	A	
	B	
	C	
	D	
R <sub>4</sub> /DNA <sub>12</sub> 20:10 [Arg]:[nt]	A	
	B	
	C	
	D	
R <sub>4</sub> /DNA <sub>12</sub> 40:5 [Arg]:[nt] <sup>a</sup>	A	
	B	
	C	
	D	
R <sub>4</sub> /DNA <sub>12</sub> 40:5 [Arg]:[nt]	A	
	B	
	C	
	D	

R <sub>6</sub> /DNA <sub>12</sub> 20:10 [Arg]:[nt] <sup>a</sup>	A	
	B	
	C	
	D	
R <sub>6</sub> /DNA <sub>12</sub> 20:10 [Arg]:[nt]	A	
	B	
	C	
	D	
R <sub>6</sub> /DNA <sub>12</sub> 40:5 [Arg]:[nt]	A	
	B	
	C	
	D	
R <sub>4</sub> /RNA <sub>12</sub> 40:5 [Arg]:[nt] <sup>a</sup>	A	
	B	
	C	
	D	
R <sub>4</sub> /RNA <sub>12</sub> 40:5 [Arg]:[nt]	A	
	B	
	C	
	D	
R <sub>6</sub> /RNA <sub>12</sub> 20:10 [Arg]:[nt]	A	
	B	

	C	
	D	
R <sub>6</sub> /RNA <sub>12</sub> 40:5 [Arg]:[nt]	A	
	B	
	C	
	D	
R <sub>6</sub> /Arich <sub>12</sub> 20:10 [Arg]:[nt] <sup>a</sup>	A	
	B	
	C	
	D	
R <sub>6</sub> /Arich <sub>12</sub> 20:10 [Arg]:[nt]	A	
	B	
	C	
	D	
R <sub>6</sub> /Arich <sub>12</sub> 40:5 [Arg]:[nt] <sup>a</sup>	A	
	B	
	C	
	D	
Control (no host) <sup>a</sup>	B	
	D	
Control (no host, w/ R <sub>4</sub> )	A	
	B	

	C	
	D	
Control (no host, w/ R <sub>6</sub> )	A	
	C	

<sup>a</sup> reactions performed with a primer/template system that is complementary to the host RNA<sub>12</sub> sequence ((ACUG)<sub>3</sub>).

**Table S15.** Average values for primer extension yields as analysed by PAGE ( $n \geq 2$  replicates). A = w/ peptide, no NaCl (coacervates); B = no peptide, no NaCl; C = w/ peptide, w/ NaCl; D = no peptide, w/ NaCl.

		Extended primer (%)			
Mixture	Time	A	B	C	D
R <sub>4</sub> /dA <sub>12</sub> 40:5 [Arg]:[nt]	0 h	0.0	0.0	0.0	0.0
	1 h	3.7	20.9	3.1	12.6
	3 h	5.6	46.5	5.0	29.7
	6 h	8.1	65.5	6.7	46.2
	24 h	14.5	91.3	11.2	80.8
R <sub>6</sub> /dA <sub>12</sub> 20:10 [Arg]:[nt] <sup>a</sup>	0 h	0.0	0.0	0.0	0.0
	1 h	21.1	24.6	8.4	12.5
	3 h	43.7	50.1	16.9	28.8
	6 h	55.6	68.2	26.9	44.8
	24 h	78.5	87.3	49.4	74.6
R <sub>6</sub> /dA <sub>12</sub> 20:10 [Arg]:[nt]	0 h	0.0	0.0	0.0	0.0
	1 h	17.4	16.0	8.9	13.0
	3 h	31.1	36.0	16.3	31.4
	6 h	35.1	54.2	25.7	48.5
	24 h	65.0	86.0	50.4	82.1
R <sub>6</sub> /rA <sub>12</sub> 20:10 [Arg]:[nt] <sup>a</sup>	0 h	0.0	0.0	0.0	0.0
	1 h	15.3	35.5	16.4	18.6
	3 h	32.1	64.3	31.5	40.6
	6 h	42.8	77.8	46.9	58.6
	24 h	58.2	90.2	73.9	83.1
R <sub>6</sub> /rA <sub>12</sub> 20:10 [Arg]:[nt] <sup>a</sup> + 50 mM NaCl	0 h	0.0			
	1 h	13.9			
	3 h	24.8			
	6 h	32.0			
	24 h	47.9			
R <sub>6</sub> /mA <sub>12</sub> 20:10 [Arg]:[nt] <sup>a</sup>	0 h	0.0	0.0	0.0	0.0
	1 h	15.5	21.6	10.4	12.2
	3 h	31.8	47.0	22.7	29.0
	6 h	44.2	64.6	30.8	44.8
	24 h	63.6	86.6	56.9	75.3
R <sub>6</sub> /dA <sub>12</sub> 40:5 [Arg]:[nt] <sup>a</sup>	0 h	0.0	0.0	0.0	0.0
	1 h	13.6	24.4	7.8	9.5
	3 h	27.7	52.9	16.8	23.8
	6 h	36.1	67.2	24.3	37.6
	24 h	55.3	88.6	43.1	68.1
R <sub>6</sub> /rA <sub>12</sub> 40:5 [Arg]:[nt] <sup>a</sup>	0 h	0.0	0.0	0.0	0.0
	1 h	12.0	22.8	12.6	13.7
	3 h	22.3	49.8	20.7	33.2
	6 h	26.3	67.2	31.7	48.2
	24 h	36.9	88.6	49.7	53.3

R <sub>6</sub> /mA <sub>12</sub> 40:5 [Arg]:[nt] <sup>a</sup>	0 h	0.0	0.0	0.0	0.0
	1 h	8.3	33.7	10.3	19.8
	3 h	17.5	65.0	18.9	43.2
	6 h	24.2	81.8	27.4	59.8
	24 h	36.0	90.4	42.1	76.5
R <sub>6</sub> /dA <sub>16</sub> 20:10 [Arg]:[nt] <sup>a</sup>	0 h	0.0	0.0	0.0	0.0
	1 h	14.2	21.2	11.7	14.1
	3 h	28.5	45.7	22.3	33.3
	6 h	40.0	62.6	35.4	49.2
	24 h	63.1	83.5	57.2	76.6
R <sub>6</sub> /rA <sub>16</sub> 20:10 [Arg]:[nt] <sup>a</sup>	0 h	0.0	0.0	0.0	0.0
	1 h	10.5	19.3	7.8	15.2
	3 h	15.9	42.9	14.7	33.8
	6 h	22.0	60.6	22.5	49.6
	24 h	31.1	87.6	38.7	78.4
R <sub>4</sub> /dT <sub>16</sub> 20:10 [Arg]:[nt]	0 h	0.0	0.0	0.0	0.0
	1 h	6.6	18.6	6.1	14.9
	3 h	13.9	41.1	12.3	34.3
	6 h	22.2	60.7	19.5	52.5
	24 h	42.9	90.3	40.5	85.6
R <sub>6</sub> /dT <sub>16</sub> 20:10 [Arg]:[nt]	0 h	0.0	0.0	0.0	0.0
	1 h	11.7	17.2	8.8	14.6
	3 h	19.0	38.9	20.3	33.7
	6 h	27.0	58.9	31.2	51.5
	24 h	42.8	90.0	62.6	85.2
R <sub>4</sub> /DNA <sub>12</sub> 20:10 [Arg]:[nt]	0 h	0.0	0.0	0.0	0.0
	1 h	6.3	16.5	5.8	13.7
	3 h	12.4	37.2	12.0	31.6
	6 h	18.6	56.2	19.2	50.8
	24 h	32.1	88.1	40.9	83.5
R <sub>4</sub> /DNA <sub>12</sub> 40:5 [Arg]:[nt] <sup>a</sup>	0 h	0.0	0.0	0.0	0.0
	1 h	5.2	9.0	3.1	8.6
	3 h	5.2	20.1	4.8	19.3
	6 h	5.6	32.0	5.9	30.9
	24 h	7.7	55.1	11.5	55.3
R <sub>4</sub> /DNA <sub>12</sub> 40:5 [Arg]:[nt]	0 h	0.0	0.0	0.0	0.0
	1 h	3.3	14.6	4.7	13.2
	3 h	6.0	32.9	7.0	29.9
	6 h	8.5	52.7	10.4	45.9
	24 h	13.8	81.7	19.3	79.4
R <sub>6</sub> /DNA <sub>12</sub> 20:10 [Arg]:[nt] <sup>a</sup>	0 h	0.0	0.0	0.0	0.0
	1 h	6.3	7.0	7.5	7.9
	3 h	9.8	16.5	14.2	17.4
	6 h	10.9	26.8	21.0	28.8
	24 h	14.2	49.6	37.6	51.2

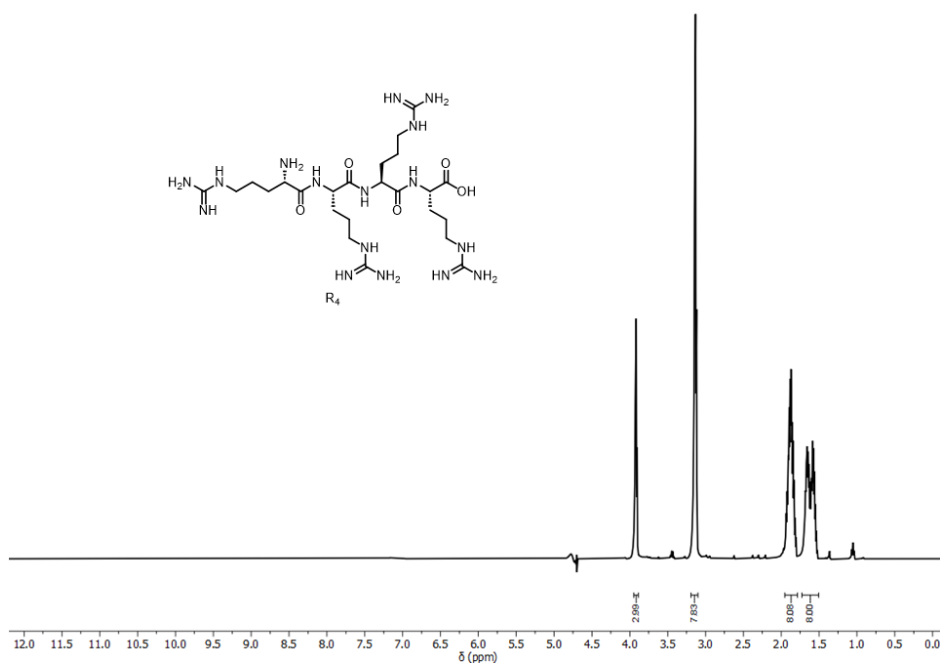
R <sub>6</sub> /DNA <sub>12</sub> 20:10 [Arg]:[nt]	0 h	0.0	0.0	0.0	0.0
	1 h	16.3	16.7	12.4	14.3
	3 h	28.4	38.1	21.6	33.6
	6 h	35.5	56.3	34.6	51.0
	24 h	41.7	87.8	61.6	78.2
R <sub>6</sub> /DNA <sub>12</sub> 40:5 [Arg]:[nt]	0 h	0.0	0.0	0.0	0.0
	1 h	10.1	15.4	5.6	16.1
	3 h	14.2	35.7	7.8	35.3
	6 h	15.7	53.1	10.0	51.5
	24 h	21.2	84.9	16.7	78.4
R <sub>4</sub> /RNA <sub>12</sub> 40:5 [Arg]:[nt] <sup>a</sup>	0 h	0.0	0.0	0.0	0.0
	1 h	0.0	0.0	0.0	0.0
	3 h	0.0	0.0	0.0	0.0
	6 h	0.0	0.0	0.0	0.0
	24 h	0.0	0.0	0.0	0.0
R <sub>4</sub> /RNA <sub>12</sub> 40:5 [Arg]:[nt]	0 h	0.0	0.0	0.0	0.0
	1 h	7.0	17.0	5.7	11.2
	3 h	8.4	36.3	6.7	25.7
	6 h	11.9	52.1	10.0	39.8
	24 h	16.2	82.9	17.6	74.3
R <sub>6</sub> /RNA <sub>12</sub> 20:10 [Arg]:[nt]	0 h	0.0	0.0	0.0	0.0
	1 h	17.5	18.8	15.4	15.3
	3 h	19.6	40.3	31.1	33.9
	6 h	23.5	59.0	43.8	52.7
	24 h	27.1	88.0	68.3	83.1
R <sub>6</sub> /RNA <sub>12</sub> 40:5 [Arg]:[nt]	0 h	0.0	0.0	0.0	0.0
	1 h	10.2	21.7	11.3	15.6
	3 h	12.4	47.5	21.2	34.9
	6 h	14.4	67.5	32.4	54.9
	24 h	23.0	82.9	52.0	84.6
R <sub>6</sub> /Arich <sub>12</sub> 20:10 [Arg]:[nt] <sup>a</sup>	0 h	0.0	0.0	0.0	0.0
	1 h	8.6	26.9	10.3	25.5
	3 h	16.3	52.9	21.3	55.4
	6 h	23.3	69.4	31.5	72.2
	24 h	36.3	85.5	56.0	93.4
R <sub>6</sub> /Arich <sub>12</sub> 20:10 [Arg]:[nt]	0 h	0.0	0.0	0.0	0.0
	1 h	8.8	11.7	6.8	15.2
	3 h	15.5	27.7	13.9	34.8
	6 h	18.4	44.6	22.2	52.3
	24 h	32.1	78.8	46.5	85.1
R <sub>6</sub> /Arich <sub>12</sub> 40:5 [Arg]:[nt] <sup>a</sup>	0 h	0.0	0.0	0.0	0.0
	1 h	8.3	25.1	7.0	12.1
	3 h	18.2	50.8	15.5	29.1
	6 h	23.1	67.4	24.6	44.3
	24 h	35.6	85.7	42.5	72.1

Control (no host) <sup>a</sup>	0 h		0.0		0.0
	1 h		20.9		11.1
	3 h		45.6		27.9
	6 h		61.0		42.5
	24 h		80.9		68.1
Control (no host, w/ R <sub>4</sub> )	0 h	0.0	0.0	0.0	0.0
	1 h	7.4	18.8	3.9	11.0
	3 h	10.6	41.1	9.2	25.1
	6 h	15.6	58.5	13.0	39.4
	24 h	30.3	89.7	23.5	75.3
Control (no host, w/ R <sub>6</sub> )	0 h	0.0	0.0	0.0	0.0
	1 h	38.8	18.8	12.2	11.0
	3 h	63.4	41.1	22.6	25.1
	6 h	86.2	58.5	34.5	39.4
	24 h	96.3	89.7	64.1	75.3

<sup>a</sup> reactions performed with a primer/template system that is complementary to the host RNA<sub>12</sub> sequence ((ACUG)<sub>3</sub>).



Supplementary Figures



**Fig. S1.** <sup>1</sup>H-NMR (500 MHz, D<sub>2</sub>O:H<sub>2</sub>O 9:1) spectrum of **R4** synthesised in-house.

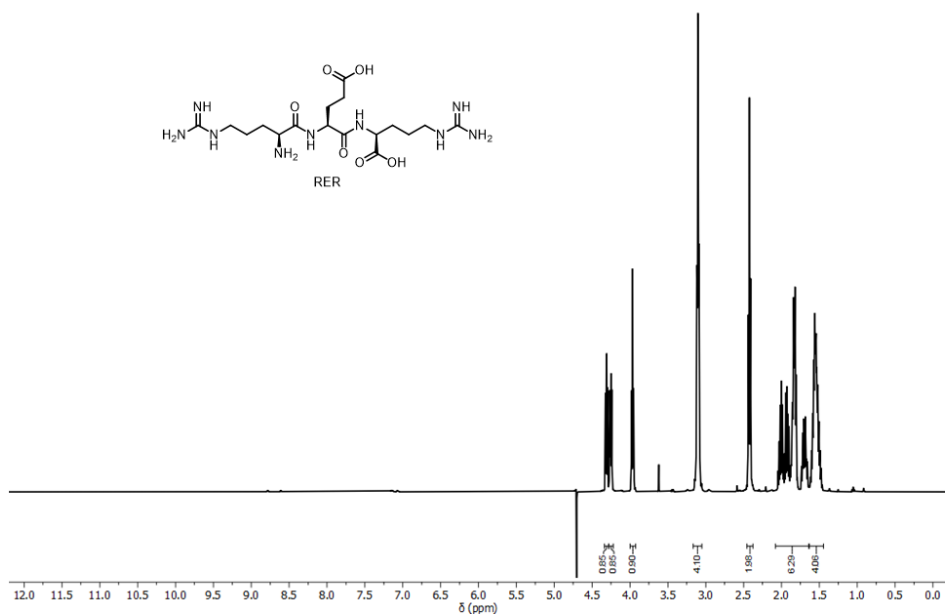
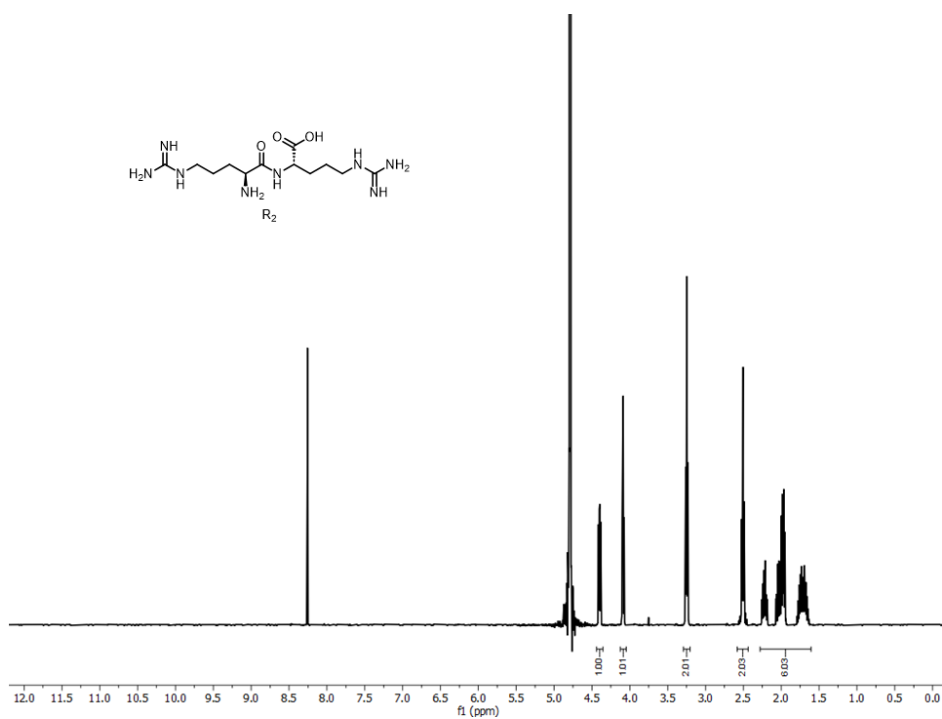
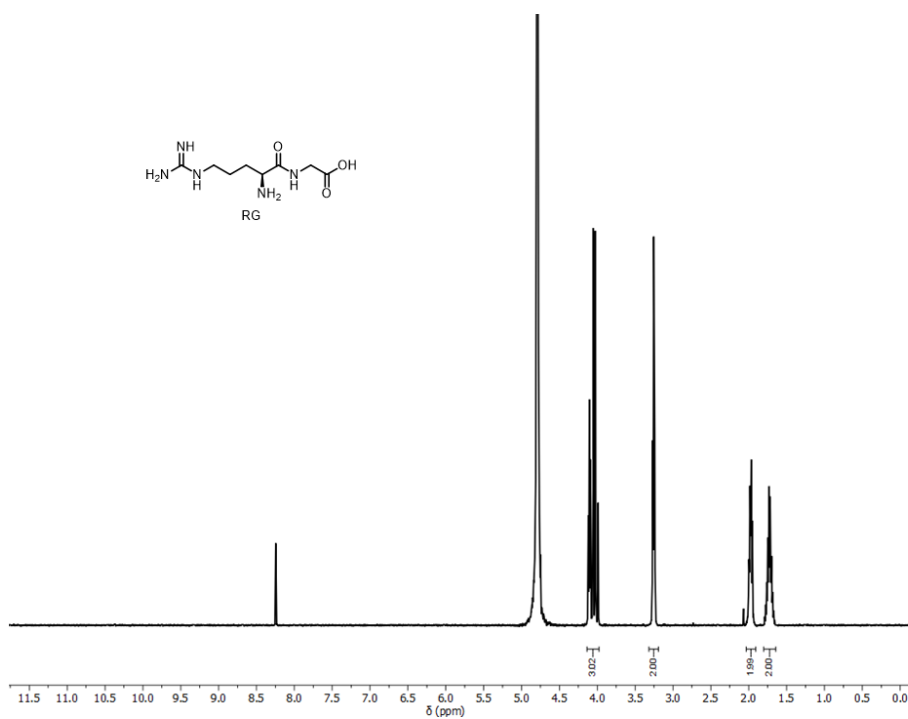


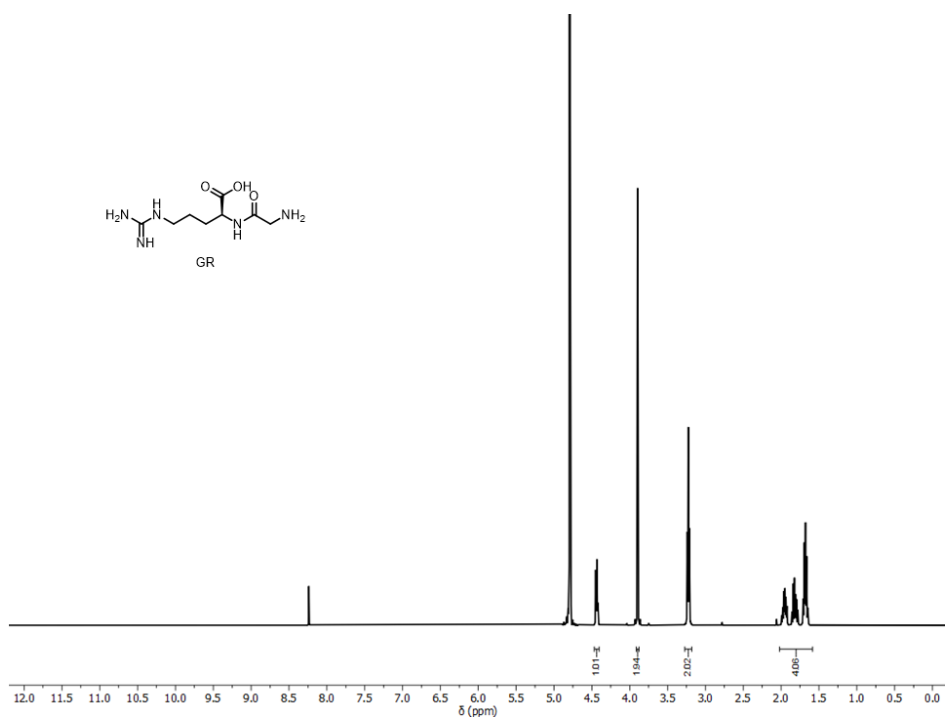
Fig. S2. <sup>1</sup>H-NMR (500 MHz, D<sub>2</sub>O:H<sub>2</sub>O 9:1) spectrum of RER synthesised in-house.



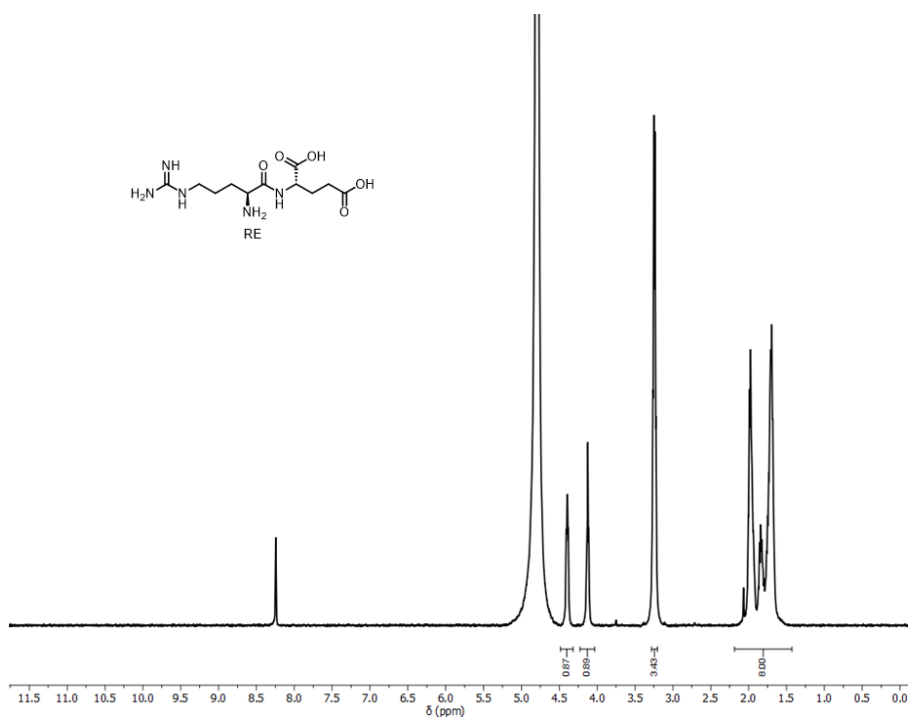
**Fig. S3.** <sup>1</sup>H-NMR (500 MHz, D<sub>2</sub>O:H<sub>2</sub>O 9:1) spectrum of **R**<sub>2</sub> synthesised in-house.



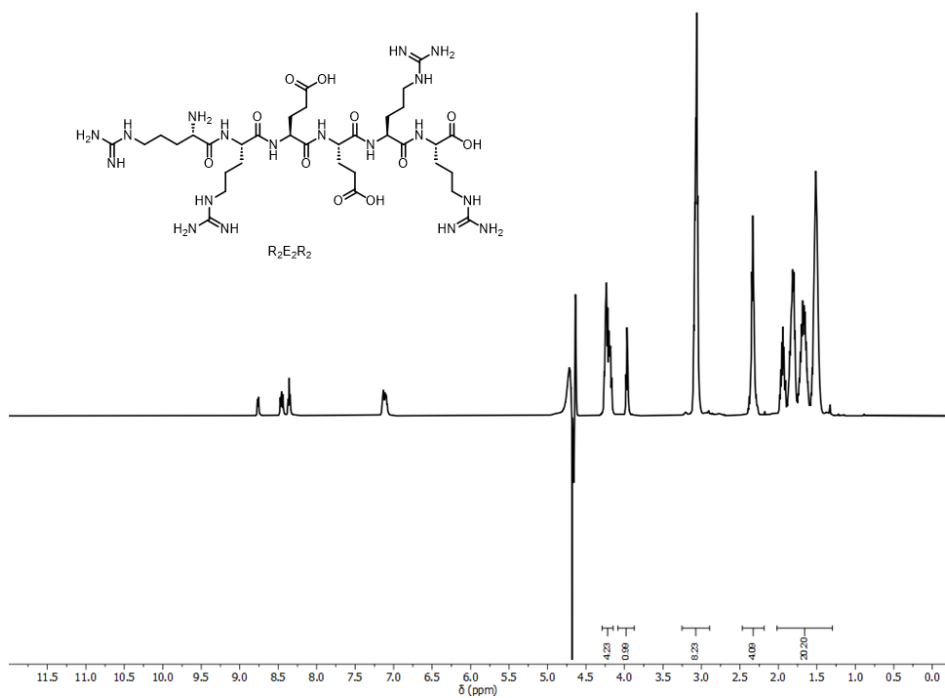
**Fig. S4.** <sup>1</sup>H-NMR (500 MHz, D<sub>2</sub>O:H<sub>2</sub>O 9:1) spectrum of RG synthesised in-house.



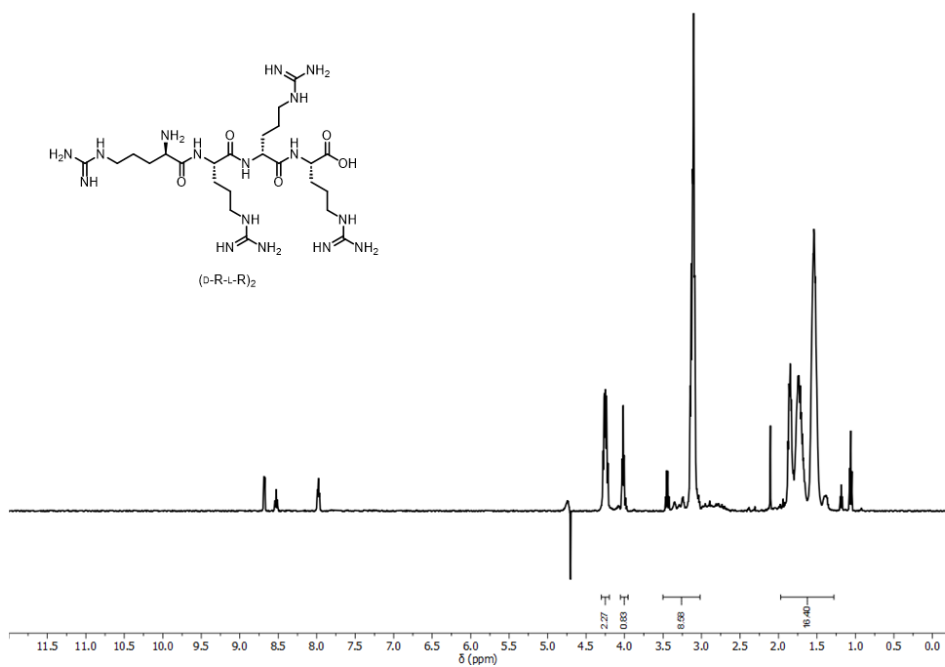
**Fig. S5.** <sup>1</sup>H-NMR (500 MHz, D<sub>2</sub>O:H<sub>2</sub>O 9:1) spectrum of GR synthesized in-house.



**Fig. S6.** <sup>1</sup>H-NMR (500 MHz, D<sub>2</sub>O:H<sub>2</sub>O 9:1) spectrum of RE synthesised in-house.



**Fig. S7.**  $^1H$ -NMR (500 MHz,  $D_2O:H_2O$  9:1) spectrum of  $R_2E_2R_2$  synthesised in-house.



**Fig. S8.** <sup>1</sup>H-NMR (500 MHz, D<sub>2</sub>O:H<sub>2</sub>O 9:1) spectrum of (D-R-L-R)<sub>2</sub> synthesised in-house.



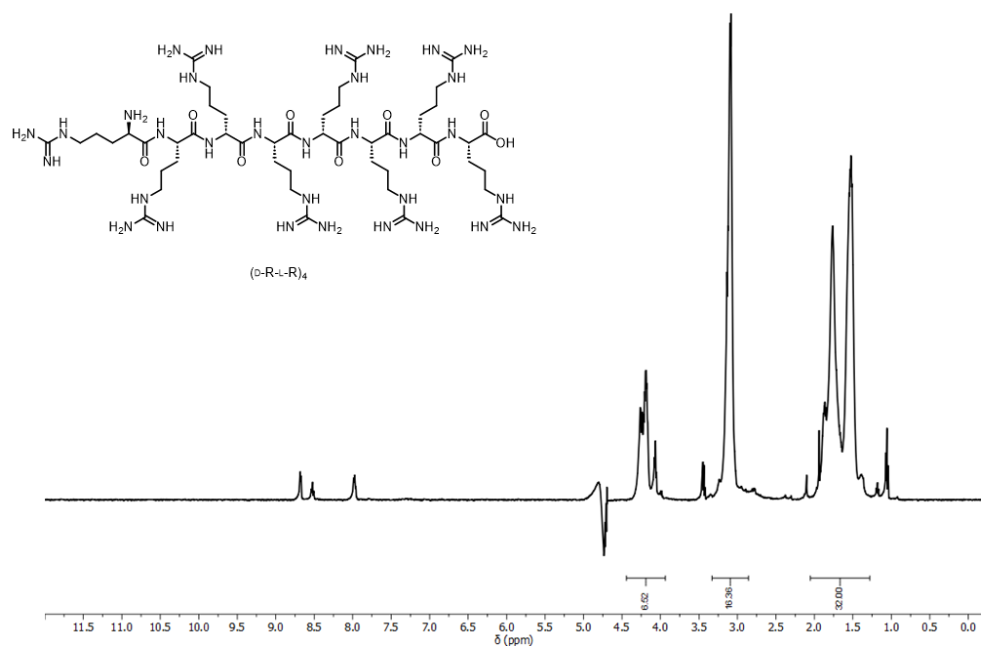
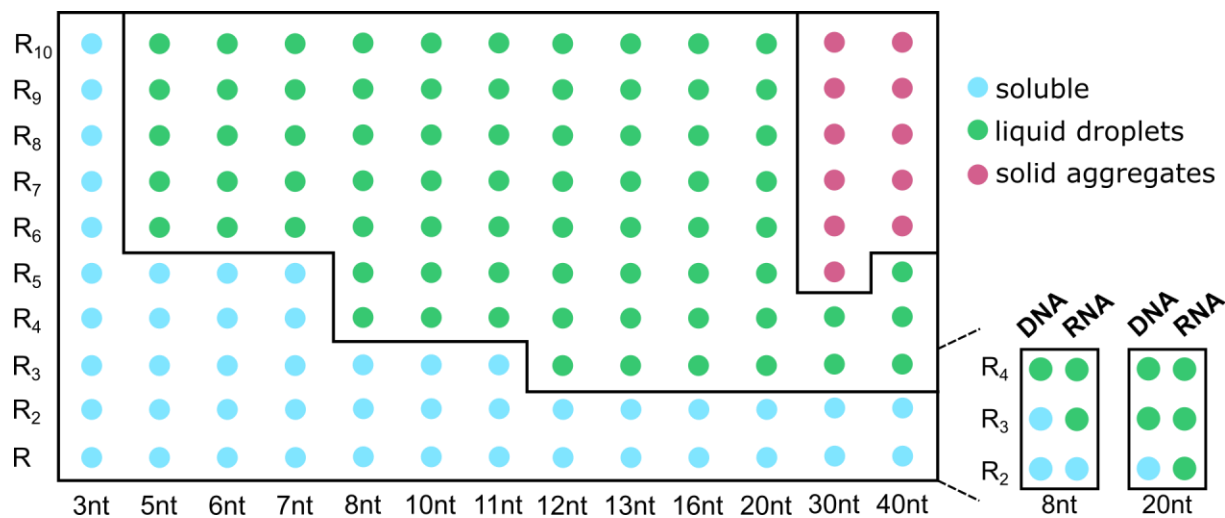
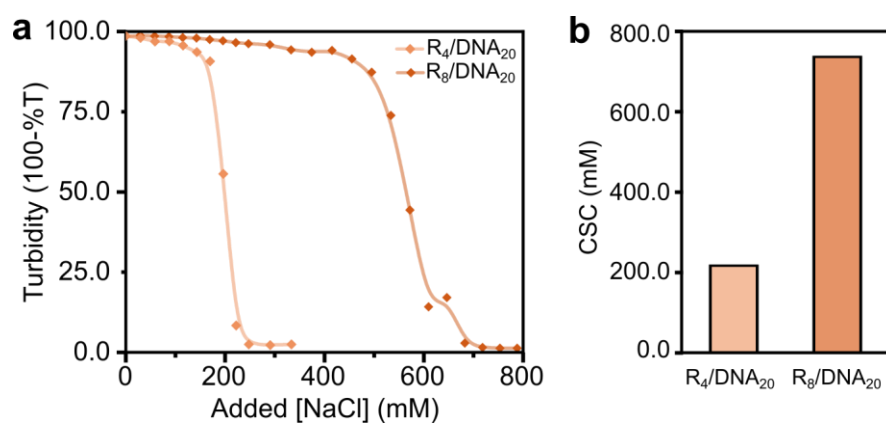


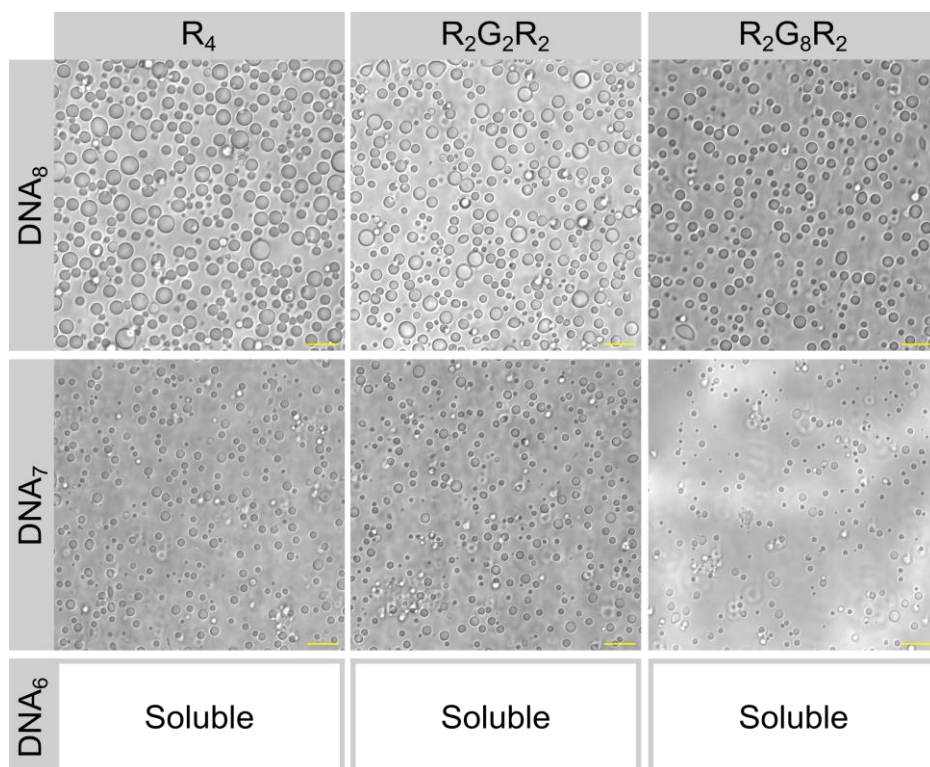
Fig. S9.  $^1H$ -NMR (500 MHz,  $D_2O:H_2O$  9:1) spectrum of  $(D-R-L-R)_4$  synthesised in-house.



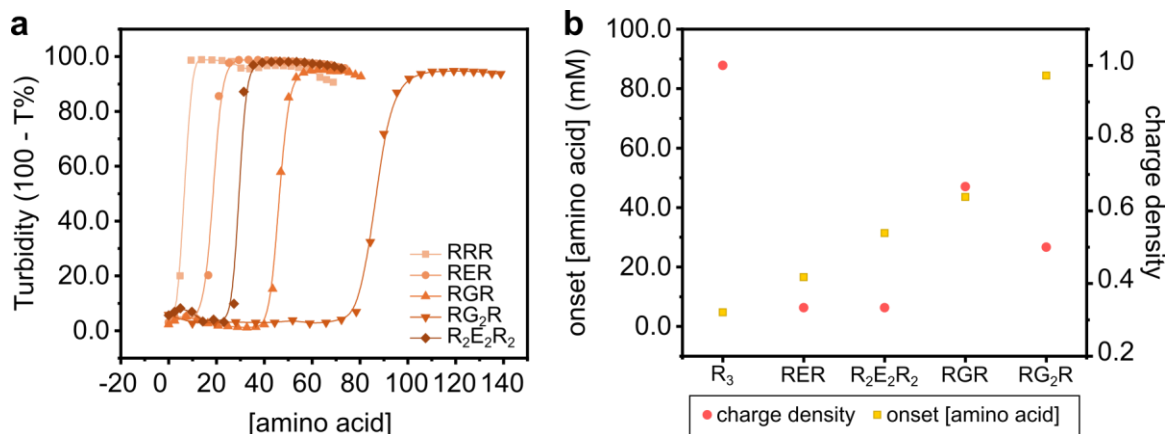
**Fig. S10.** Extended screening of peptide/DNA mixtures obtained by varying both peptide (vertical axis) and DNA lengths (horizontal axis). DNA sequences follow the motif ACTG, except for 3nt, which is dA<sub>3</sub>. The inset to the right shows the screening results with RNA oligonucleotides alongside those obtained with DNA oligonucleotides of the same length (and motif). The “liquid droplets” region (green) expands with RNA. All mixtures were screened at 20 mM amino acid, 5 mM nucleotide, 25 mM HEPES pH 7.4 and room temperature.



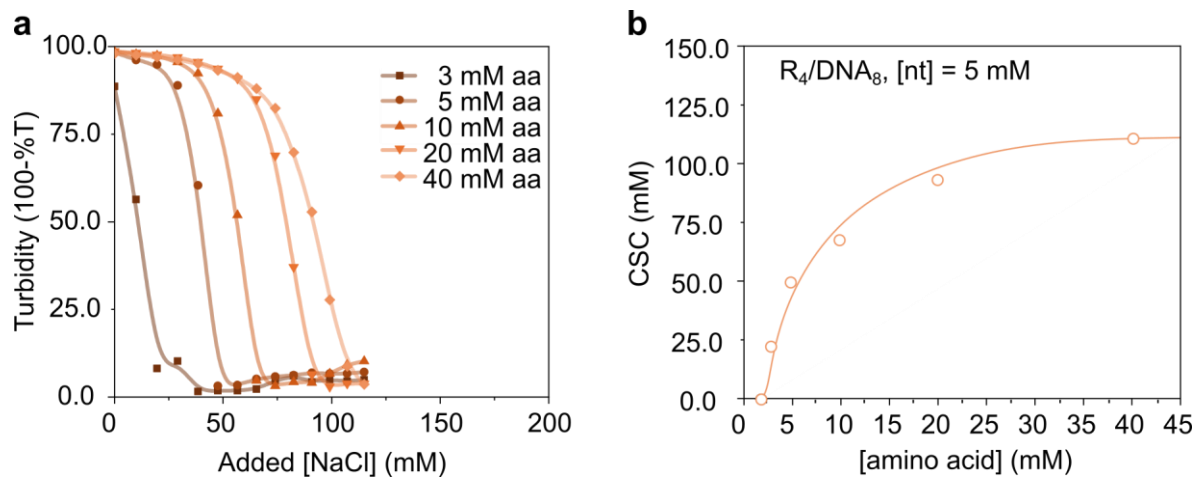
**Fig. S11.** (a) Salt titration curves used to determine the CSC values (b) for R<sub>4</sub>/DNA<sub>20</sub> and R<sub>8</sub>/DNA<sub>20</sub> at 20 mM arginine and 5 mM nucleotide concentrations.



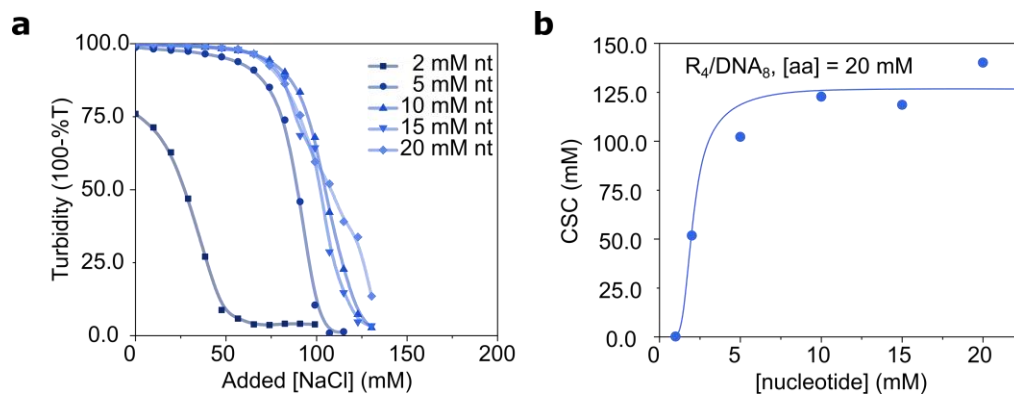
**Fig. S12.** Screening of minimal DNA oligonucleotide length required to form coacervates with a series of  $R_2G_NR_2$  peptides ( $N = 0, 2, 8$ ). Scale bar = 10  $\mu\text{m}$ , bright-field microscopy.



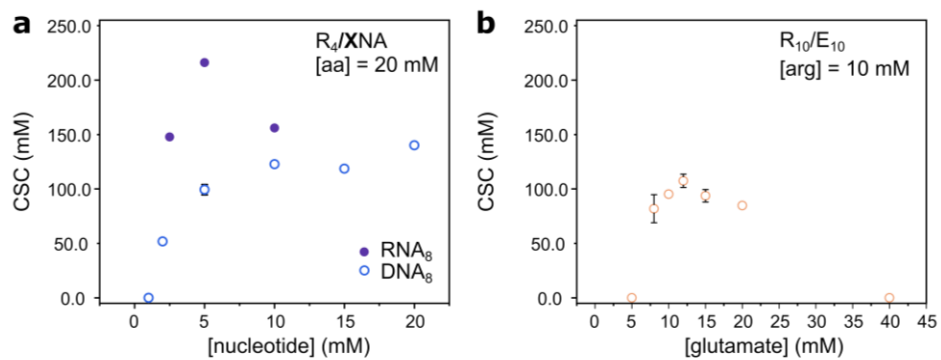
**Fig. S13. (a)** Extended data for the amino acid concentration leading to an onset of turbidity and, therefore, coacervation. All curves were recorded titrating a DNA<sub>16</sub> solution ([nt] = 10 mM) with concentrated stocks of t peptides in the legend. **(b)** Relation between the amino acid concentration at which turbidity sharply increases (onset [amino acid]) and peptide charge density. Onset amino acid concentrations measured are 4.8 mM (R<sub>3</sub>), 16.6 mM (RER), 31.4 mM (R<sub>2</sub>E<sub>2</sub>R<sub>2</sub>), 43.5 mM (RGR) and 84.4 mM (RG<sub>2</sub>R).



**Fig. S14.** (a) Salt titration curves of  $R_4/DNA_8$  mixtures at 5 mM nucleotide. These curves are used to determine (b) the phase diagram of the mixture. CSC values were measured at different amino acid concentrations.

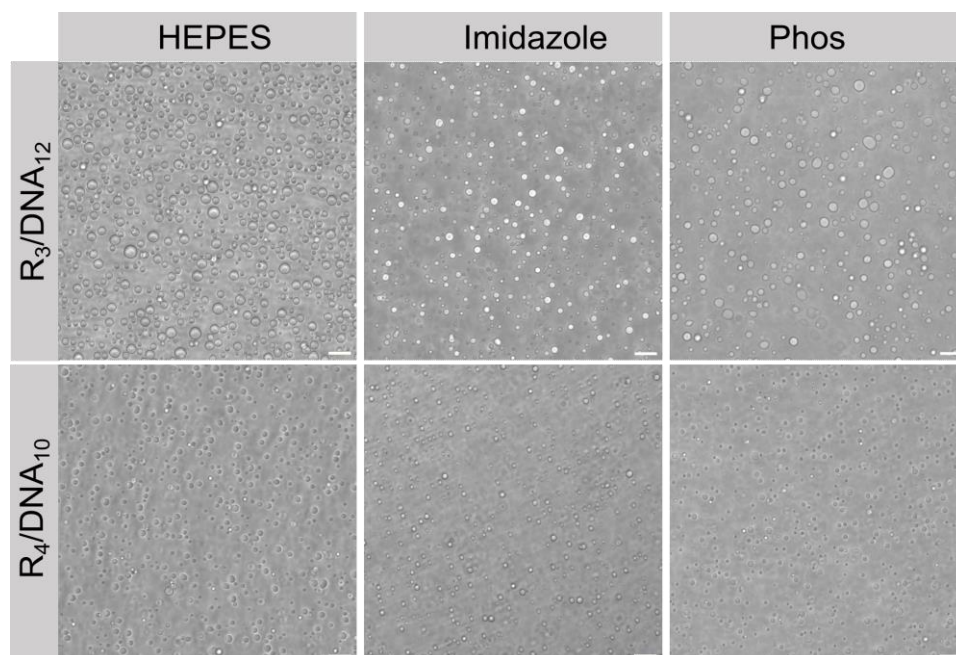


**Fig. S15. (a)** Salt titration curves of  $R_4/DNA_8$  mixtures at 20 mM amino acid. These curves are used to determine **(b)** the phase diagram of the mixture. The CSC values were measured at different nucleotide concentrations.

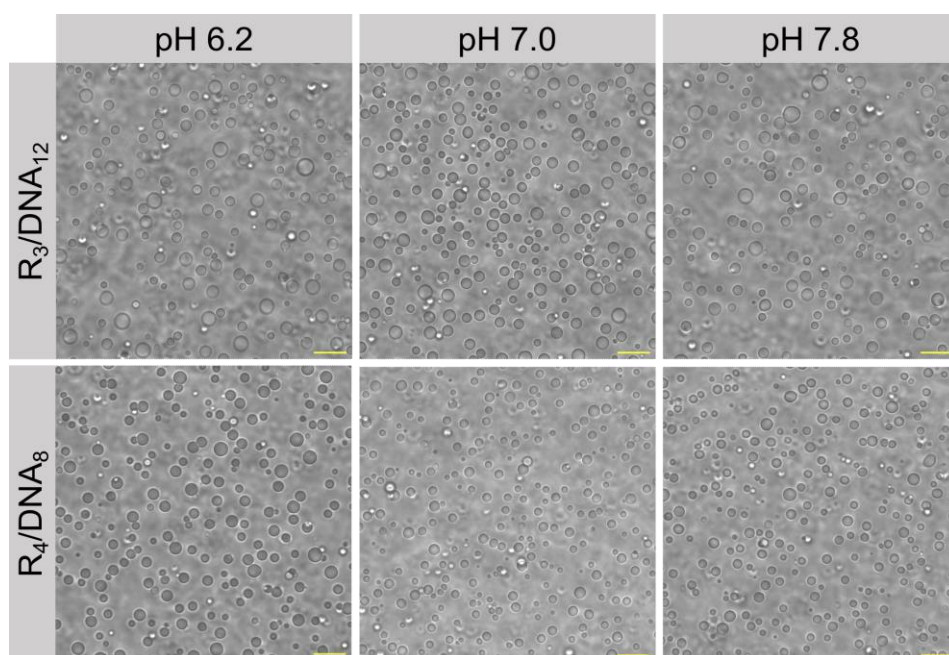


**Fig. S16.** Phase diagram of the mixtures in **Figure 2** (main text), obtained by varying the concentration of the anionic monomer: nucleotide in the case of peptide/oligonucleotide mixtures **(a)**; glutamic acid in the case of the peptide/peptide coacervates **(b)**.

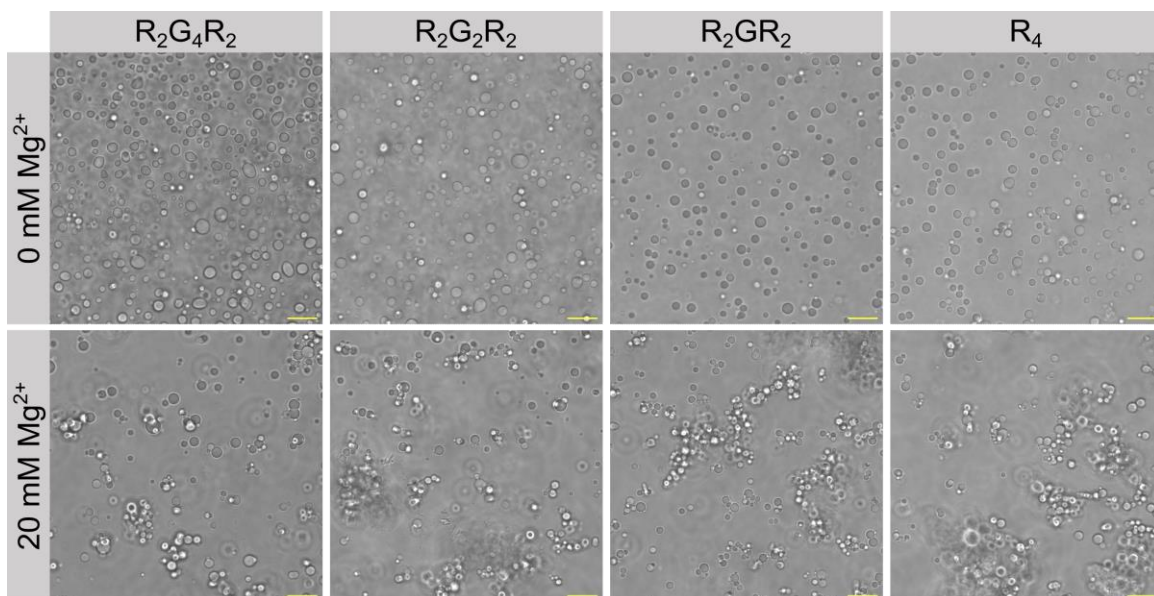




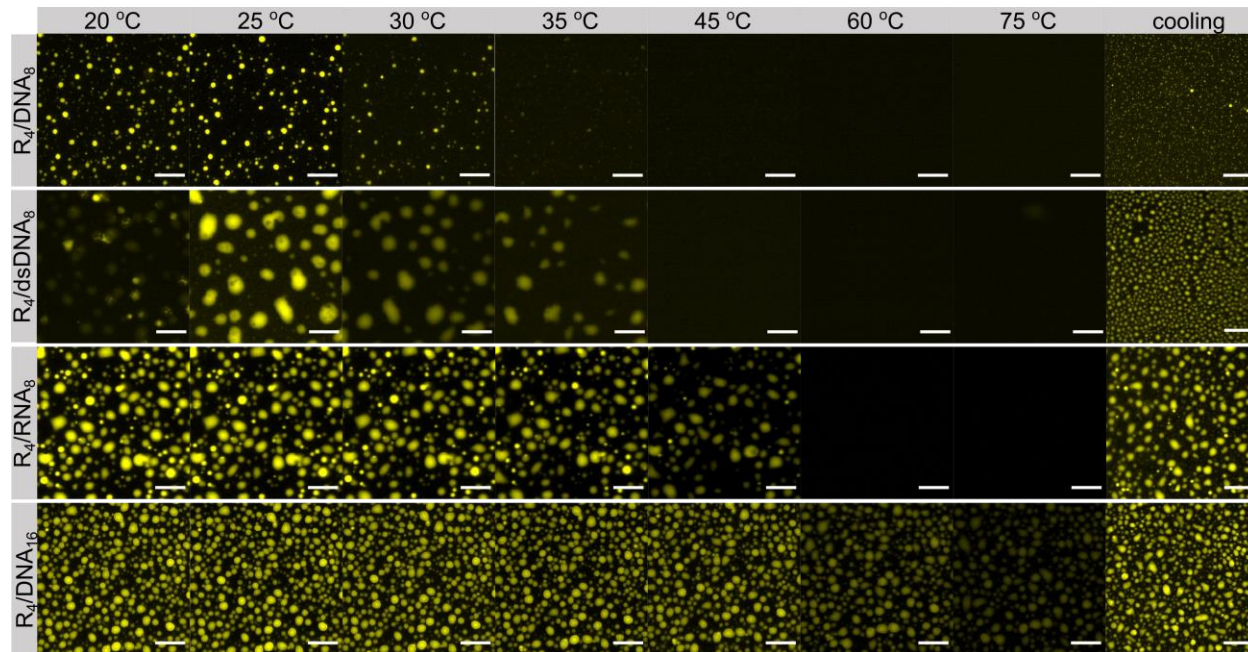
**Fig. S17.** Bright-field images of minimal coacervates in 25 mM HEPES pH 7.4, 25 mM imidazole pH 7.5 or 25 mM phosphate buffer pH 7.5. Scale bar = 10  $\mu$ m.



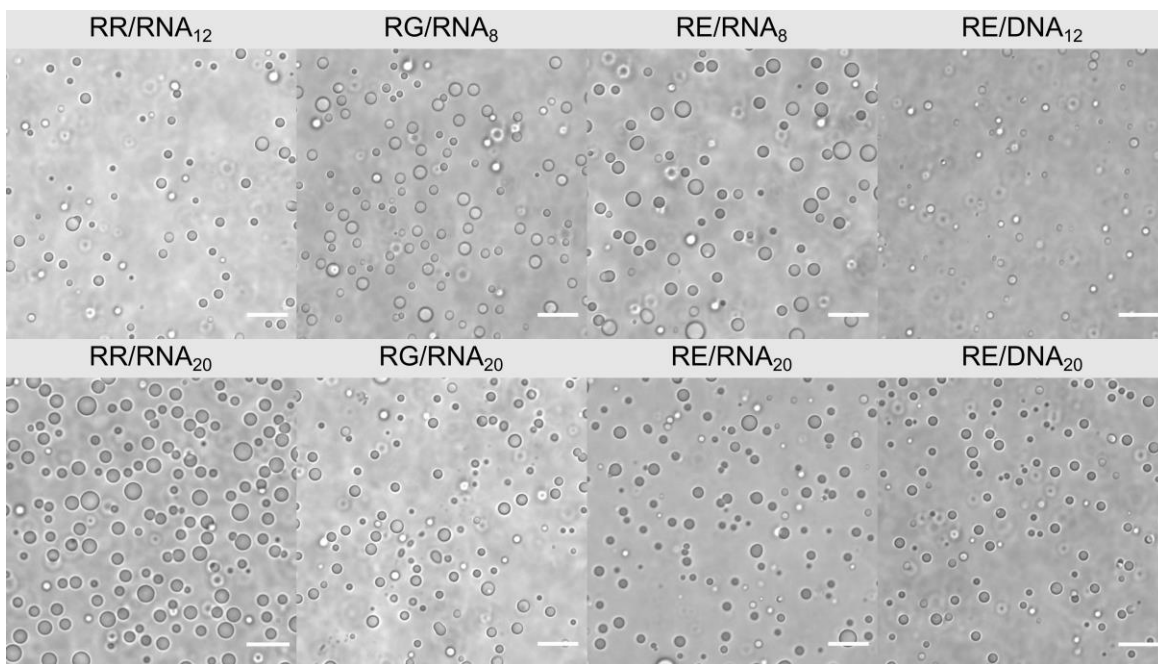
**Fig. S18.** Minimal coacervates in 25 mM imidazole buffer at different pH values, observed by bright-field microscopy. Scale bar = 10  $\mu$ m.



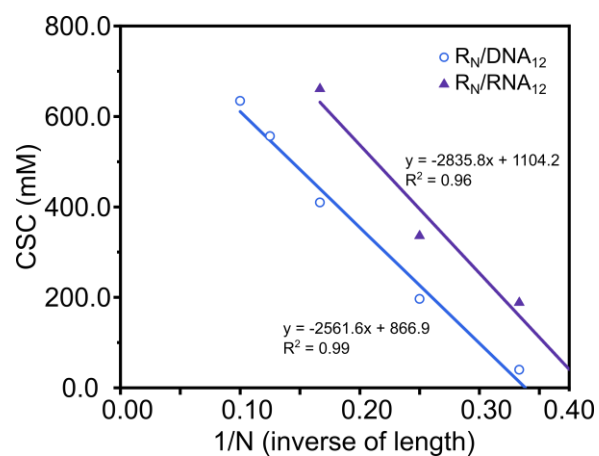
**Fig. S19.**  $R_2G_NR_2/DNA_{20}$  coacervates at different  $Mg^{2+}$  concentrations. Scale bar = 10  $\mu m$ , bright-field microscopy.



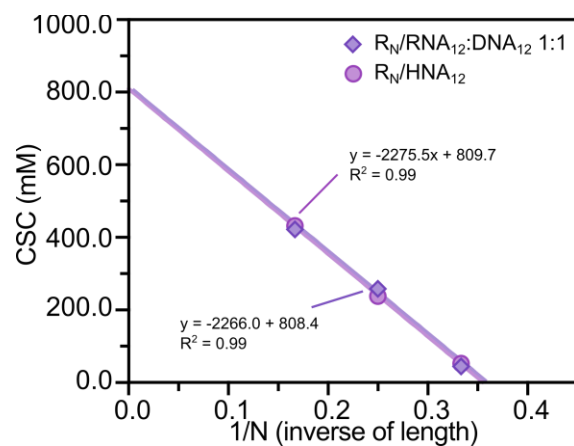
**Fig. S20.** Extended dataset for the thermal stability of peptide/oligonucleotide mixtures as in **Figure 2** (main text). The  $R_4$ /dsDNA<sub>8</sub> mixture is added for comparison and shows an additional phase transition before room temperature.  $R_4$ /DNA<sub>16</sub>, despite its similar CSC to  $R_4$ /RNA<sub>8</sub>, did not fully dissolve in the heating ramp. All mixtures reassemble into droplets upon cooling, and coacervate fluorescence is recovered. Scale bar: 10  $\mu$ m, fluorophore: Cy3-(TGAC)<sub>2</sub>.



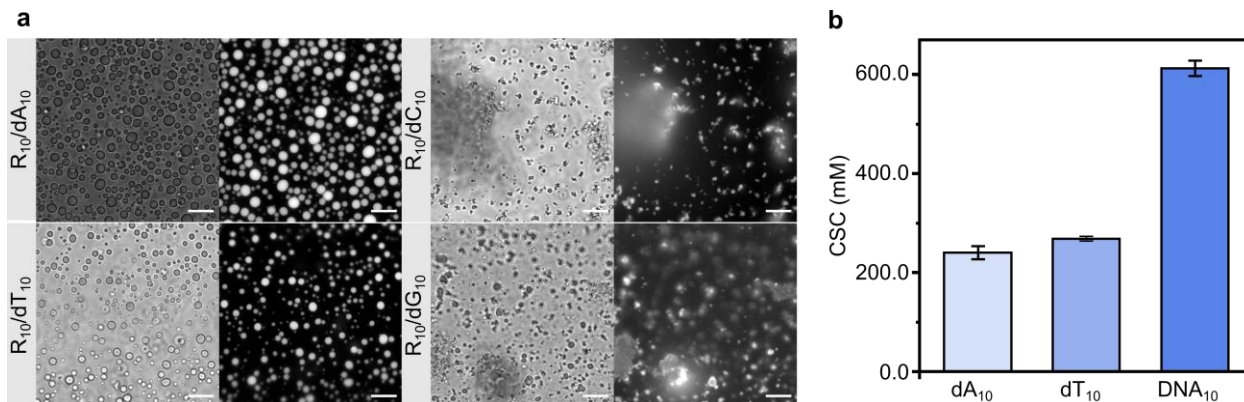
**Fig. S21.** Coacervates composed of peptide dimers and oligonucleotides (8-20 nt). Required concentrations of the components are listed in **Table S7**. Scale bar = 10  $\mu\text{m}$ , bright-field microscopy.



**Fig. S22.** CSC dependence on the inverse of the length of different peptides and oligonucleotides enabling the prediction of the shortest peptide to form coacervates with DNA<sub>12</sub> or RNA<sub>12</sub> (motif ACTG, open circles; or ACUG, purple triangles). The details of the linear regression are shown to calculate the length for CSC > 0.

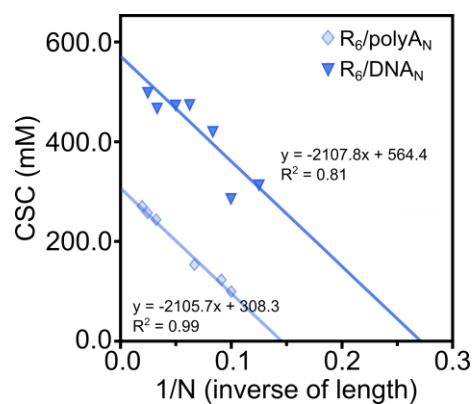


**Fig. S23.** CSC dependence on the inverse of the length of different peptides and oligonucleotides enabling the prediction of the shortest peptide to form coacervates with a mixture of DNA<sub>12</sub> and RNA<sub>12</sub> (purple diamonds) or with the hybrid strand HNA<sub>12</sub> (magenta circles). The linear fits overlap, and details are shown in **Table S5**. The details of the linear regression are shown to calculate the length for CSC > 0.

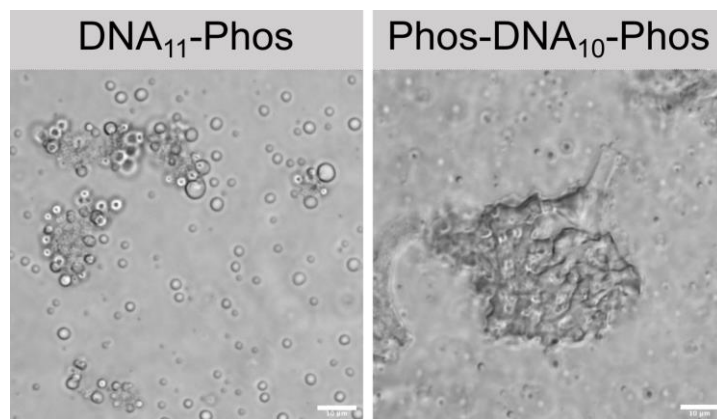


**Fig. S24. (a)** Mixtures of  $R_{10}/dX_{10}$  imaged by epifluorescence microscopy (probe: Cy3-10nt). Decamers of C and G, the bases capable of three hydrogen bonds, lead to solid aggregation instead of liquid droplets. **(b)** Critical salt concentrations (CSCs) of  $R_{10}/X_{10}$  mixtures that form coacervates, measured at 20 mM amino acid and 5 mM nucleotide, without any labelled oligo added. The CSC of solid aggregates is not a defined property.





**Fig. S25.** CSC dependence on the inverse of the length of different peptides and oligonucleotides enabling the prediction of the shortest homopolymeric DNA (polyA<sub>N</sub>, diamonds) to form coacervates with peptide R<sub>6</sub>, in comparison to when a heteropolymeric DNA sequence is used (inverted triangles). The details of the linear regression are shown to calculate the length for CSC > 0.



**Fig. S26.** R<sub>4</sub>-based coacervates made with phosphate-modified oligos. Scale bar = 10 µm, bright-field microscopy.

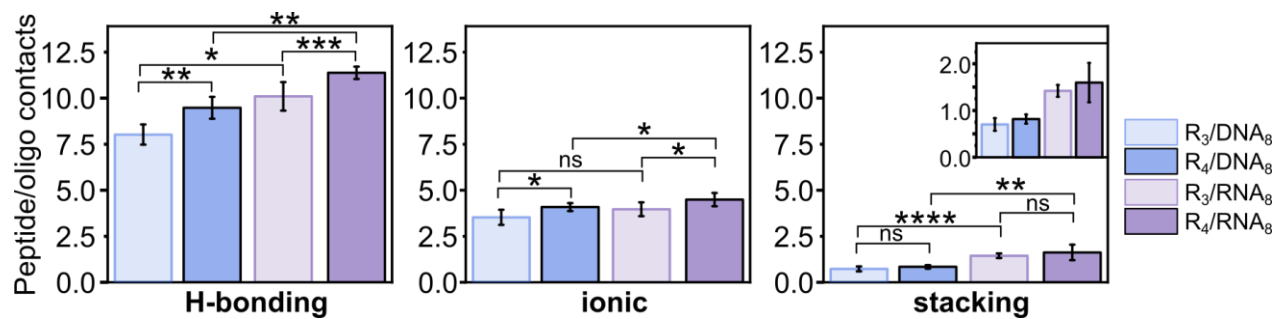
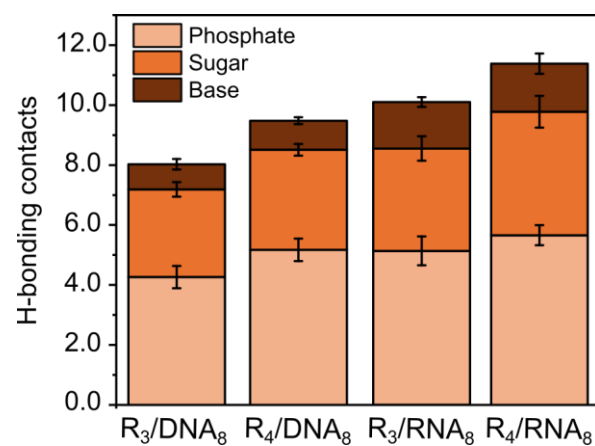
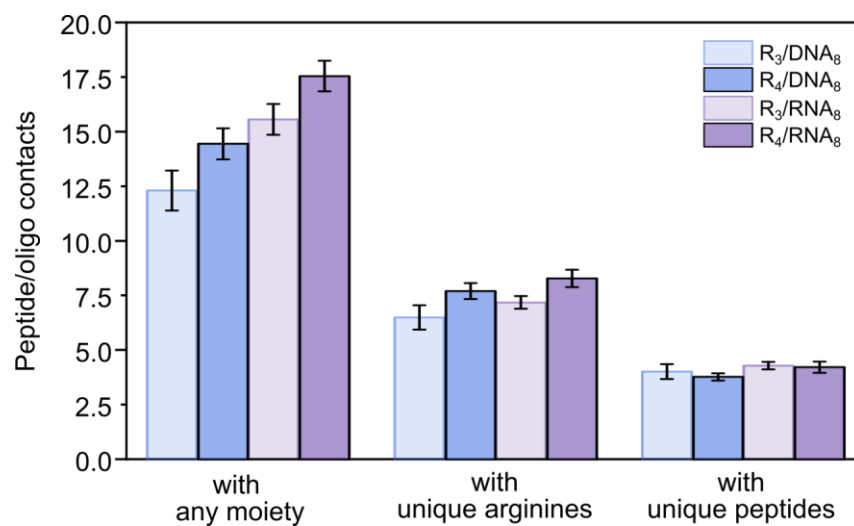


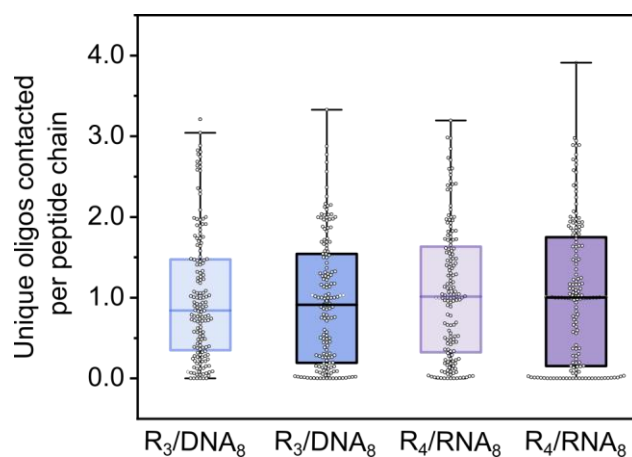
Fig. S27. Number of contacts per nucleotide through all three interaction modes for the four systems simulated atomistically. Error bars represent the standard deviation across 5 repeats.



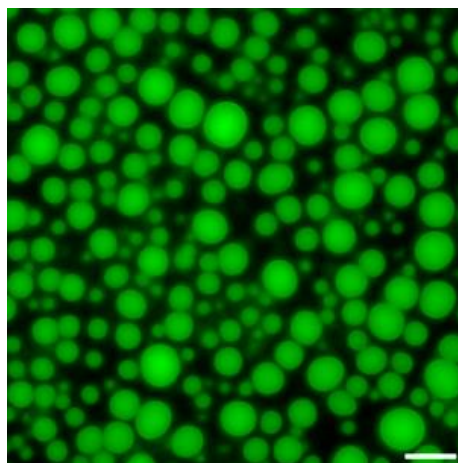
**Fig. S28.** Number of contacts *via* H-bonding, per nucleotide, established through the phosphate, sugar and base moieties. Error bars represent the standard deviation across 5 repeats.



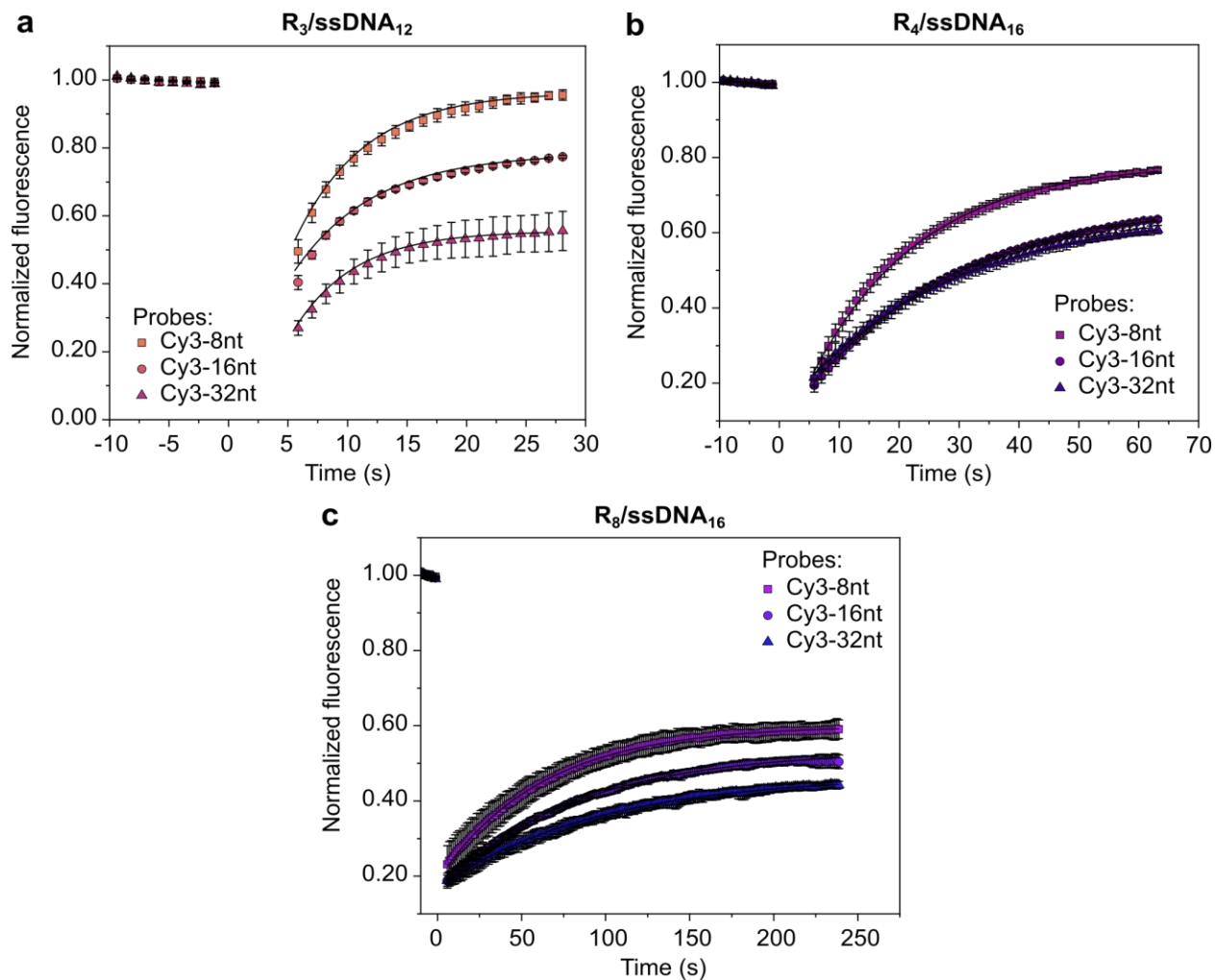
**Fig. S29.** Number of contacts established per oligonucleotide, grouped into three types of contact: with any peptide moiety, with unique arginine residues, or with unique peptide chains. Error bars represent the standard deviation across 5 repeats. The number of contacts with any peptide moiety is the “total valency” represented in **Figure 3** (main text).



**Fig. S30.** Unique oligonucleotide chains contacted by a peptide chain for the different mixtures simulated atomistically. The mixture R<sub>3</sub>/DNA<sub>8</sub> is the only one with a median <1, *i.e.*, on average, the peptide R<sub>3</sub> is free in the presence of DNA<sub>8</sub> chains. In this case, we represent each peptide chain sampled (36 chains, 5 repeats) instead of an average. Boxplots contain 50% of the data points measured for the 36 peptide chains in the simulation, averaged over time per simulation repeat (5x). The horizontal line represents the median.

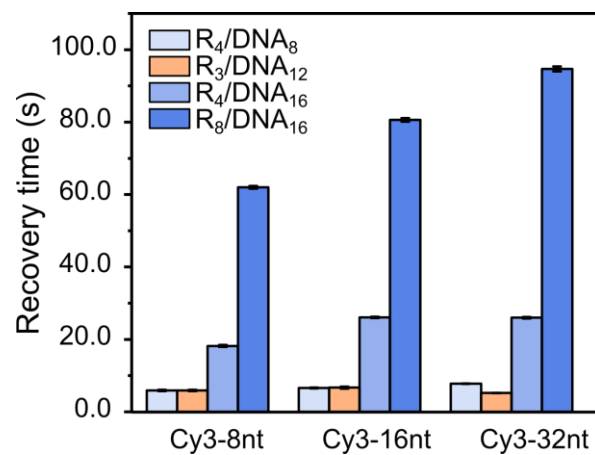


**Fig. S31.**  $\text{Cy}_3\text{-DNA}_5$  in  $\text{R}_4/\text{DNA}_{20}$  coacervates, showing that a DNA pentamer is recruited in the droplets. Scale bar = 10  $\mu\text{m}$ , epifluorescence microscopy.

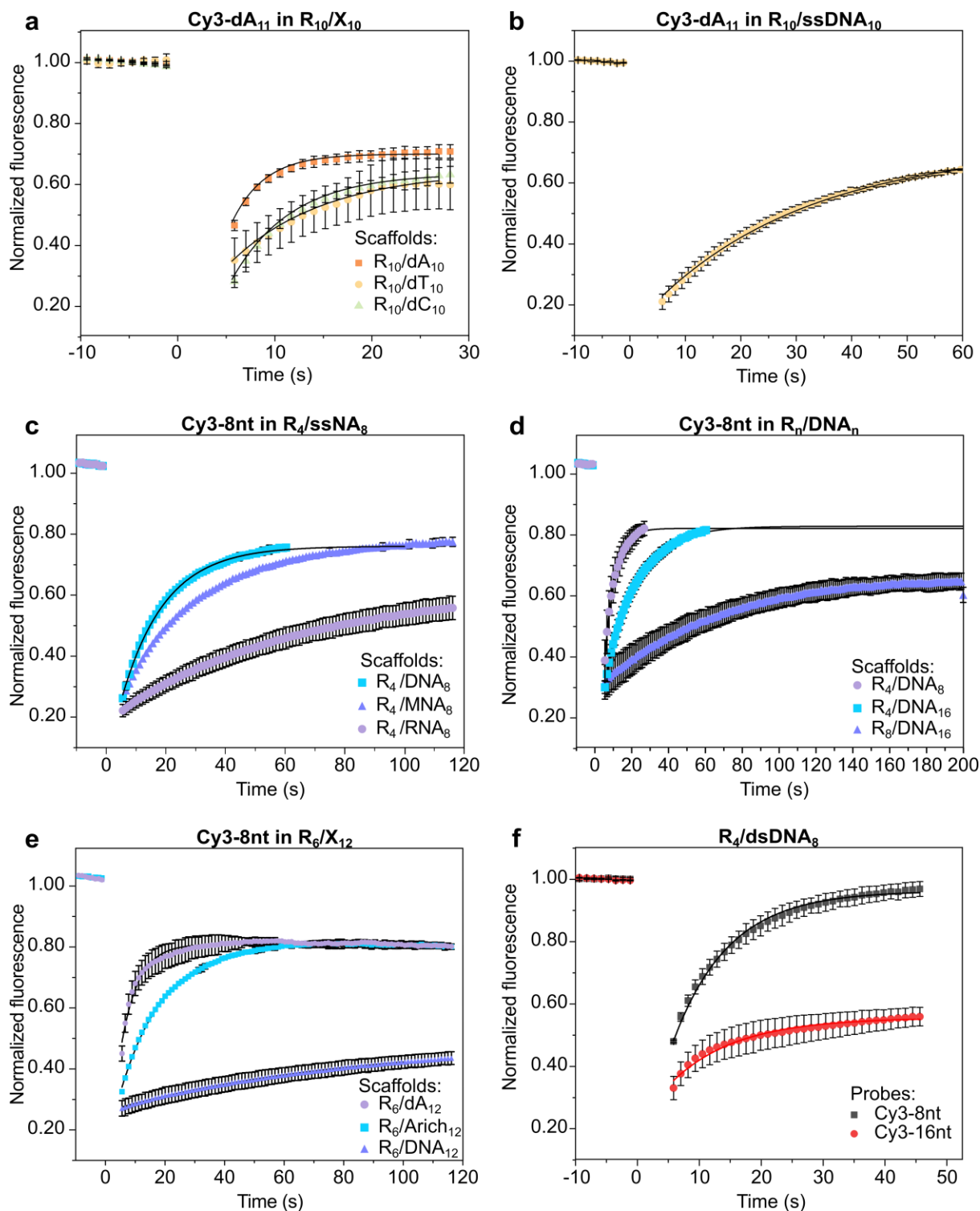


**Fig. S32.** FRAP profiles of a series of coacervates where peptide and DNA length were varied. Non-complementary probes of three lengths were tested for each coacervate system: 8, 16 and 32nt.

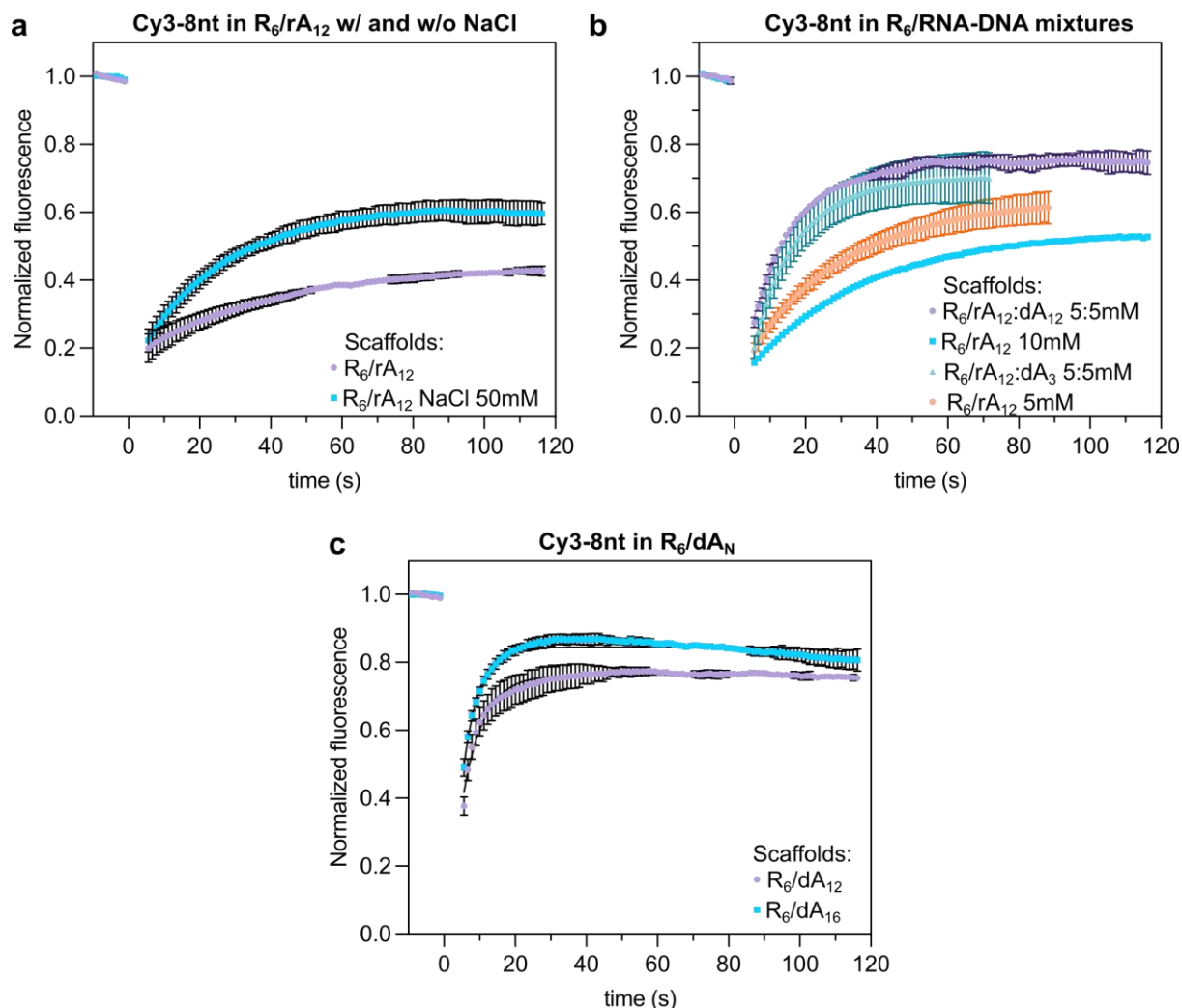




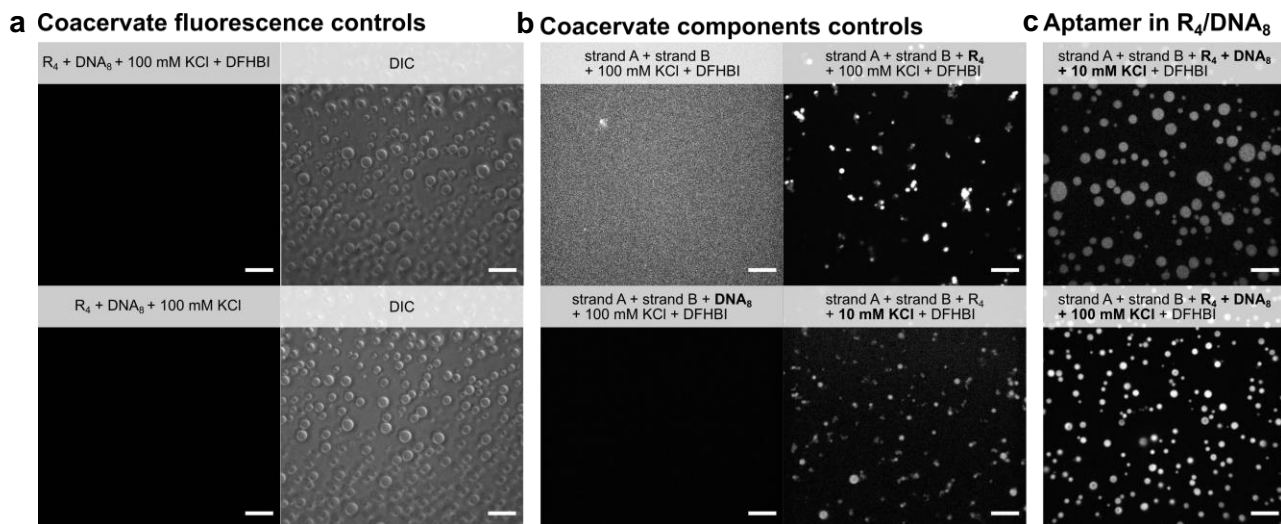
**Fig. S33.** Expanded dataset of FRAP recovery times for peptide-, DNA- and probe-length series as shown in **Figure 4** (main text).



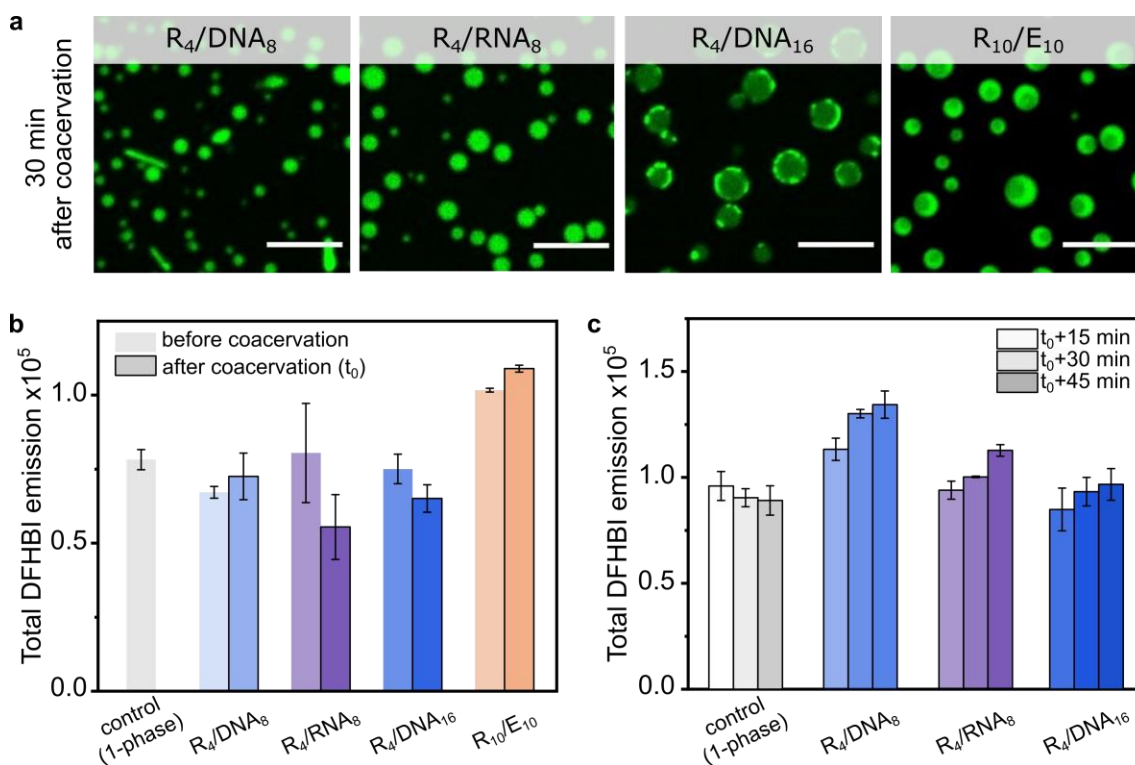
**Fig. S34.** FRAP profiles of coacervates showcasing the effect of the nature of the scaffold. **(a)** and **(b)** refer to the effect of homopolymers and heteropolymers of DNA. **(c)** probes the effect of DNA versus RNA as scaffold strands. **(d)** shows the effect of the scaffold polymer length (both peptide and DNA). **(e)** compares diffusion in DNA 12mers of different sequences. **(f)** shows the effect of having dsDNA as scaffold strands.



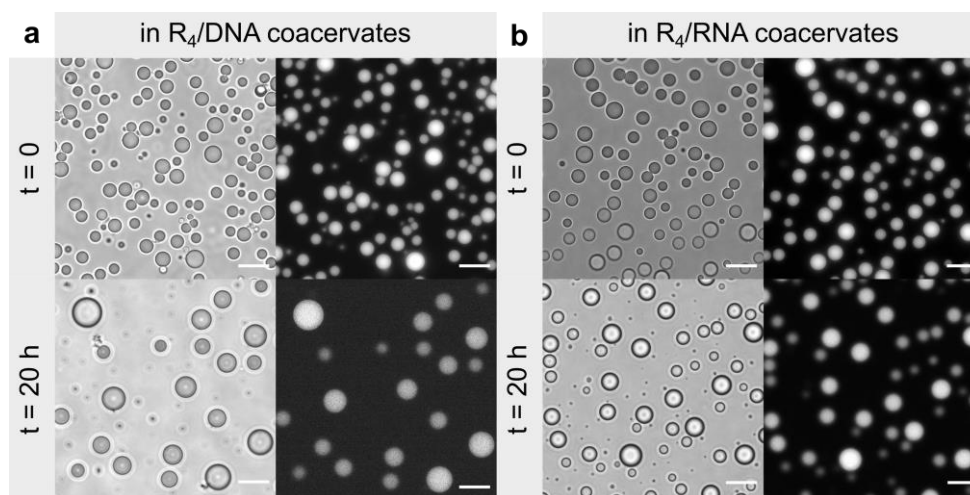
**Fig. S35. FRAP profiles of RNA- and DNA-based coacervates in the presence of  $R_6$ .** (a) shows the effect of having salt (50mM NaCl) in solution, which partially dissolves the coacervates and seemingly fluidizes the system. (b) compares RNA-based coacervates with coacervates made of mixtures of RNA and DNA of the same length ( $rA_{12}$ ,  $dA_{12}$ ) or different lengths ( $rA_{12}$ ,  $dA_3$ ) in equimolar quantities. The presence of DNA actively fluidizes the coacervates as they are more fluid than those made up of half concentration of RNA only ( $rA_{12}$  5mM). (c) shows the length component in DNA polyA systems ( $dA_{12}$  and  $dA_{16}$ , respectively).



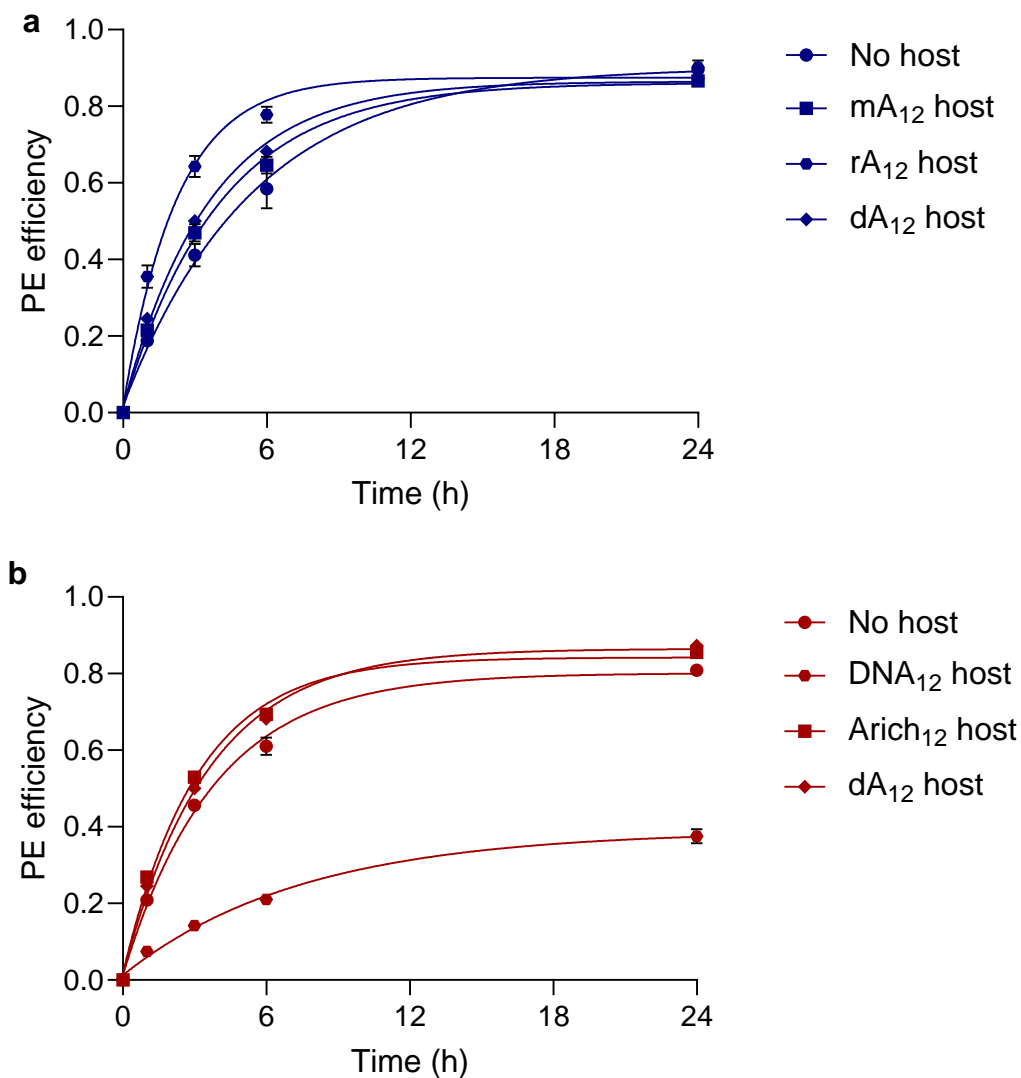
**Fig. S36.** Confocal micrographs of aptamer reconstitution in coacervates. **(a)** Confocal fluorescence micrographs of different controls and test samples under constant irradiation conditions in the 488 nm channel (DFHBI). The DIC channel is only shown for (1) and (2) to confirm the presence of coacervates. **(b)** Quantification of the total DFHBI emission in the field of view shown in (a). Error bars come from measurements in triplicate. **(c)** DFHBI emission in the presence of coacervates, now separating emission from all droplets in the FOV and the background (dilute phase). Samples were prepared adding DFHBI as the last component.



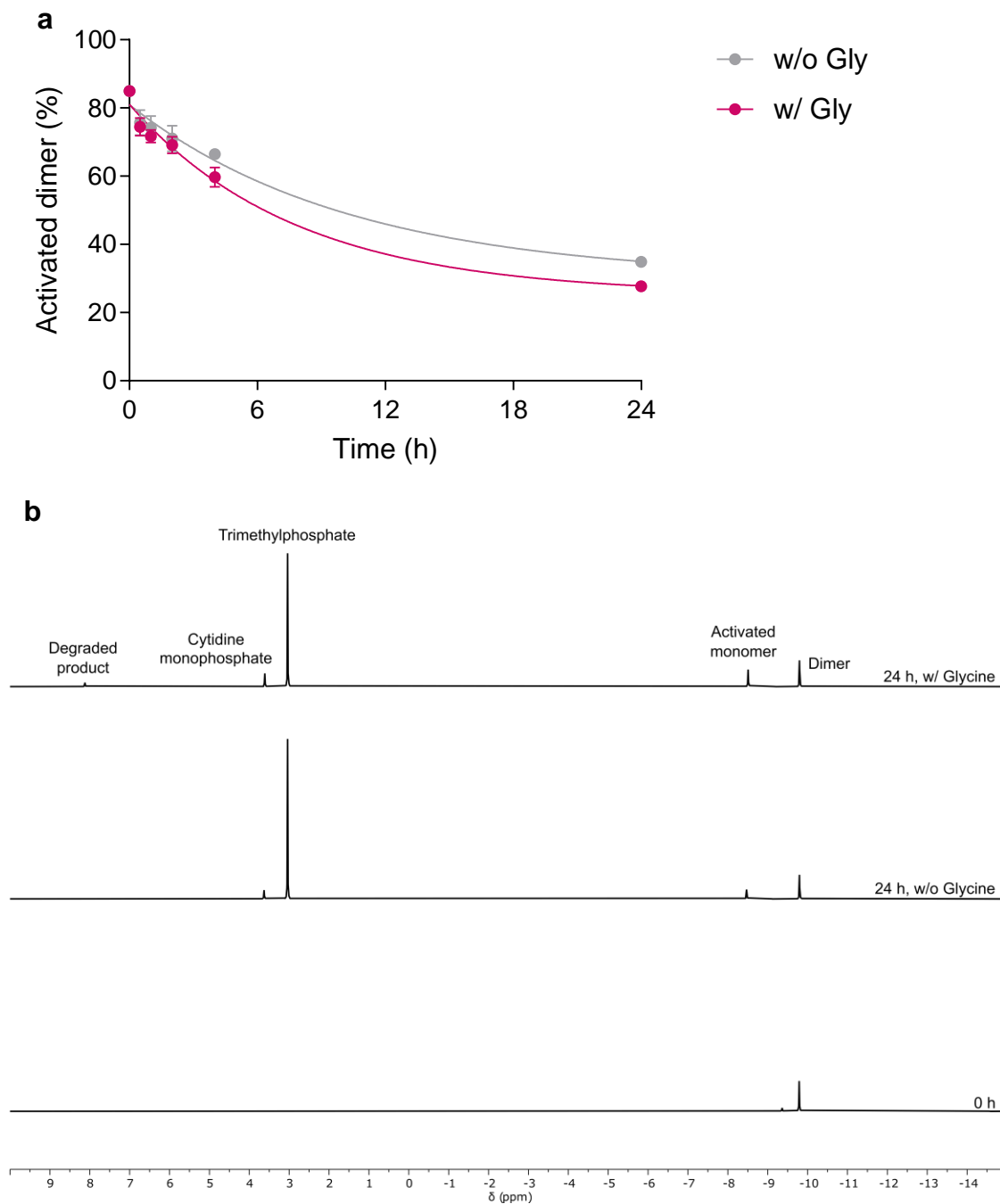
**Fig. S37.** DFHBI/Brocколи aptamer emission measured by confocal microscopy and fluorescence spectroscopy (bulk). **(a)** Confocal micrographs of coacervates containing the DFHBI/Brocколи aptamer complex imaged ca. 30 min after preparation. Scale bars are 10  $\mu\text{m}$ . **(b)** Expanded dataset shown in **Figure 5** (main text), including the effect of  $R_4/DNA_{16}$  and  $R_{10}/E_{10}$  coacervates on emission, measured before and immediately after coacervation. Samples were prepared by adding the peptide as the last component, *i.e.*, coacervation occurs in the presence of the reconstituted aptamer. **(c)** Time course of DFHBI emission (15, 30 and 45 min after mixing). In this setup, the different partitioning of the aptamer among the coacervates tested is evident.



**Fig. S38.** Stability of peptide/nucleic acid coacervates during primer extension. Micrographs of reaction mixtures for primer extension by transmission and epifluorescence (FAM-labelled primer). The coacervate scaffold is composed of: **(a)** 40 mM (aa)  $R_4$ , 5 mM (nt)  $(ACTG)_3$ , **(b)** 40 mM  $R_4$ , 5 mM  $(ACUG)_3$ . **(a)** and **(b)** contain 1% of the FAM-labelled primer strand and 1% of the template strand. (a-c) contain  $Mg^{2+}$  5 mM, activated dimer 5.0 mM and 25 mM HEPES pH 7.4.

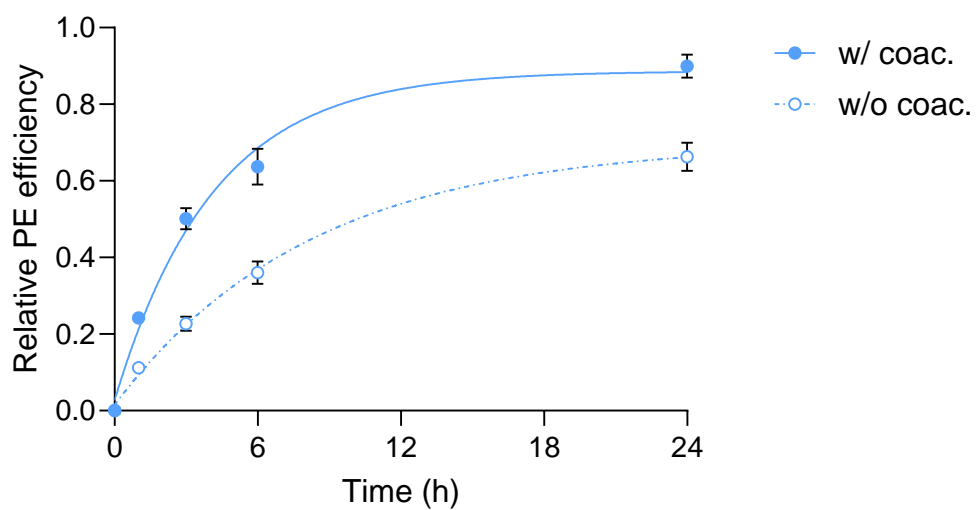


**Fig. S39.** Primer extension efficiencies over time in the presence or absence of bystander (host) oligonucleotides. PE was tested with a primer/template system with no complementarity with the host oligonucleotide **(a)**, and a primer/template system with complementarity with the host  $DNA_{12}$  oligonucleotide **(b)**. Data were fit to first order exponential. Abbreviations: PE = primer extension,  $dA_{12}$  = 12-deoxyribonucleotide-long polyadenine oligonucleotide,  $rA_{12}$  = 12-ribonucleotide-long polyadenine oligonucleotide,  $mA_{12}$  =  $dA_{12}:rA_{12}$  1:1 ratio,  $Arich_{12}$  = 12-deoxyribonucleotide-long A-rich-sequence oligonucleotide,  $DNA_{12}$  = 12-deoxyribonucleotide-long mixed-sequence oligonucleotide ((ACTG)<sub>3</sub>).

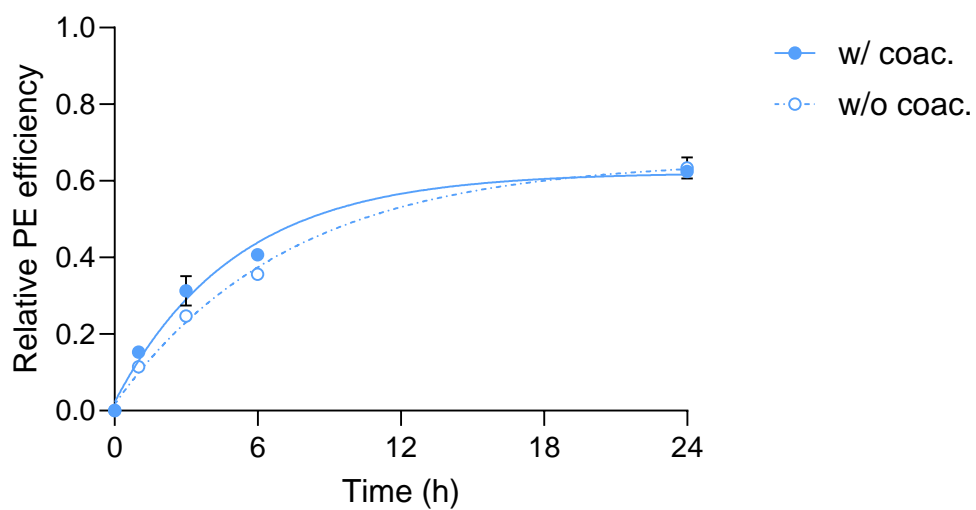


**Fig. S40. (a)** Degradation profile of the activated imidazolium-bridged dicytidyl dimer in the absence (grey filled dots) and in the presence of glycine (red filled dots). **(b)** Representative NMR spectra after 24 hours, highlighting degradation products (e.g., cytidine monophosphate and activated monomer), are shown for the activated dimer with and without glycine.

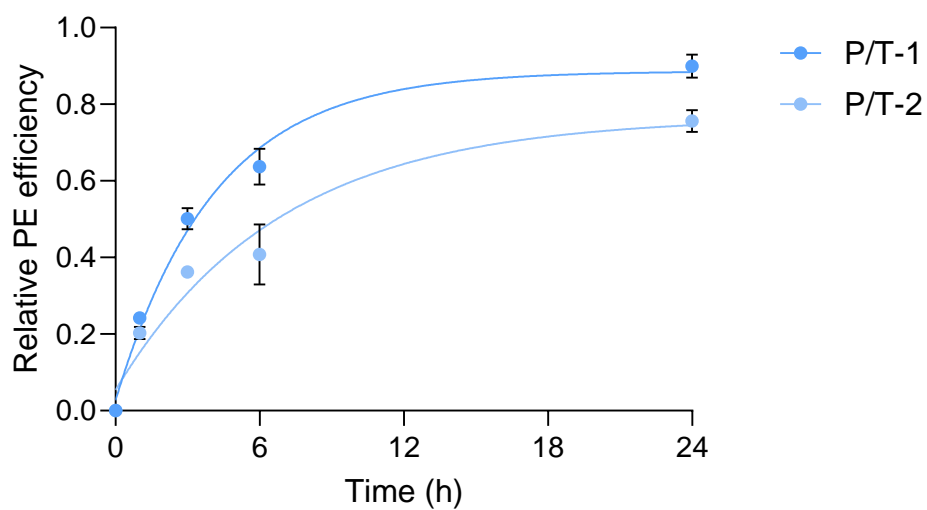




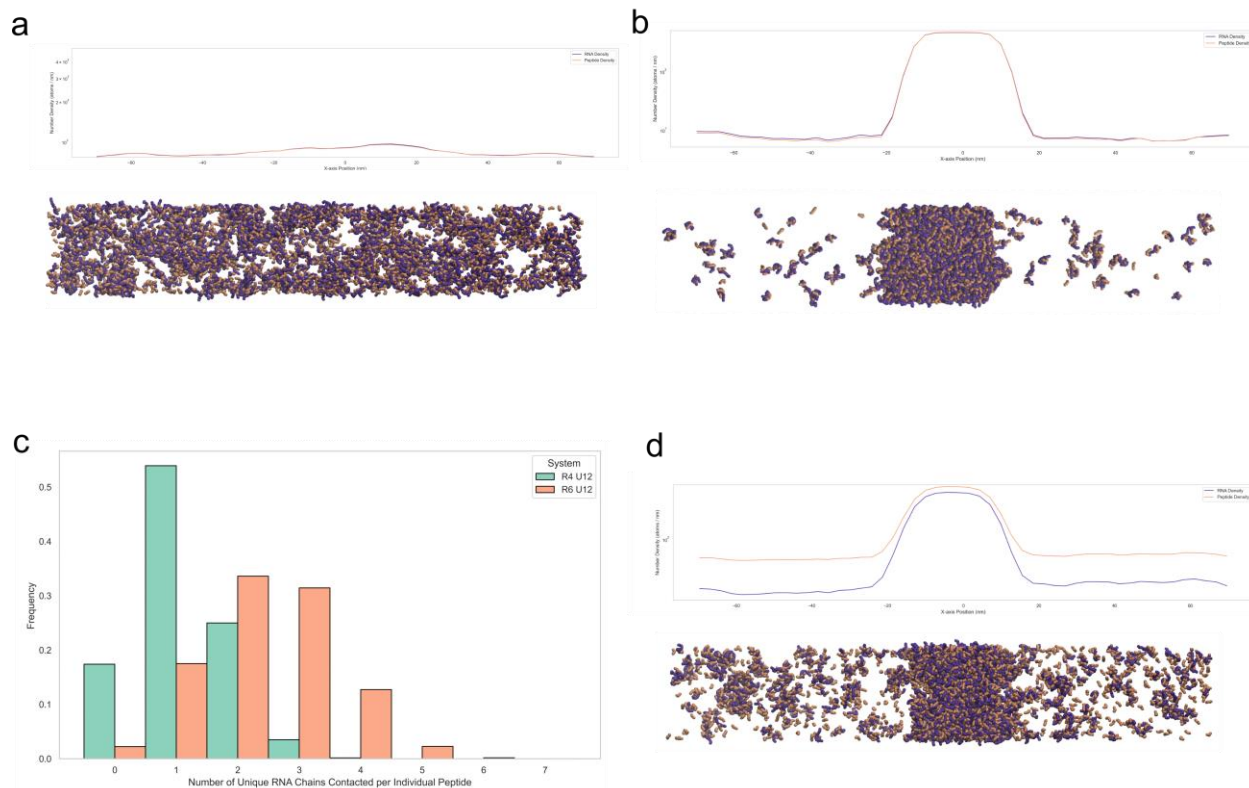
**Fig. S41.** Primer extension efficiencies over time in the presence of  $dA_{12}$  and  $R_6$  (20:10 [Arg]:[nt] ratio) without NaCl to enable coacervation (filled circles) or with NaCl to prevent coacervation (empty circles). PE efficiencies were normalised against their respective control reactions. Data were fit to first order exponential.



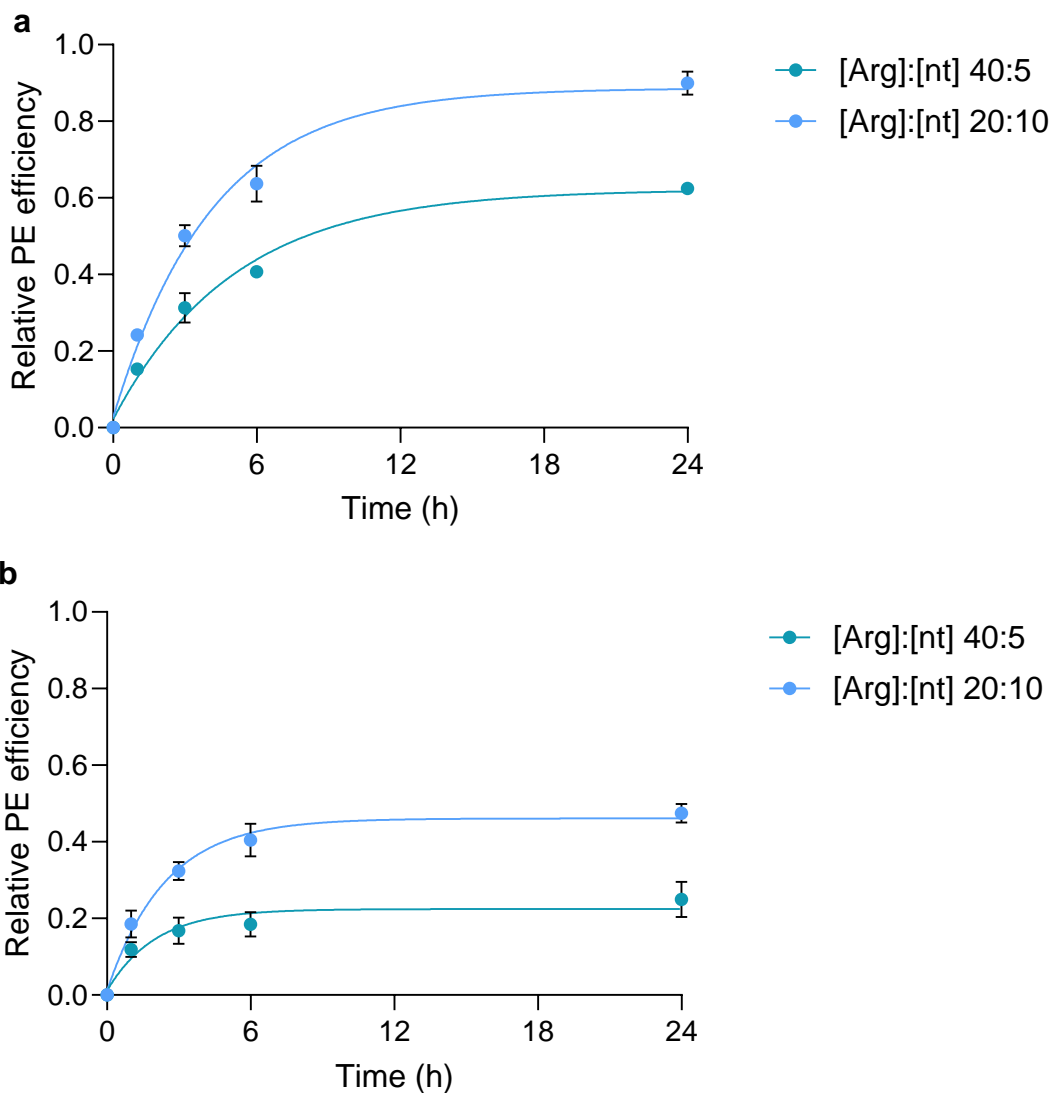
**Fig. S42.** Primer extension efficiencies over time in the presence of  $dA_{12}$  and  $R_6$  (40:5 [Arg]:[nt] ratio) without NaCl to enable coacervation (filled circles) or with NaCl to prevent coacervation (empty circles). PE efficiencies were normalised against their respective control reactions. Data were fit to first order exponential.



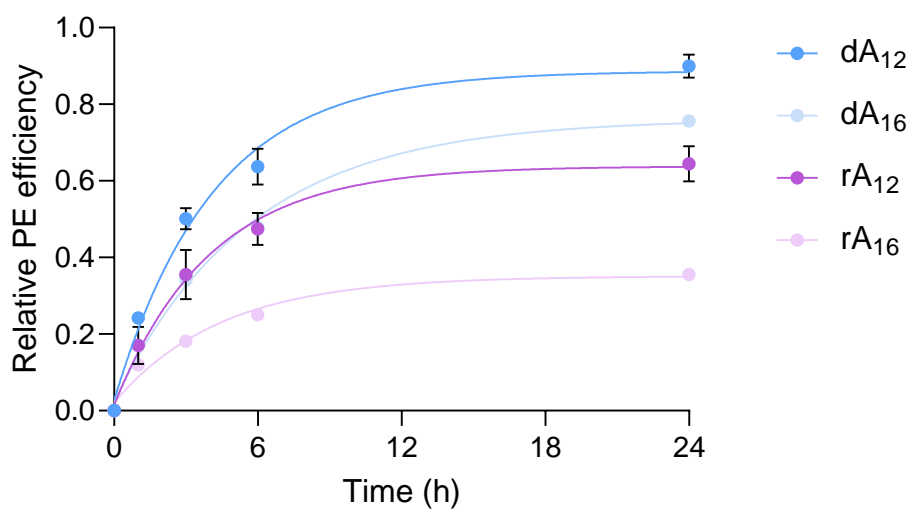
**Fig. S43.** Primer extension efficiencies over time in the presence of  $dA_{12}$  and  $R_6$  (20:10 [Arg]:[nt] ratio) with two different primer/template (P/T) pairs. PE efficiencies were normalised against their respective control reactions. Data were fit to first order exponential.



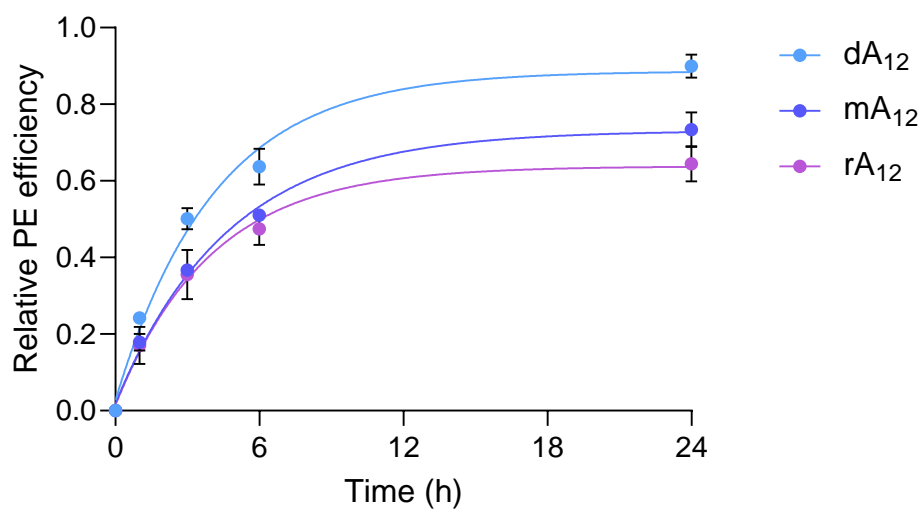
**Fig. S44.** Coarse-grain simulation of  $U_{12}$  system. **(a)** Density profile and simulation snapshot for the 3 R4 : 1 U12 system, showing an approximately uniform density throughout the box, indicating that liquid-liquid phase separation (LLPS) does not occur for this mixture. **(b)** Density profile and simulation snapshot for the 2 R6 : 1 U12 system, showing a pronounced peak in the density of RNA and peptide at the center of the box, corresponding to the formation of a condensate. **(c)** Histogram showing differences in valency in the charge-balanced 3 R4 : 1 U12 and 2 R6 : 1 U12 systems. The R6 system shows many peptides simultaneously contacting 3,4, or 5 unique RNA chains, whilst in the R4 system very few peptides contact more than 2 RNA chains simultaneously. **(d)** Density profile and simulation snapshot for the 3 R6 : 1 U12 system, illustrating the effects of oversaturating with peptide. While the peptide:RNA ratio increases only moderately ( $\sim 19\%$ ) in the central dense region, a much larger ( $\sim 140\%$ ) increase is observed in the dilute phase.



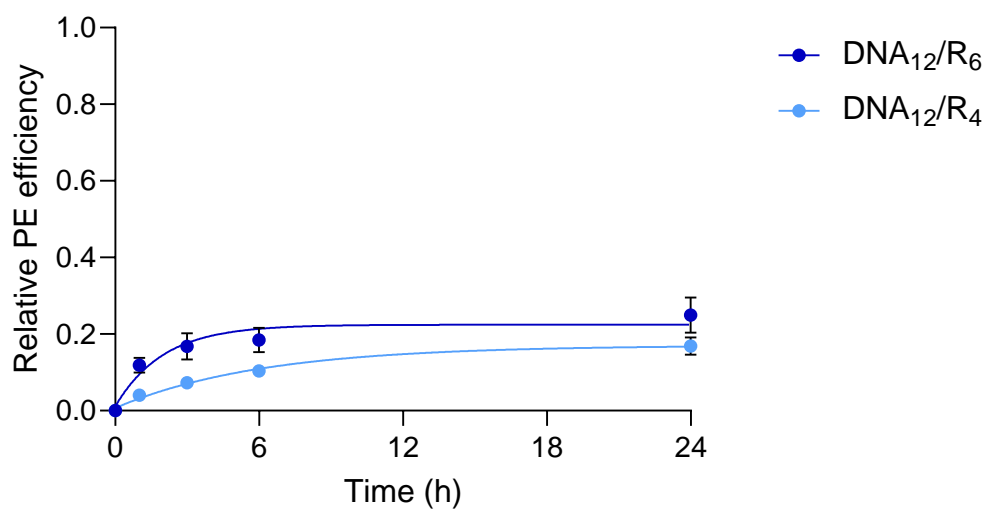
**Fig. S45. (a)** Primer extension efficiencies over time in the presence of  $dA_{12}$  and  $R_6$  at different charge ratios between peptide and oligonucleotide. **(b)** Primer extension efficiencies over time in the presence of  $DNA_{12}$  and  $R_6$  at different charge ratios between peptide and oligonucleotide. PE efficiencies were normalised against their respective control reactions. Data were fit to first order exponential.



**Fig. S46.** Primer extension efficiencies over time in the presence of R<sub>6</sub> (20:10 [Arg]:[nt] ratio) and dA<sub>12</sub>, dA<sub>16</sub>, rA<sub>12</sub> and rA<sub>16</sub>. PE efficiencies were normalised against their respective control reactions. Data were fit to first order exponential.

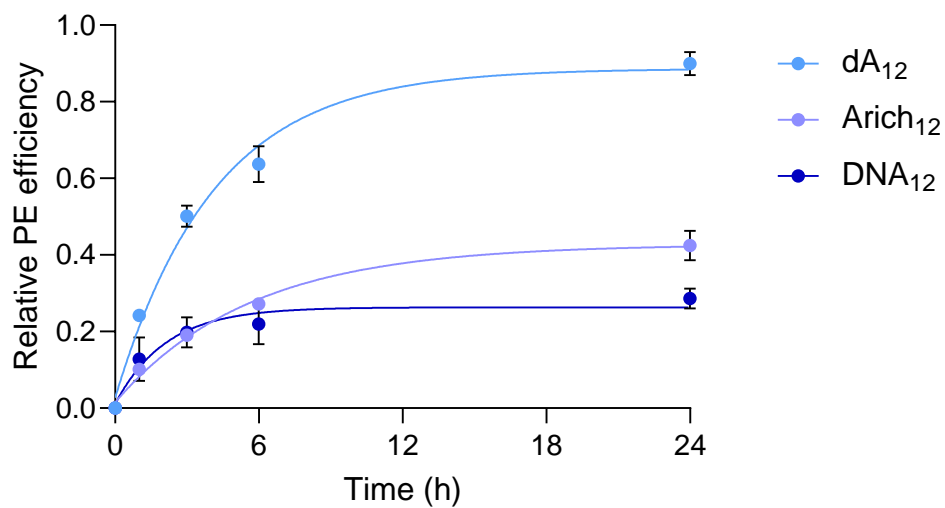


**Fig. S47.** Primer extension efficiencies over time in the presence of  $R_6$  (20:10 [Arg]:[nt] ratio) and dA<sub>12</sub>, mA<sub>12</sub> (dA<sub>12</sub>:rA<sub>12</sub> 1:1) and rA<sub>12</sub>. PE efficiencies were normalised against their respective control reactions. Data were fit to first order exponential.

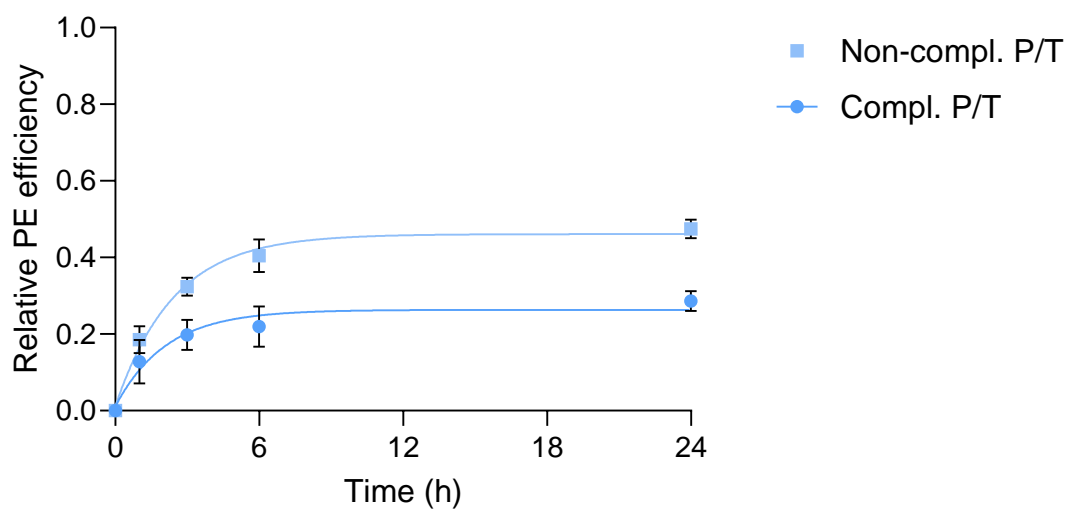


**Fig. S48.** Primer extension efficiencies over time in the presence of DNA<sub>12</sub> (40:5 [Arg]:[nt] ratio) and R<sub>6</sub> or R<sub>4</sub>. PE efficiencies were normalised against their respective control reactions. Data were fit to first order exponential.





**Fig. S49.** Primer extension efficiencies over time in the presence of R<sub>6</sub> (20:10 [Arg]:[nt] ratio) and dA<sub>12</sub>, Arich<sub>12</sub> and DNA<sub>12</sub>. PE efficiencies were normalised against their respective control reactions. Data were fit to first order exponential.



**Fig. S50.** Primer extension efficiencies over time in the presence of DNA<sub>12</sub> and R<sub>6</sub> with primer/template systems that are complementary or non-complementary to the host strand. PE efficiencies were normalised against their respective control reactions. Data were fit to first order exponential.

## References

1. Jensen, K. J. ; T. S., Pernille; Pedersen, Søren L. *Peptide Synthesis and Applications*. 252 (Humana Press, Totowa, NJ, 2013).
2. Robinson, J. D., Sammons, S. R. & O'Flaherty, D. K. Preparation of 2-Aminoimidazole-Activated Substrates for the Study of Nonenzymatic Genome Replication. *Current Protocols* **4**, e1119 (2024).
3. Nakashima, K. K., André, A. A. M. & Spruijt, E. Chapter Thirteen - Enzymatic control over coacervation. in *Methods in Enzymology* (ed. Keating, C. D.) vol. 646 353–389 (Academic Press, 2021).
4. Maier, J. A. *et al.* ff14SB: Improving the Accuracy of Protein Side Chain and Backbone Parameters from ff99SB. *J. Chem. Theory Comput.* **11**, 3696–3713 (2015).
5. Zgarbová, M. *et al.* Refinement of the Cornell *et al.* Nucleic Acids Force Field Based on Reference Quantum Chemical Calculations of Glycosidic Torsion Profiles. *J. Chem. Theory Comput.* **7**, 2886–2902 (2011).
6. Ivani, I. *et al.* Parmbsc1: a refined force field for DNA simulations. *Nat Methods* **13**, 55–58 (2016).
7. Wang, L.-P., Martinez, T. J. & Pande, V. S. Building Force Fields: An Automatic, Systematic, and Reproducible Approach. *J. Phys. Chem. Lett.* **5**, 1885–1891 (2014).
8. Åqvist, J., Wennerström, P., Nervall, M., Bjelic, S. & Brandsdal, B. O. Molecular dynamics simulations of water and biomolecules with a Monte Carlo constant pressure algorithm. *Chemical Physics Letters* **384**, 288–294 (2004).
9. Zhang, Z., Liu, X., Yan, K., Tuckerman, M. E. & Liu, J. Unified Efficient Thermostat Scheme for the Canonical Ensemble with Holonomic or Isokinetic Constraints via Molecular Dynamics. *J. Phys. Chem. A* **123**, 6056–6079 (2019).
10. Eastman, P. & Pande, V. S. Constant Constraint Matrix Approximation: A Robust, Parallelizable Constraint Method for Molecular Simulations. *J. Chem. Theory Comput.* **6**, 434–437 (2010).
11. Essmann, U. *et al.* A smooth particle mesh Ewald method. *The Journal of Chemical Physics* **103**, 8577–8593 (1995).

12. Eastman, P. *et al.* OpenMM 8: Molecular Dynamics Simulation with Machine Learning Potentials. *J. Phys. Chem. B* **128**, 109–116 (2024).
13. Liu, D. C. & Nocedal, J. On the limited memory BFGS method for large scale optimization. *Mathematical Programming* **45**, 503–528 (1989).
14. PyMOL | pymol.org. <https://pymol.org/>.
15. Martínez, L., Andrade, R., Birgin, E. G. & Martínez, J. M. PACKMOL: A package for building initial configurations for molecular dynamics simulations. *Journal of Computational Chemistry* **30**, 2157–2164 (2009).
16. McGibbon, R. T. *et al.* MDTraj: A Modern Open Library for the Analysis of Molecular Dynamics Trajectories. *Biophysical Journal* **109**, 1528–1532 (2015).
17. Wernet, Ph. *et al.* The Structure of the First Coordination Shell in Liquid Water. *Science* **304**, 995–999 (2004).
18. Paloni, M., Bussi, G. & Barducci, A. Arginine multivalency stabilizes protein/RNA condensates. *Protein Science* **30**, 1418–1426 (2021).
19. Tejedor, A. R. *et al.* Chemically-informed coarse-graining of electrostatic forces in charge-rich biomolecular condensates. Preprint at <https://doi.org/10.1101/2024.07.26.605370> (2024).
20. Ladd, A. J. C. & Woodcock, L. V. Triple-point coexistence properties of the lennard-jones system. *Chemical Physics Letters* **51**, 155–159 (1977).
21. Okuta, R., Unno, Y., Nishino, D., Hido, S. & Loomis, C. CuPy: A NumPy-Compatible Library for NVIDIA GPU Calculations. in *Proceedings of Workshop on Machine Learning Systems (LearningSys) in The Thirty-first Annual Conference on Neural Information Processing Systems (NIPS)* (2017).